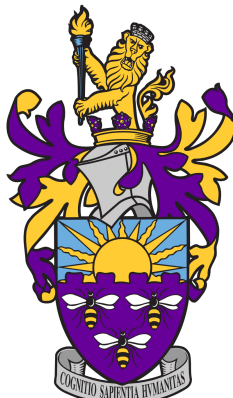


Cosmological constraints from tSZ power spectrum and cluster counts

Boris Bolliet

Jodrell Bank Centre for Astrophysics
The University of Manchester



Objectives of the talk:

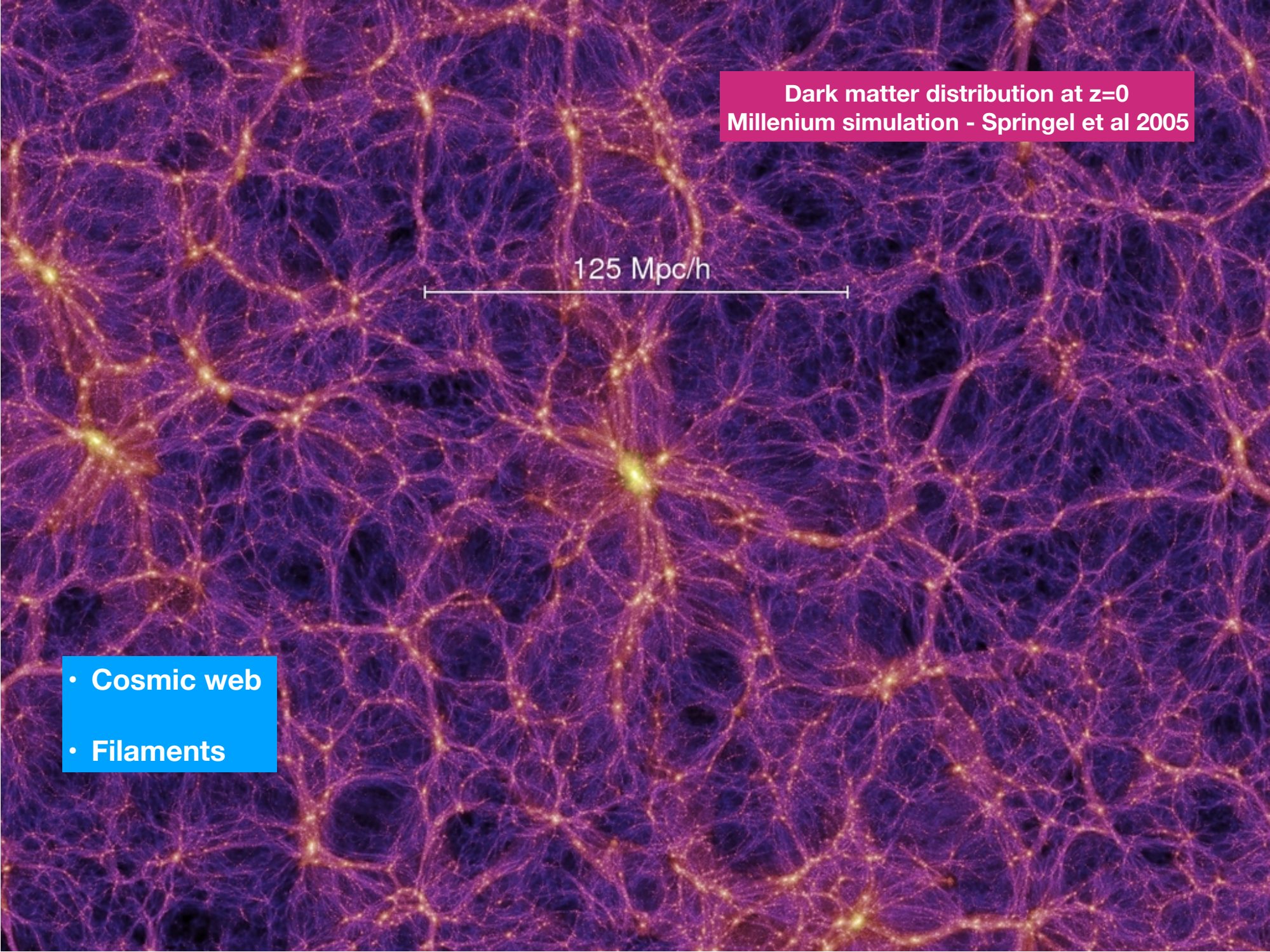
- Planck SZ cluster counts and power spectrum fully consistent with other SZ observation and galaxy surveys.
- Discuss the tension:
Primary CMB predicts more clusters than we see.
- What will we learn from SZ in the next 15 years?

some material in this talk from work with:

Richard Battye, Thejs Brinckmann, Barbara Comis, Jens Chluba, Eiichiro Komatsu, Julien Lesgourgues, Juan Macias-Perez, Aditya Rotti, Mathieu Remazeilles

Density field at $z=18.3$
Millenium simulation - Springel et al 2005

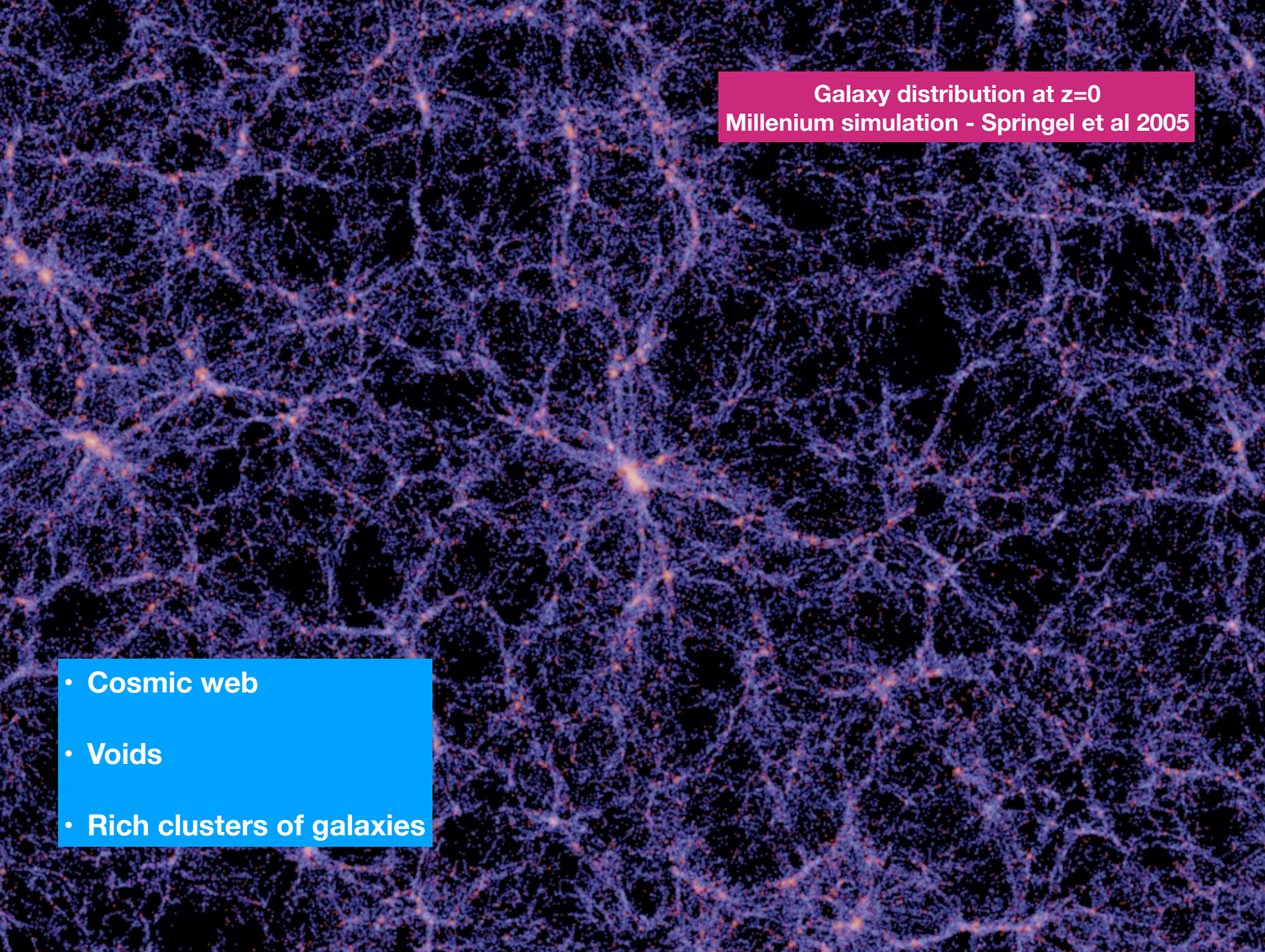
500 Mpc/h



Dark matter distribution at $z=0$
Millenium simulation - Springel et al 2005

125 Mpc/h

- Cosmic web
- Filaments



Galaxy distribution at $z=0$
Millenium simulation - Springel et al 2005

- Cosmic web
- Voids
- Rich clusters of galaxies

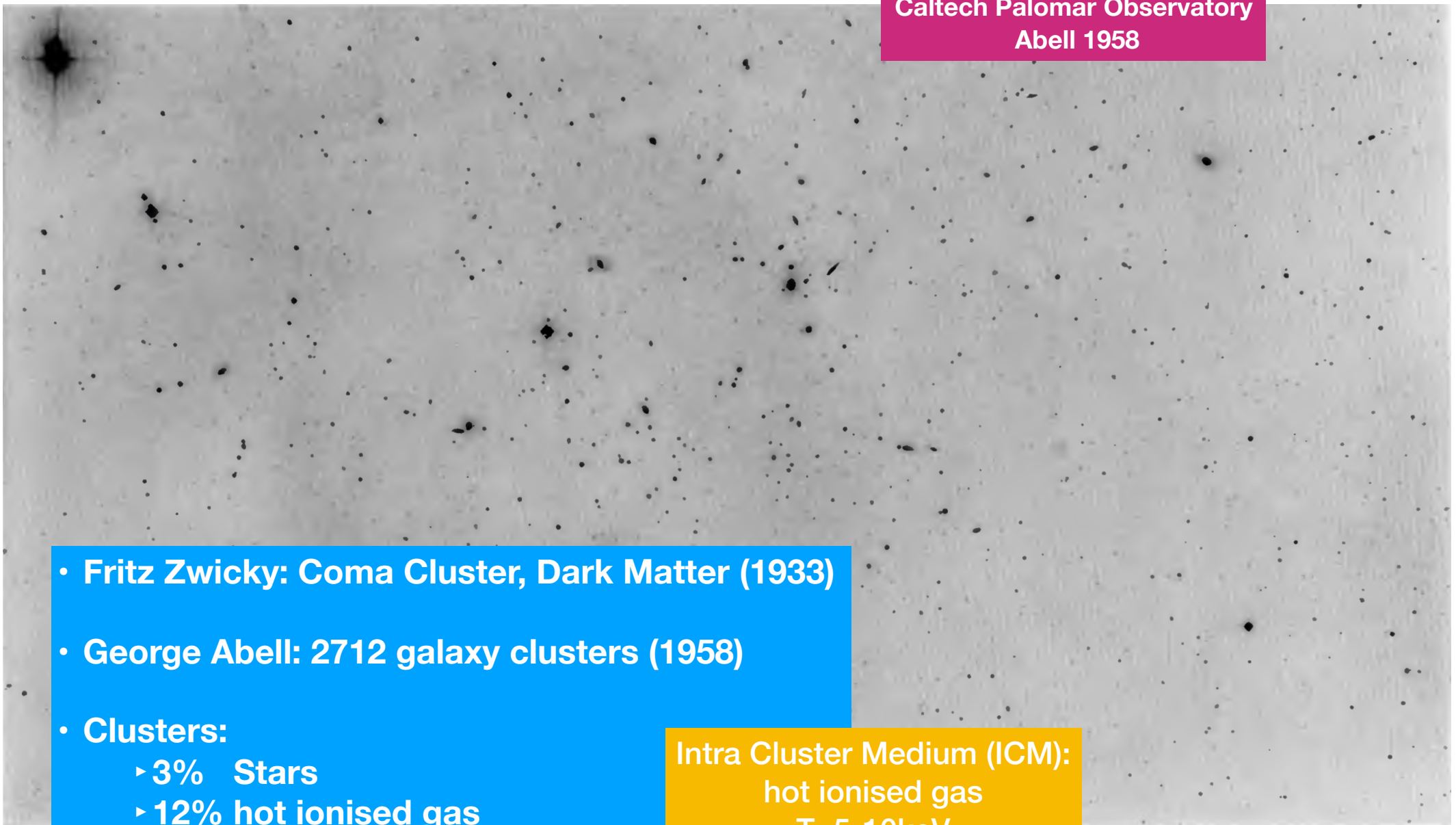
Galaxy distribution at $z=0$
Millenium simulation - Springel et al 2005

- $10^2 - 10^3$ galaxies
- $10^{14} - 10^{15} M_{\text{sun}}$
- $\sim 1 \text{Mpc}$

2 Mpc/h

- Methods to observe clusters:
 - Optical

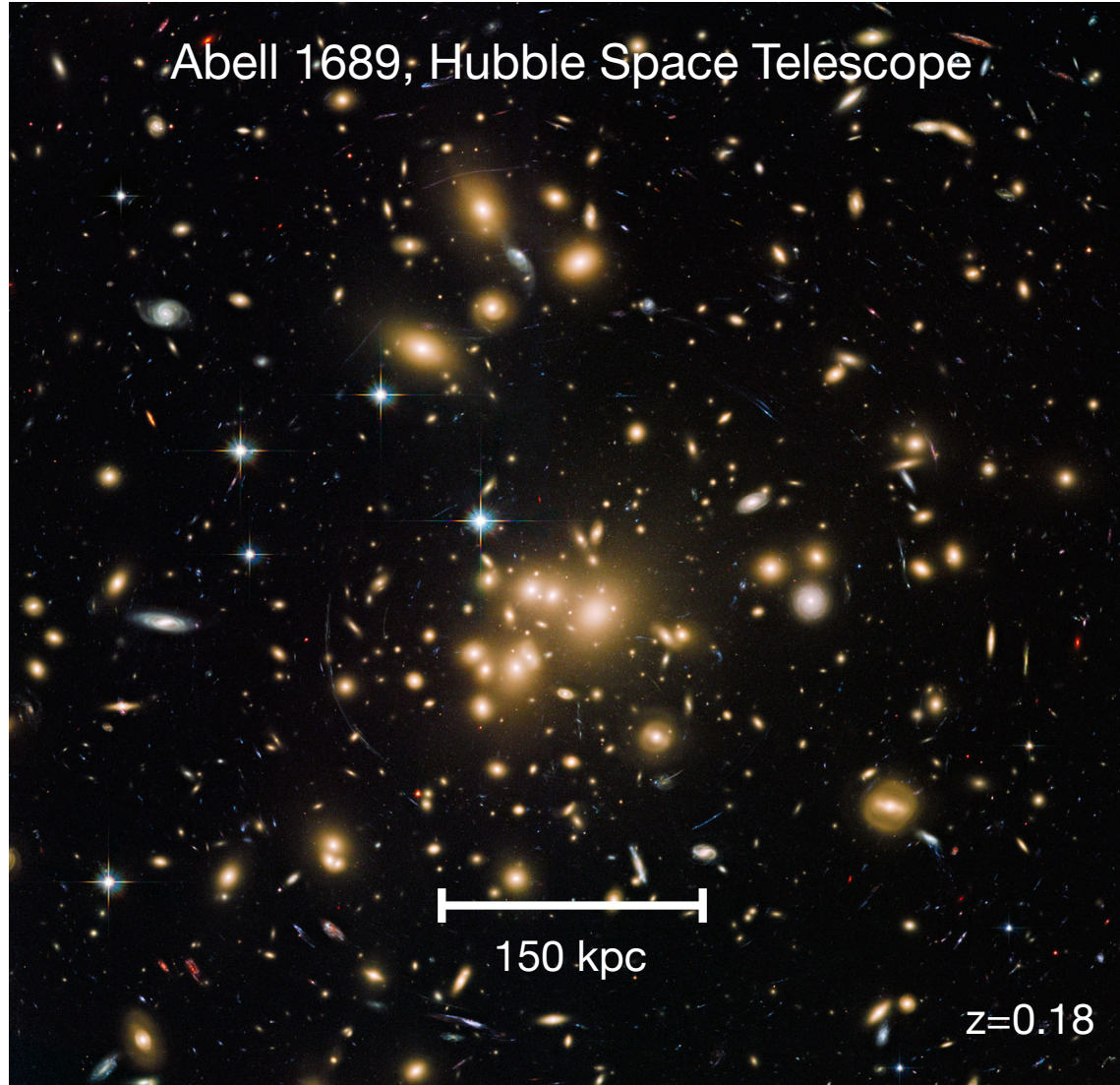
Leo Cluster (Abell 1367)
Caltech Palomar Observatory
Abell 1958



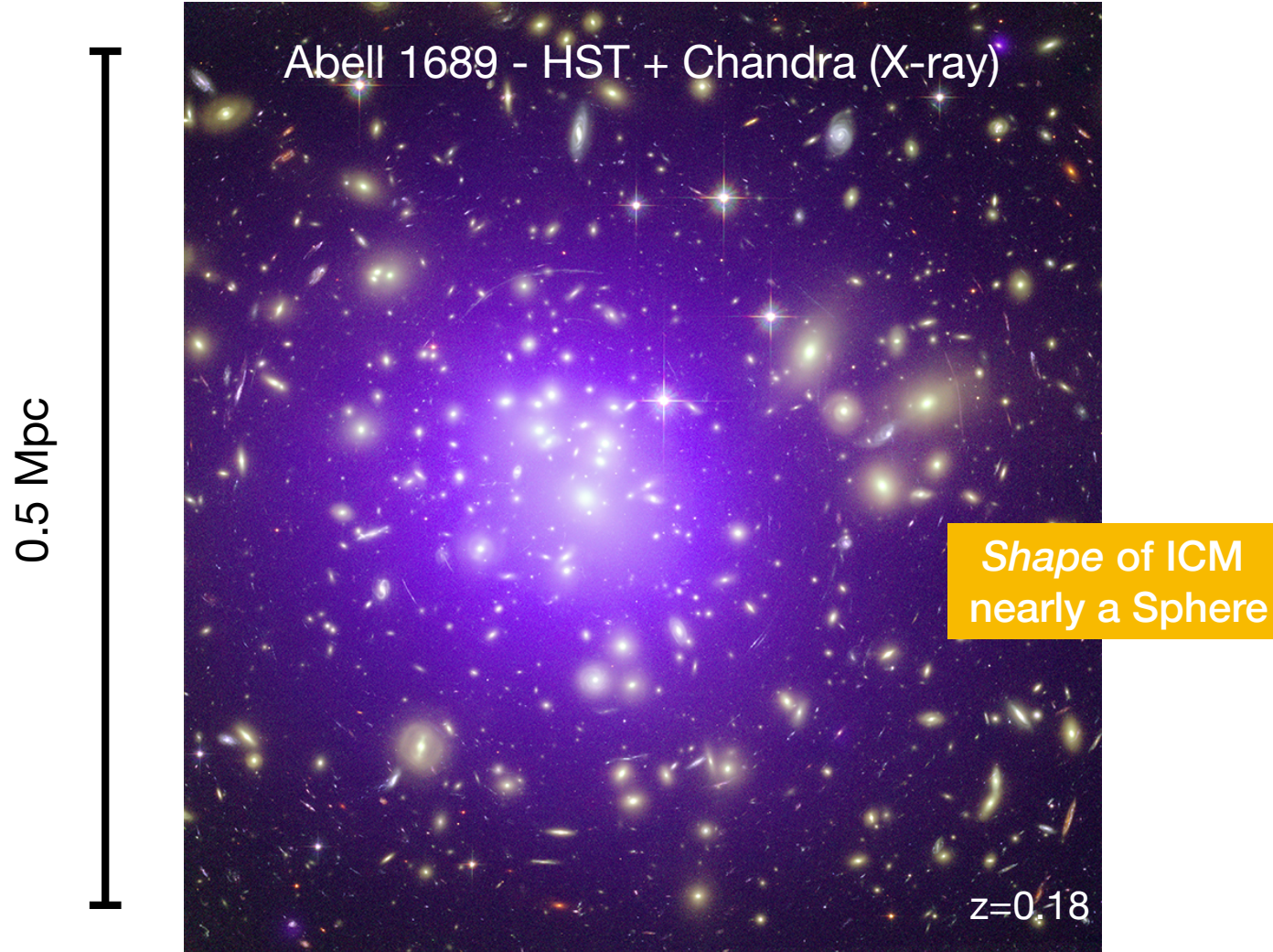
- Fritz Zwicky: Coma Cluster, Dark Matter (1933)
- George Abell: 2712 galaxy clusters (1958)
- Clusters:
 - 3% Stars
 - 12% hot ionised gas
 - 85% Dark Matter

Intra Cluster Medium (ICM):
hot ionised gas
 $T \sim 5\text{-}10\text{keV}$

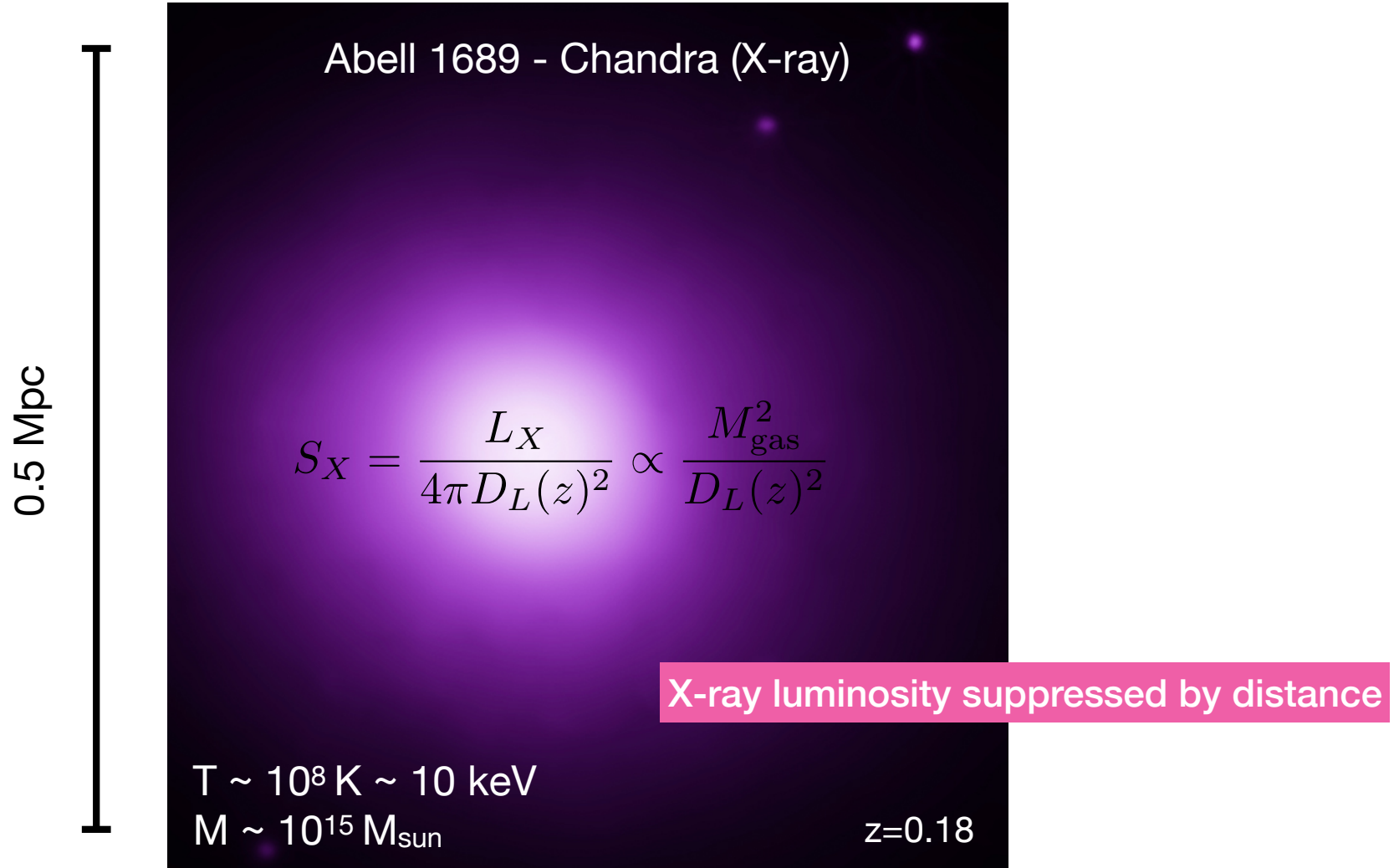
- Methods to observe clusters:
 - Optical



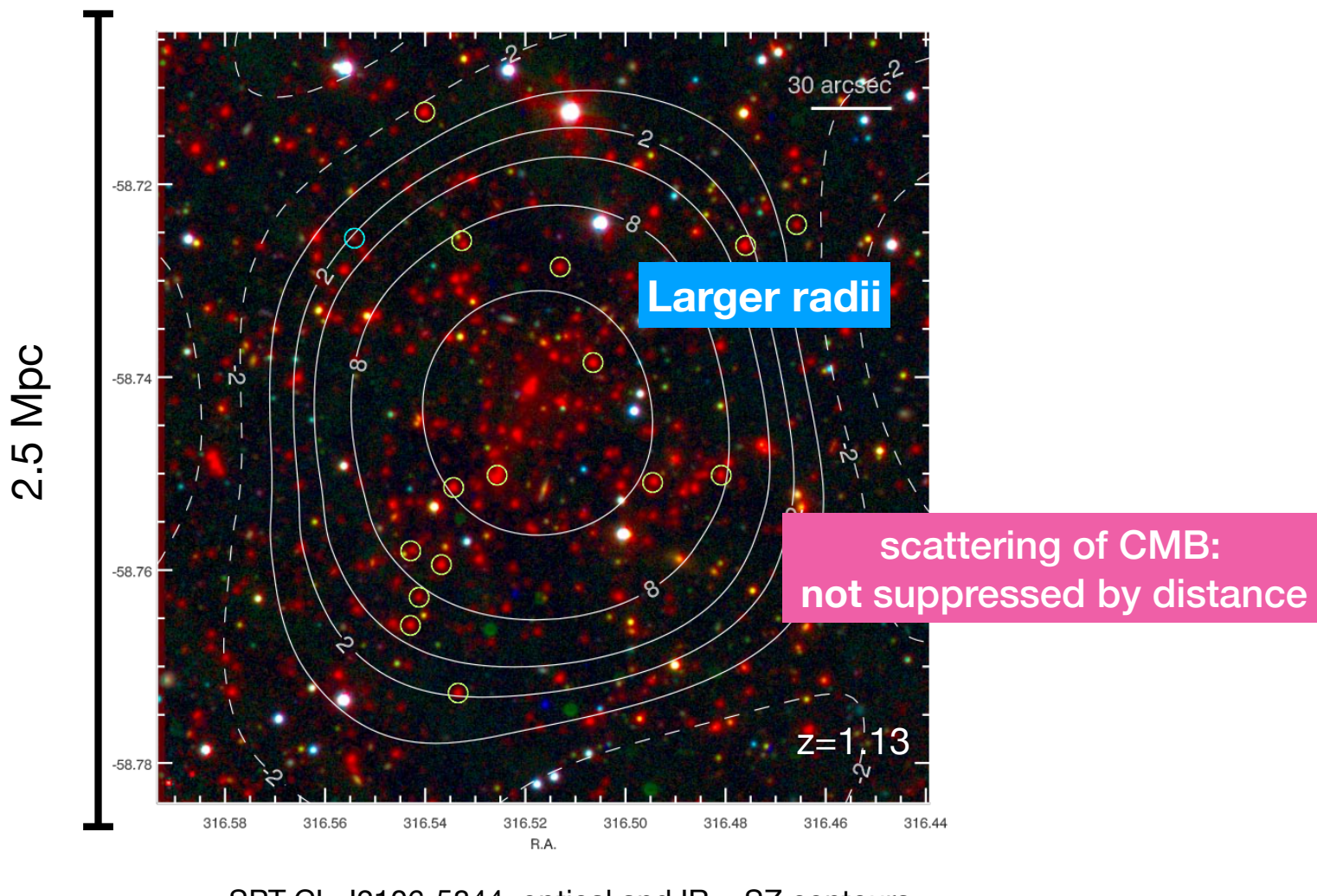
- Methods to observe clusters:
 - Optical
 - X-ray



- Methods to observe clusters:
 - Optical
 - X-ray

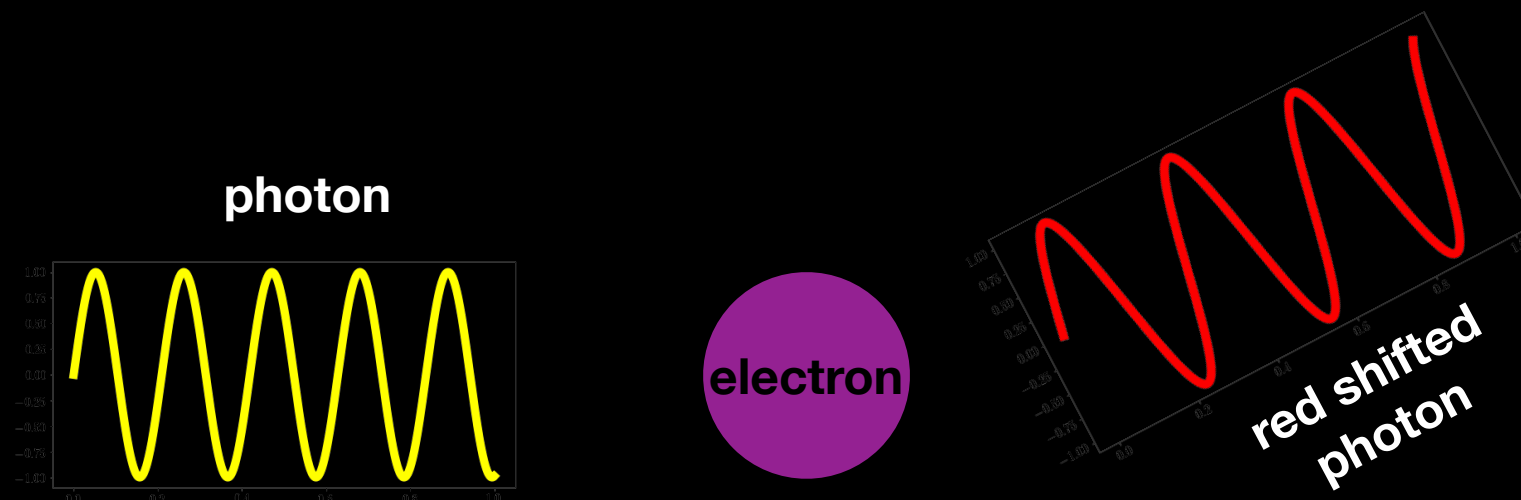


- Methods to observe clusters:
 - Optical
 - X-ray
 - Sunyaev-Zeldovich effect



Compton Scattering

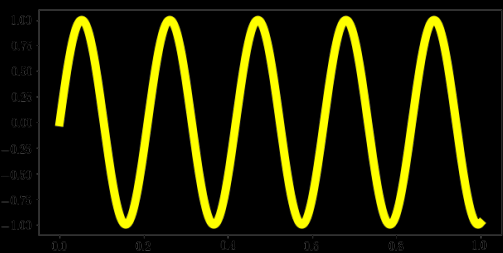
Photon give energy to electron



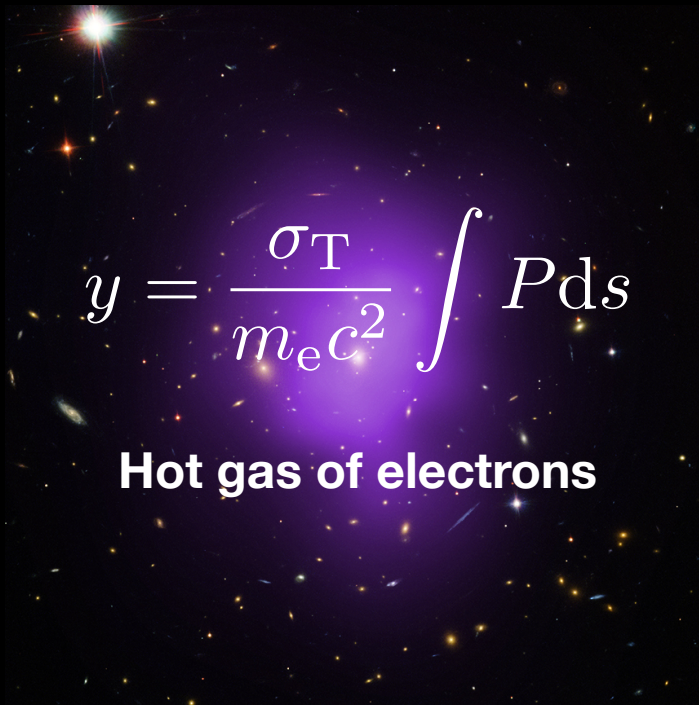
Inverse Compton Scattering

Electron give energy to photon

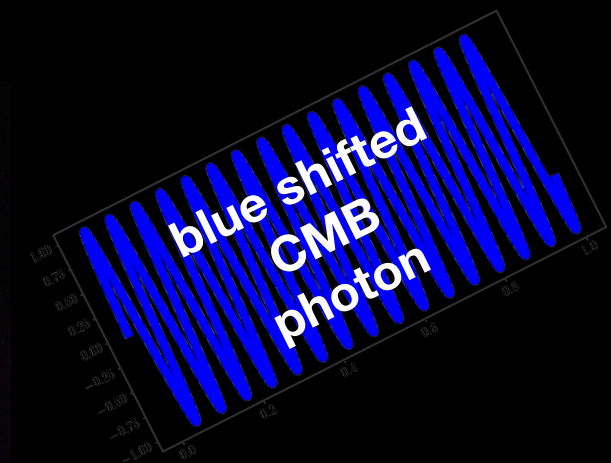
CMB
photon



Galaxy Cluster



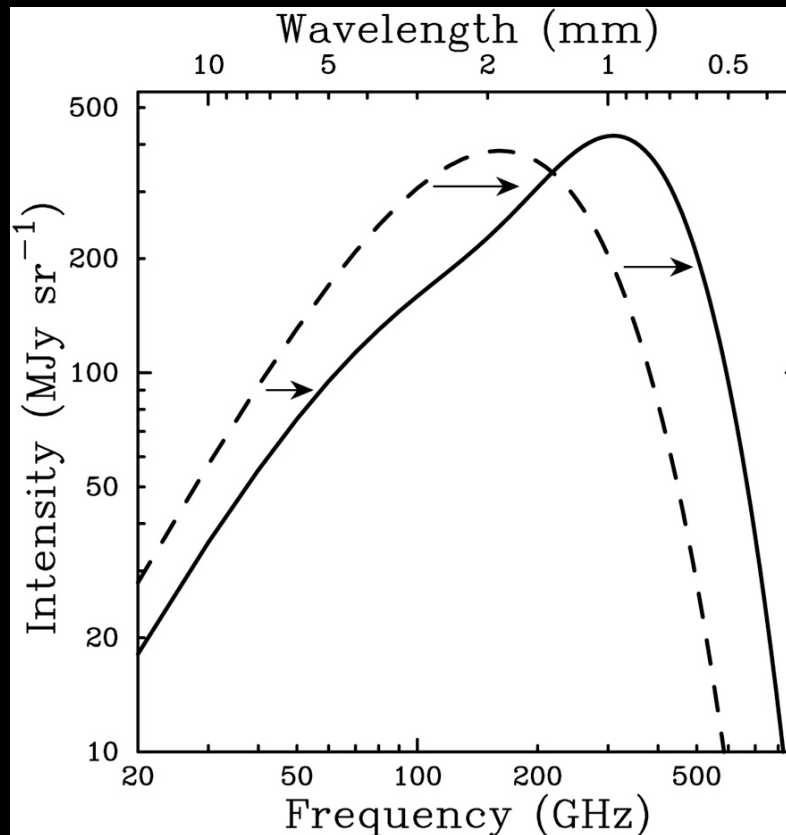
Hot gas of electrons



THERMAL SUNYAEV ZELDOVICH EFFECT



Rashid Sunyaev
(b. 1943)



Sunyaev & Zeldovich 1972



Yakov Zeldovich
(1914-1987)

- CMB Spectral distortion
- Frequency dependent
- “redshift independent”

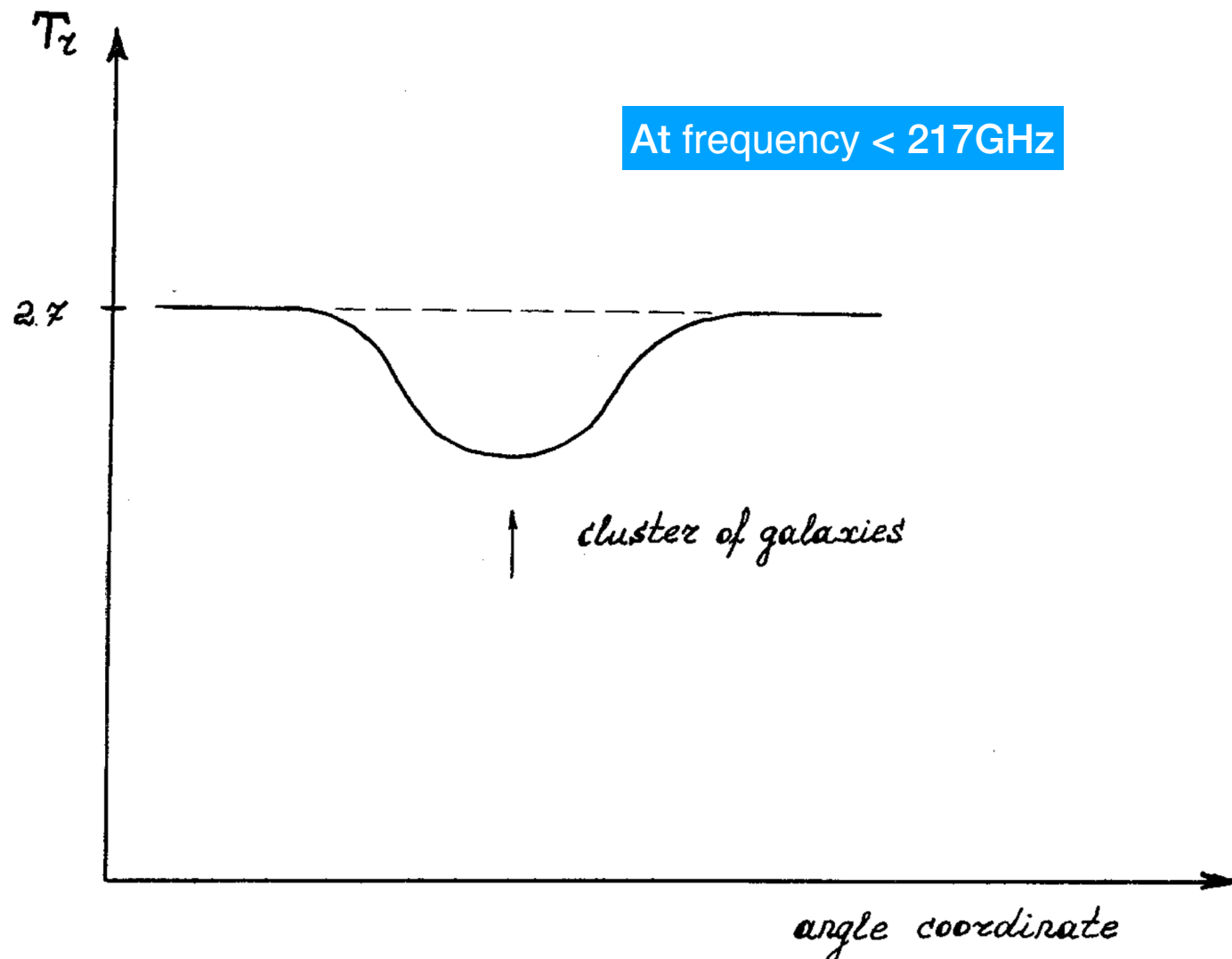
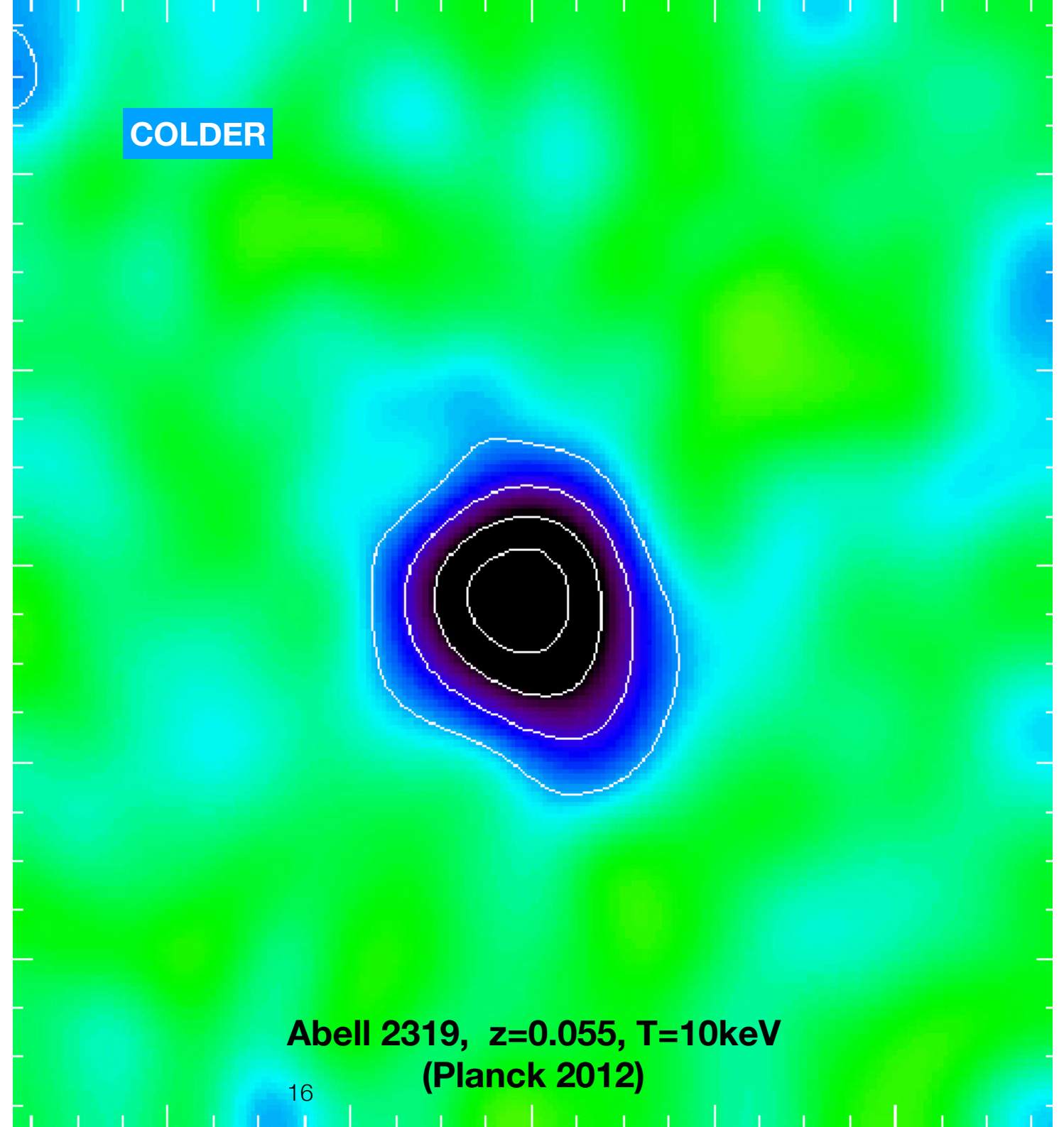
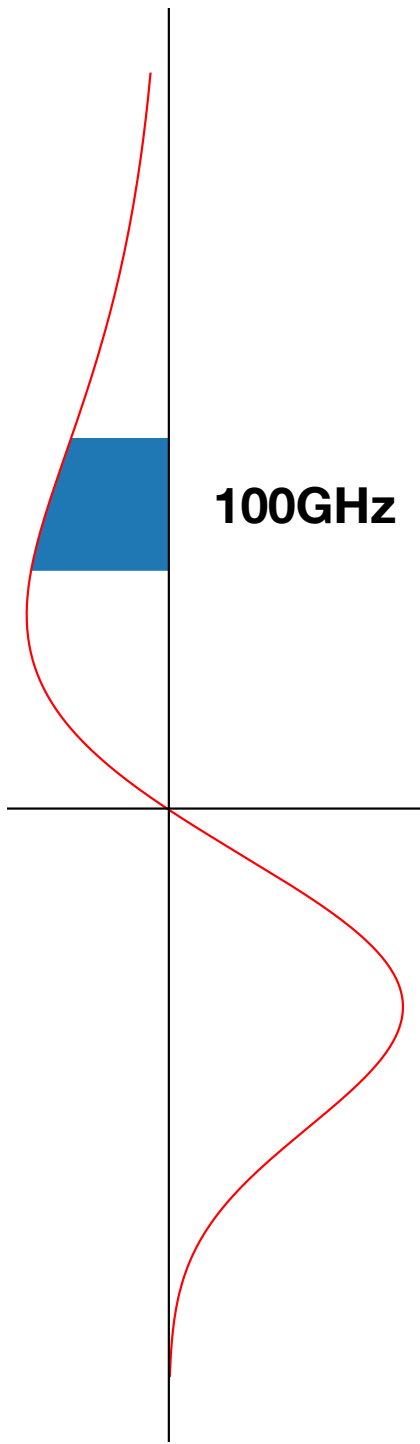
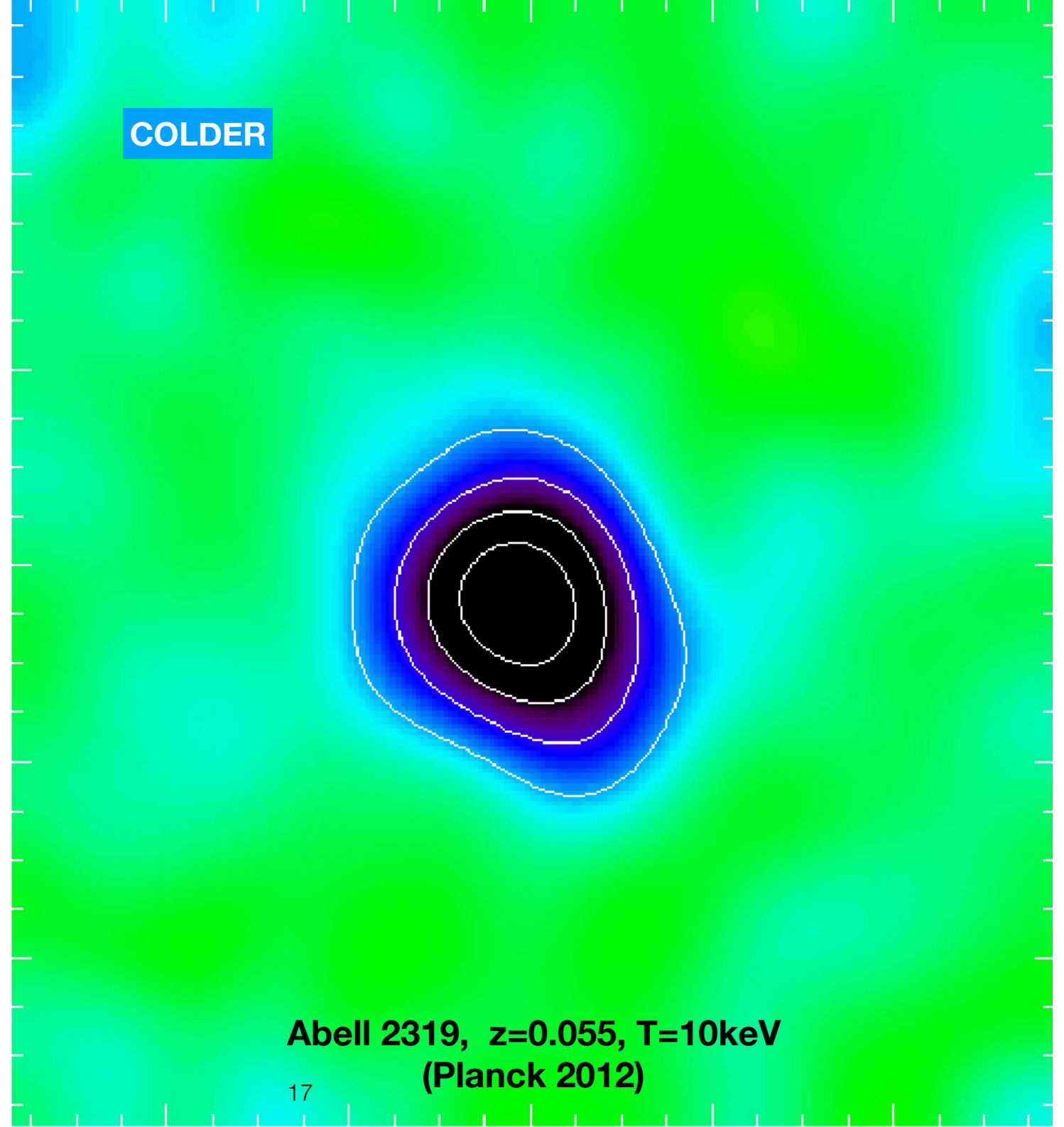
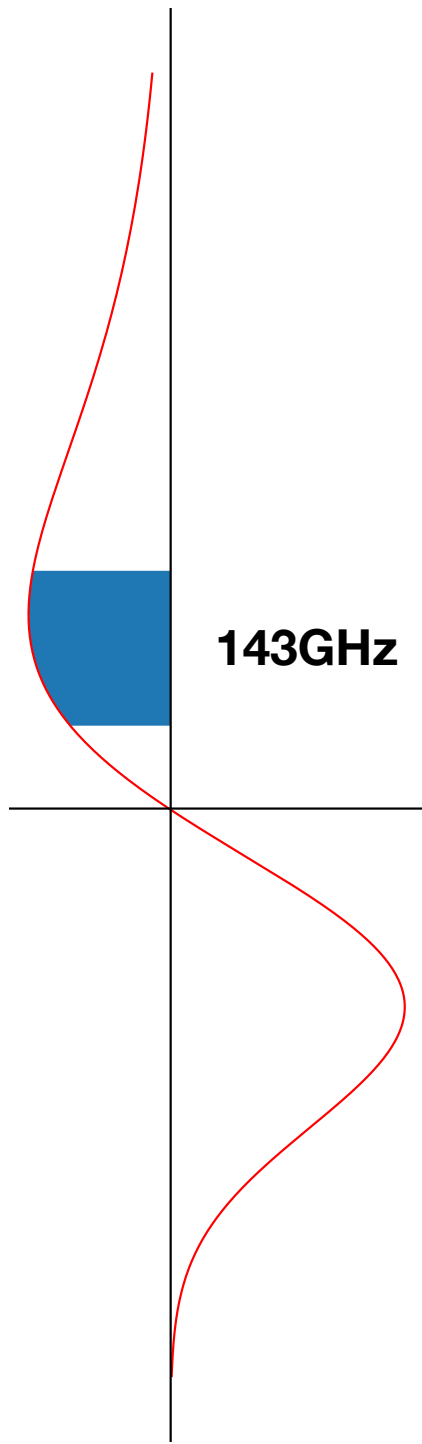
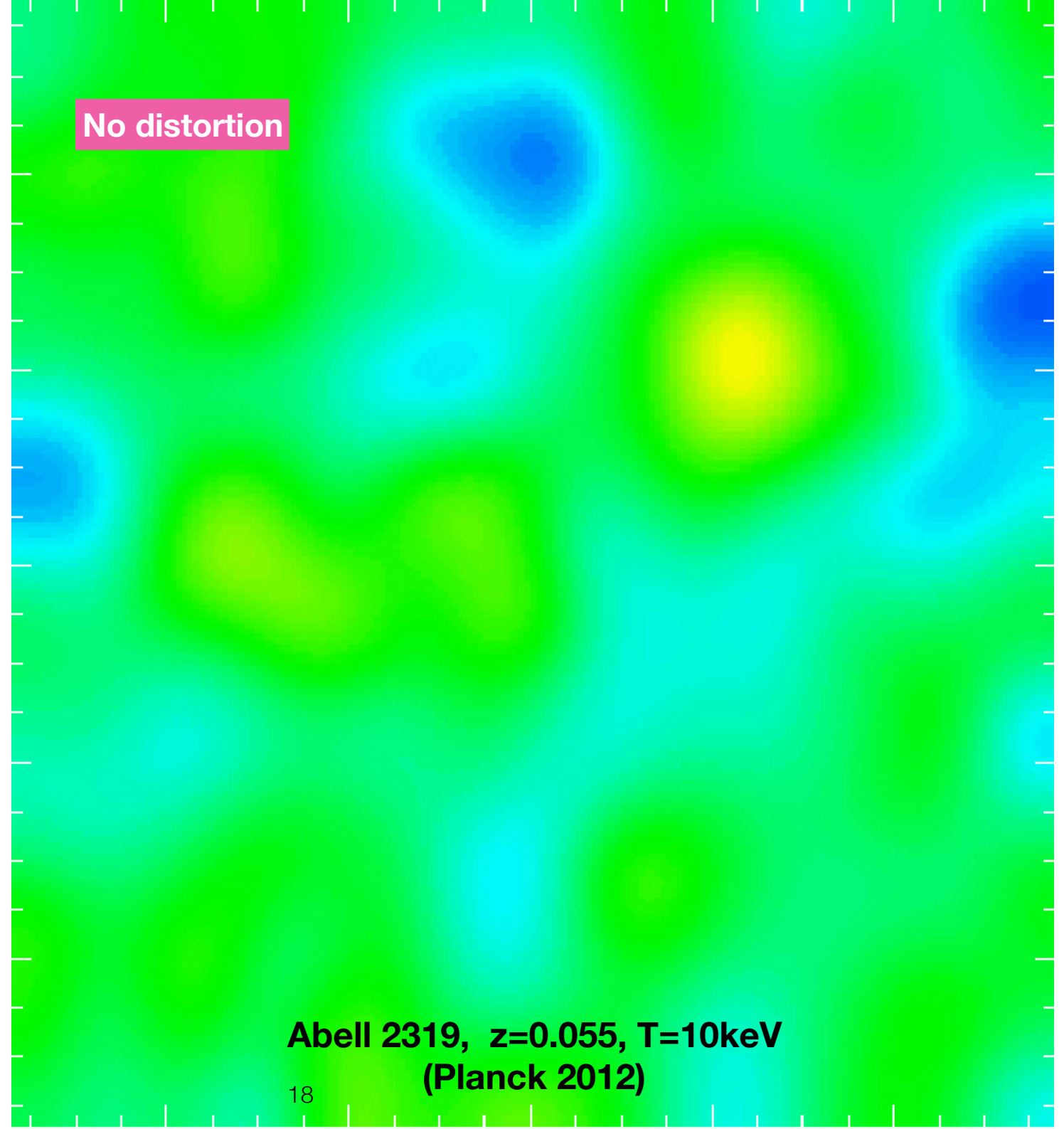
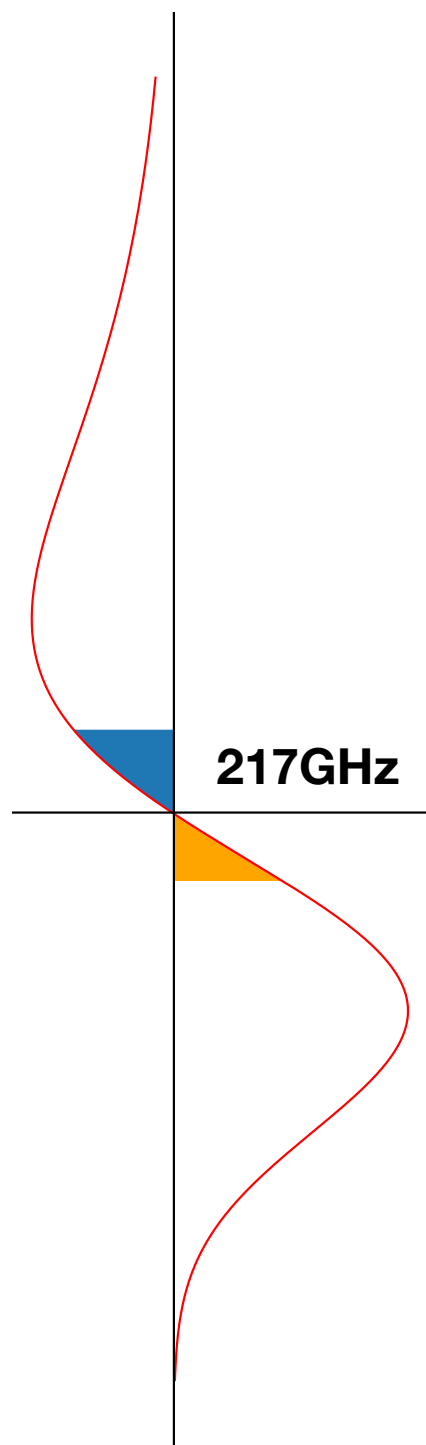
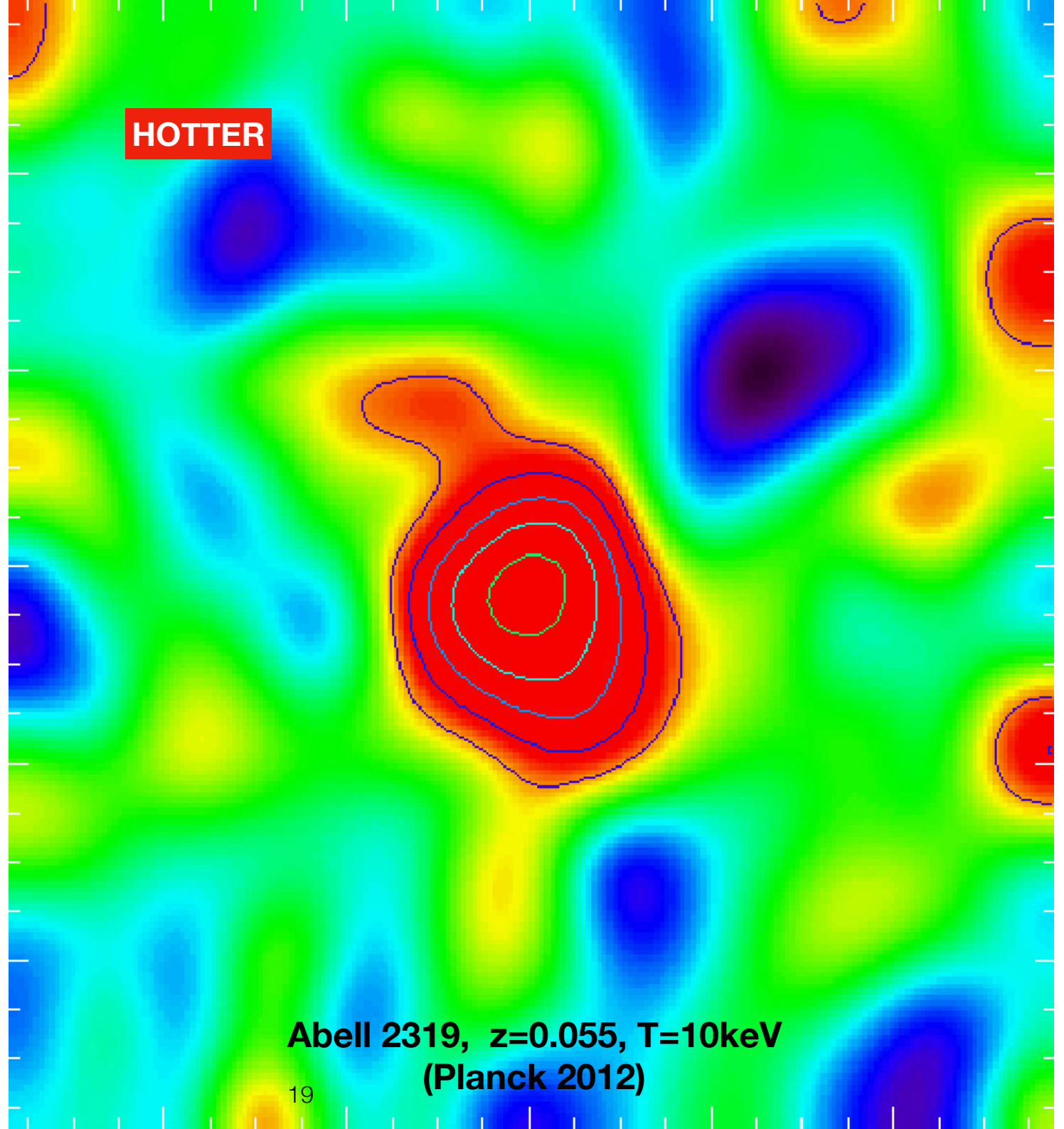
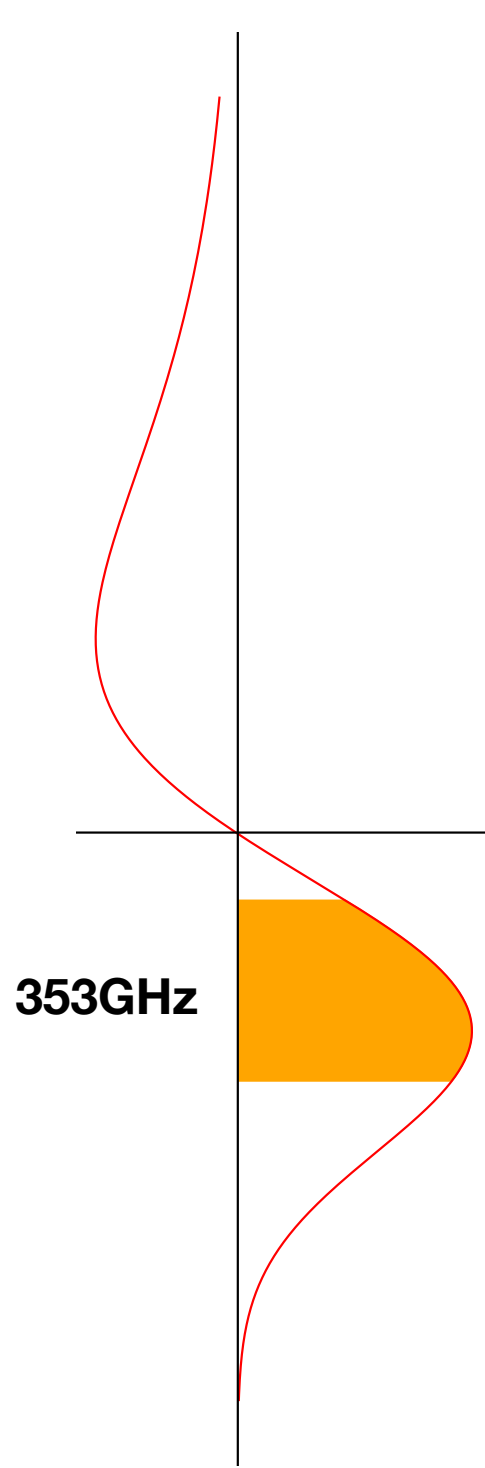


Figure: Sunyaev and Zeldovich 1972







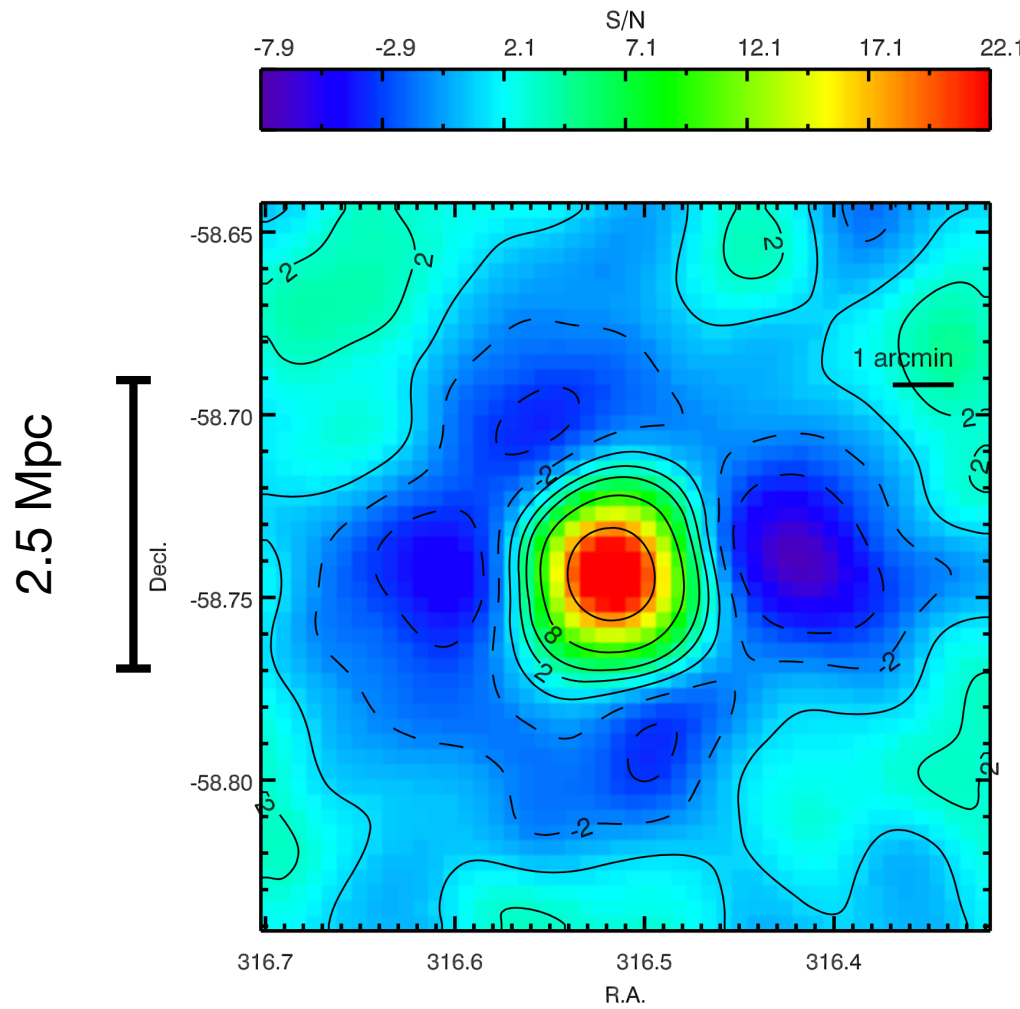


- Methods to observe clusters:
 - Optical
 - X-ray
 - Sunyaev-Zeldovich effect

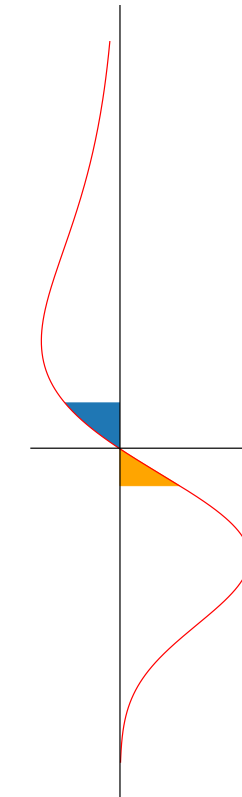
Compton y parameter

$$y = \frac{\sigma_T}{m_e c^2} \int P ds$$

$$\frac{\Delta T_{\text{CMB}}}{T_{\text{CMB}}} = g(\nu)y$$



SPT-CL J2106-5844, SZ contours



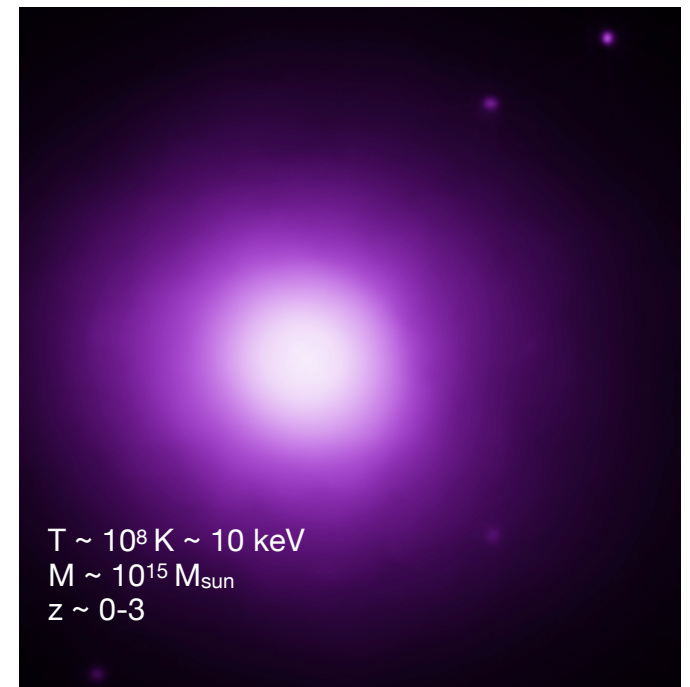
Clusters: summary

- Observations
- Largest matter-made gravitationally bound objects

- “self-similarity”

→ cosmological probe

(see, e.g., Weinberg et al [1201.2434])

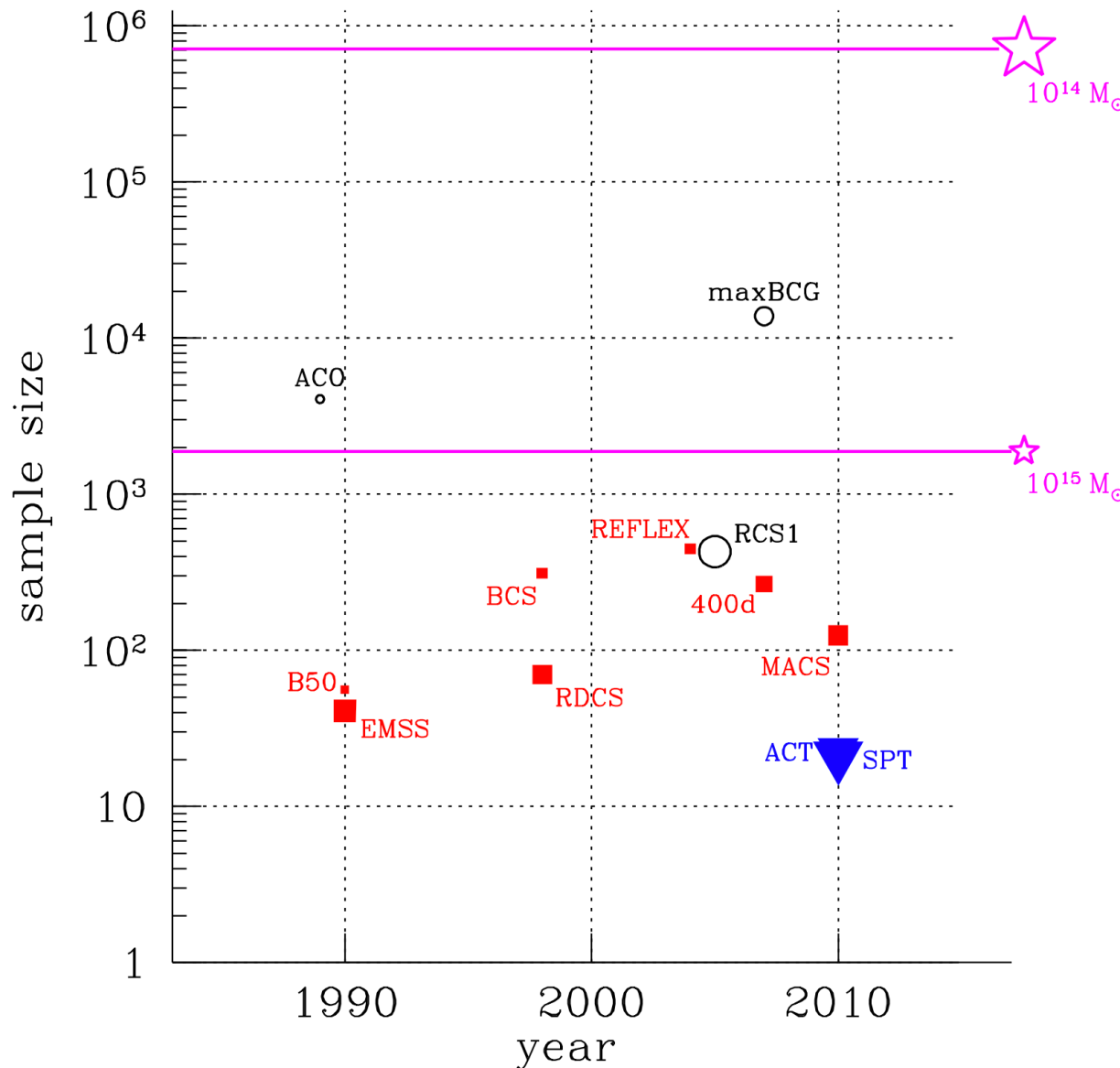


$T \sim 10^8$ K ~ 10 keV

$M \sim 10^{15}$ M_{\odot}

$z \sim 0-3$

- How many clusters in the observable universe?

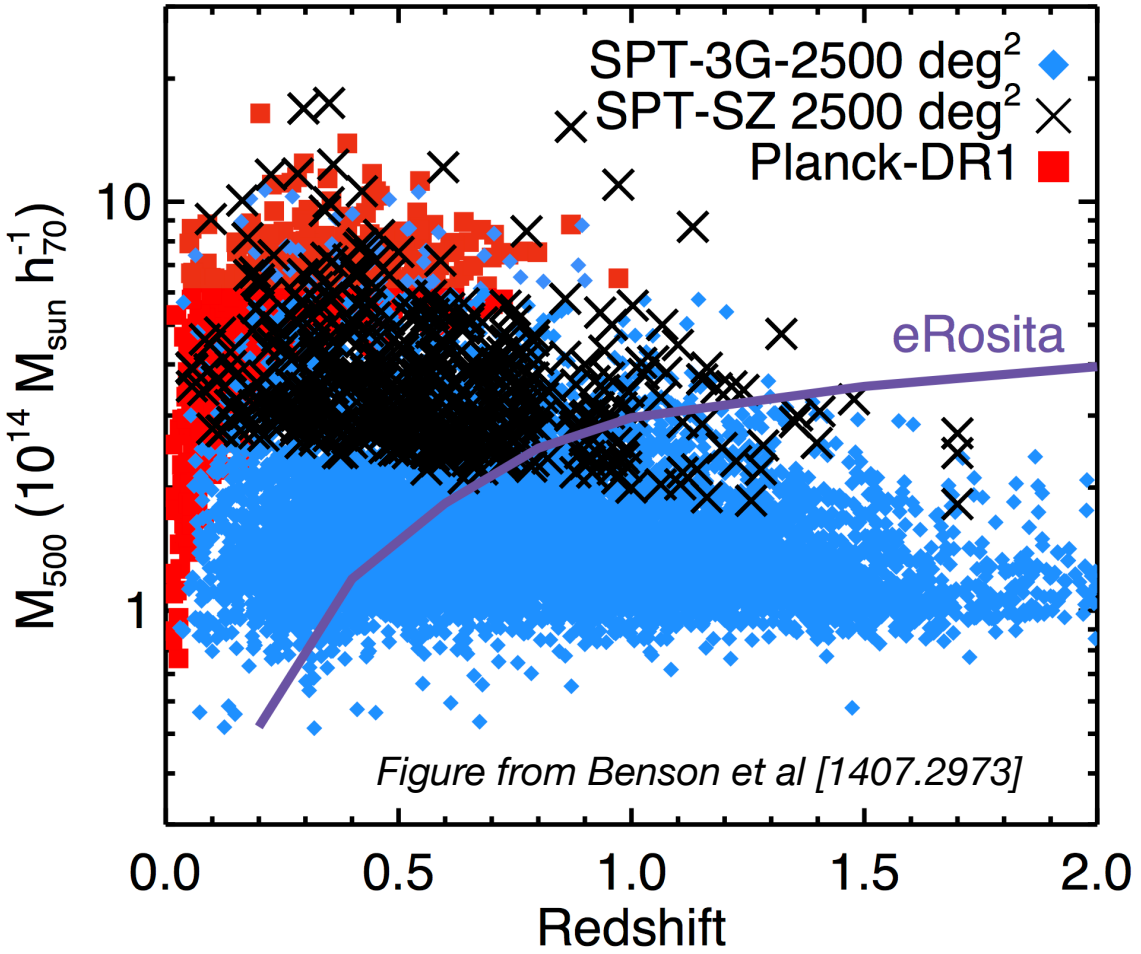


- Benchmark ideas:

- * Neyman, Scott, Layzer, + (1952-58)
- * Gott, Rees, Peebles, Press, Schechter, + (1974-75)
- * Zeldovich, Sunyaev, + (1972-80)
- * White, Navarro, Frenk, + (1993-96)

Future surveys:
~ALL the clusters

Figure from Allen et al [1103.4829v2]



- X-ray flux

$$S_X = \frac{L_X}{4\pi D_L(z)^2} \propto \frac{M_{\text{gas}}^2}{D_L(z)^2}$$

→ Suppressed by redshift

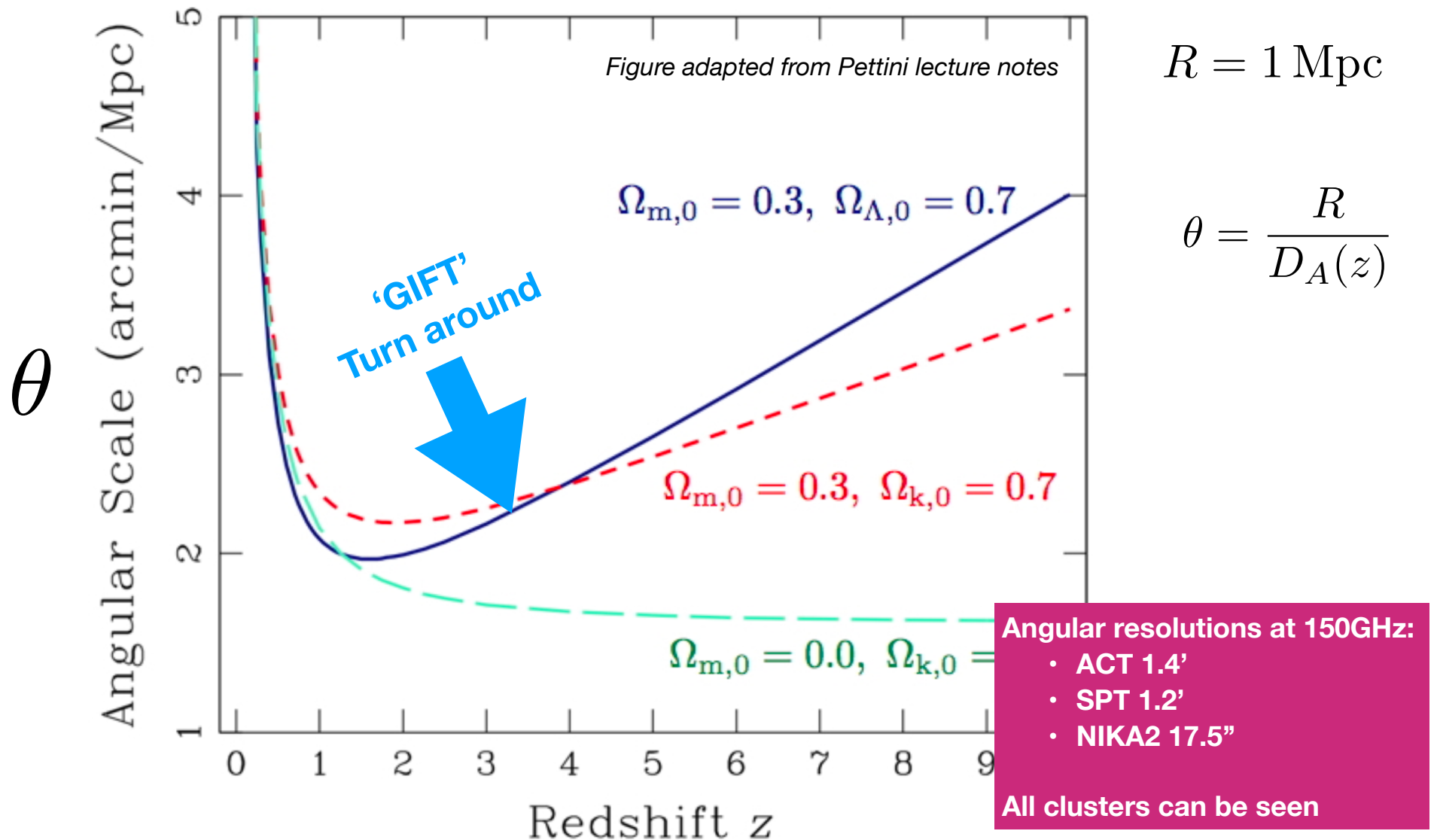
$$D_L(z) = (1 + z)^2 D_A(z)$$

- SZ flux depends on redshift only via angular size

$$S_{\text{SZ}} \propto \int y d\Omega \propto \frac{1}{D_A(z)^2} \int n_e T_e dV \propto \frac{M_{\text{gas}} \langle T_e \rangle}{D_A(z)^2}$$

Cluster of size $R=1$ Mpc: angular size at high redshift?

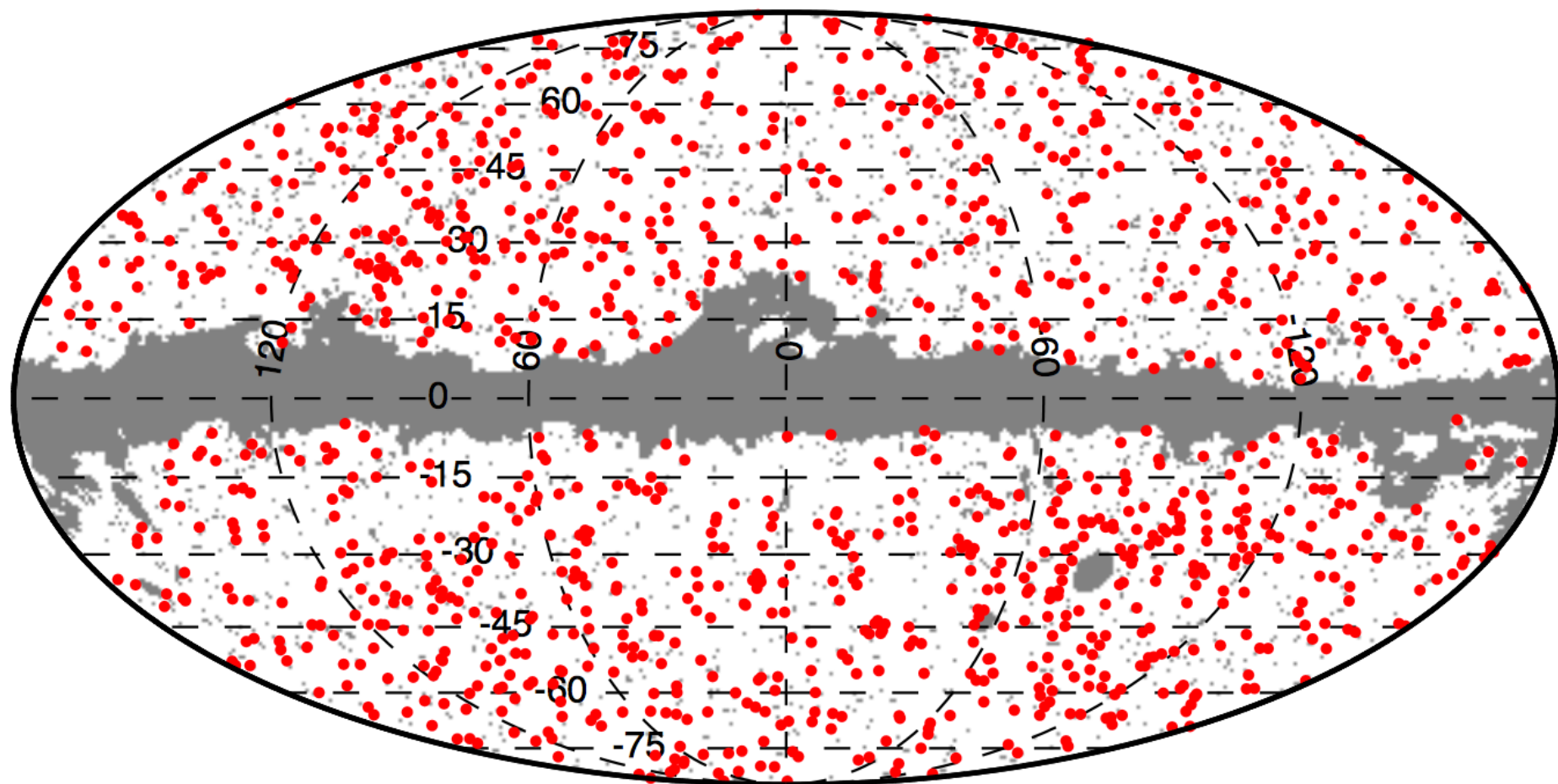
Objects of 1Mpc appears larger at z=3 than z=1



Galaxy Clusters detected by Planck

Planck SZ Cluster Catalogue

**Full mission data
1653 detections with S/N>4.5**



Planck SZ Cluster Catalogue

- Detection (same technique as ACT and SPT)
- Blind search (i.e., no prior info on location)
- **Matched Multi-filters** (Herranz et al 2002, Melin et al 2006)

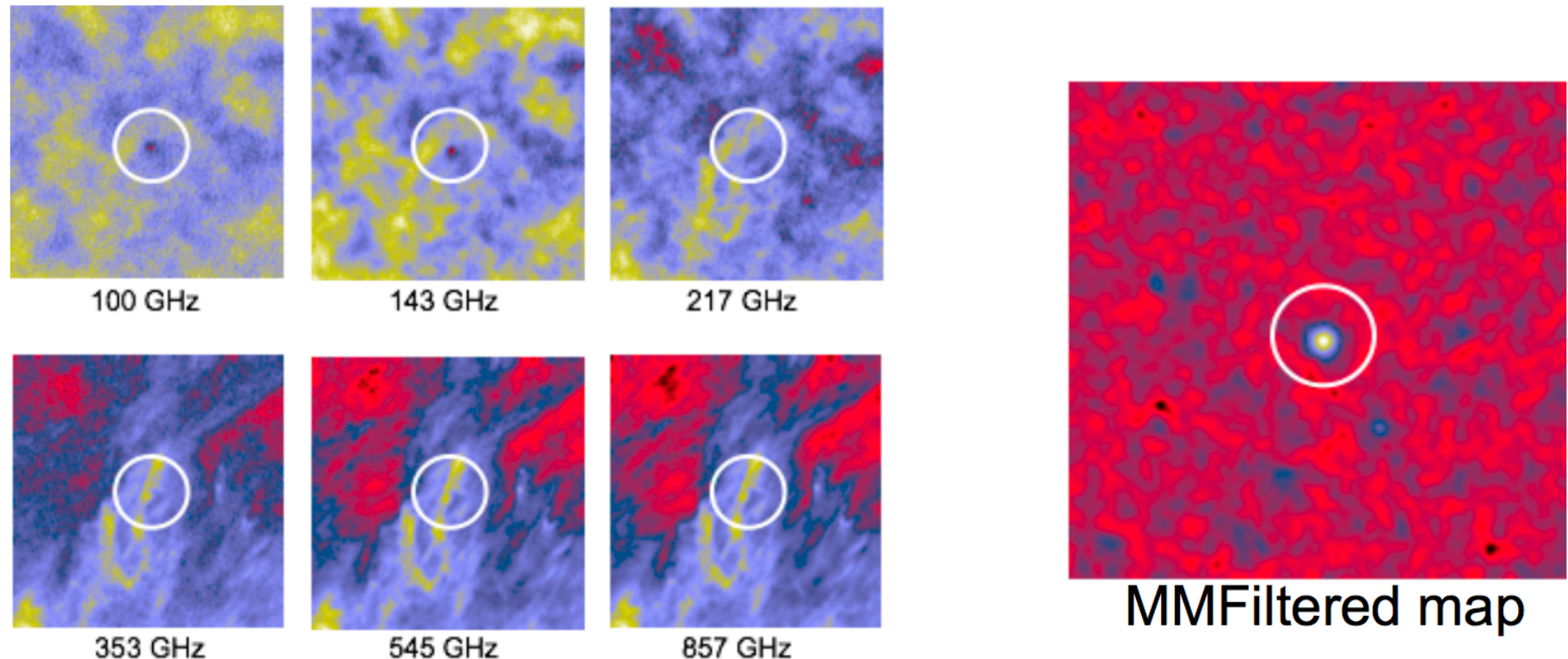


Image from Melin's talk

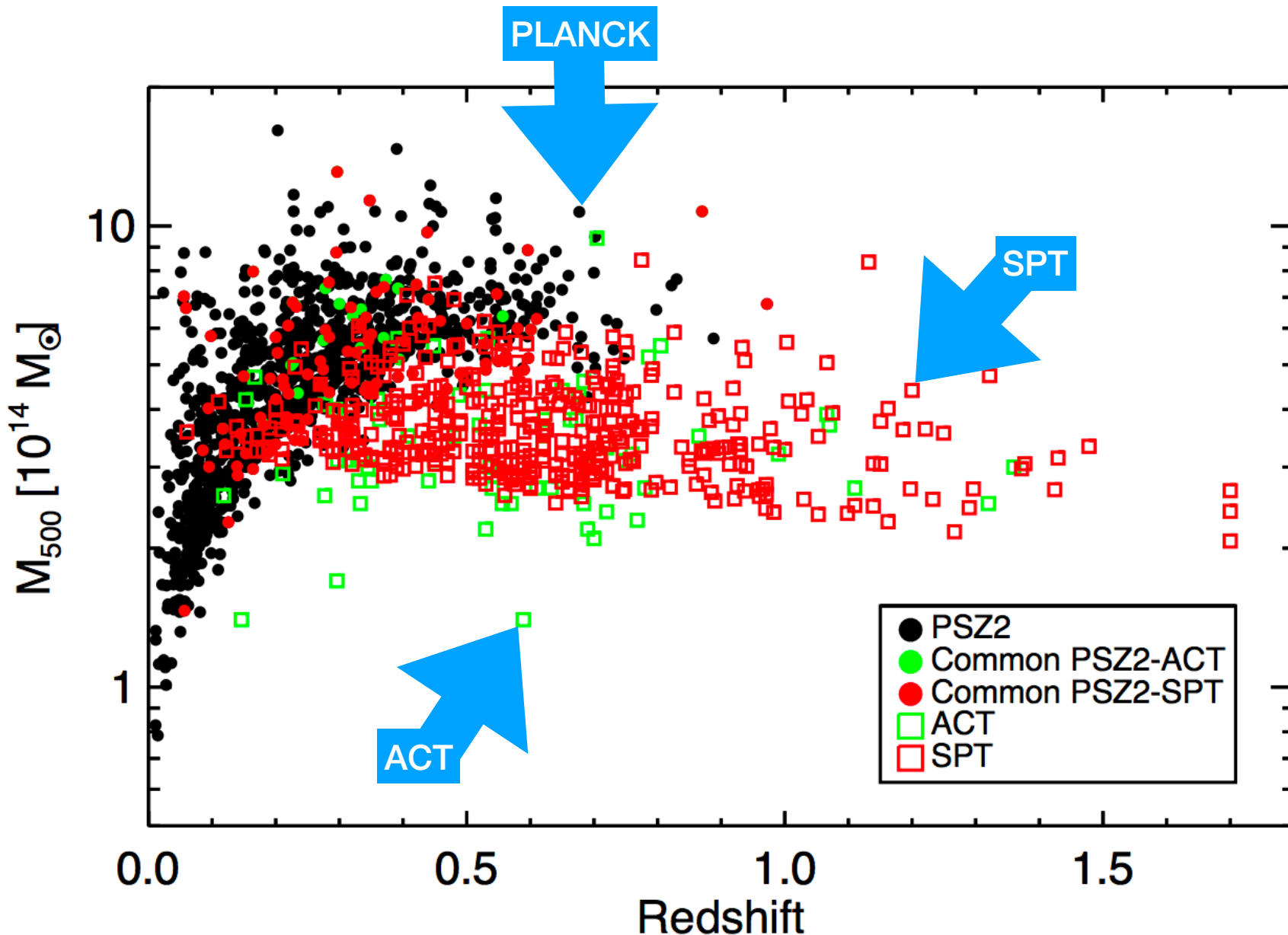


Figure from Planck XX

Cosmological sample: 439 clusters with S/N>6

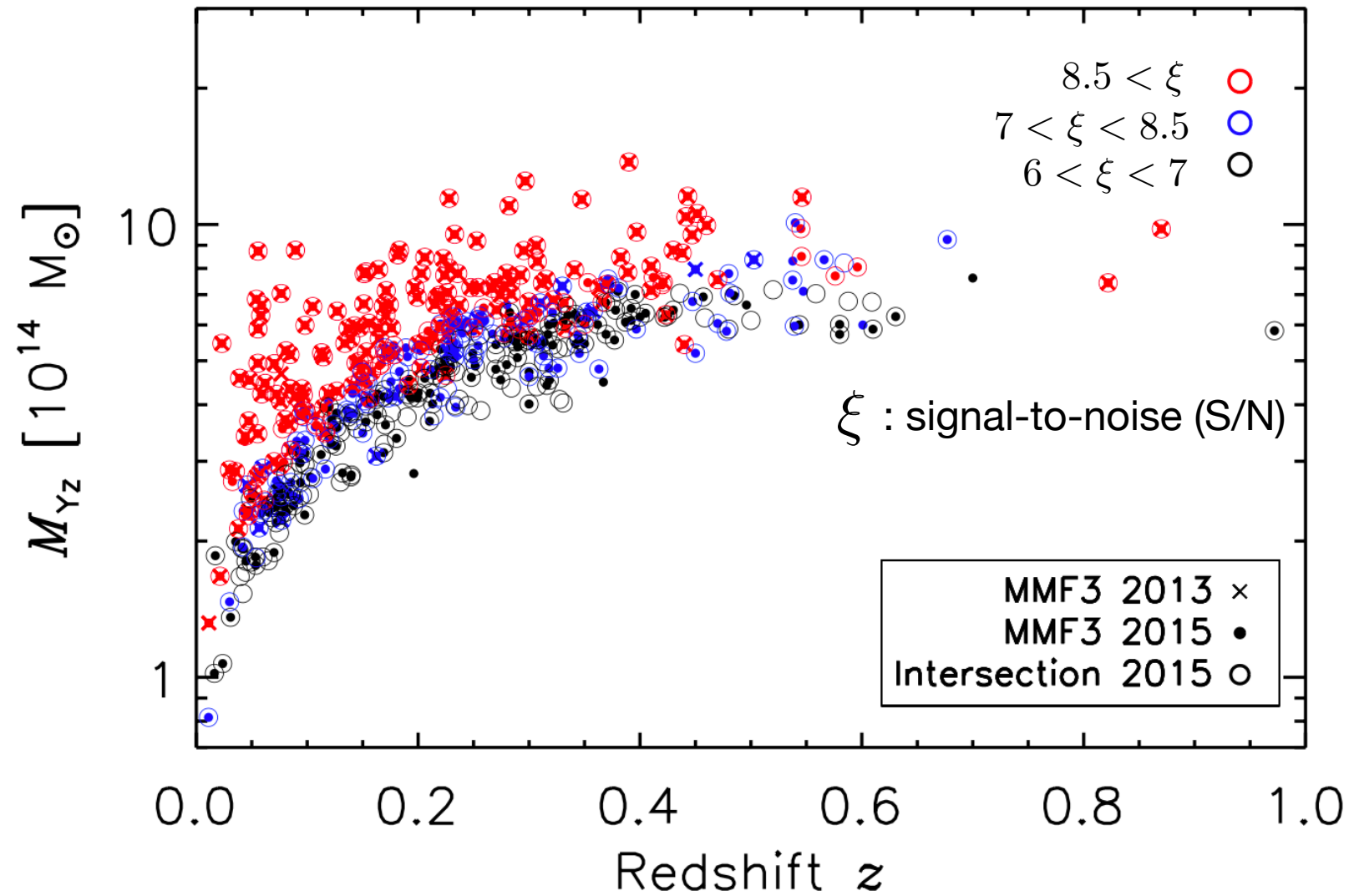


Figure from Planck XX

Planck SZ Cluster Catalogue

- **Redshifts:**

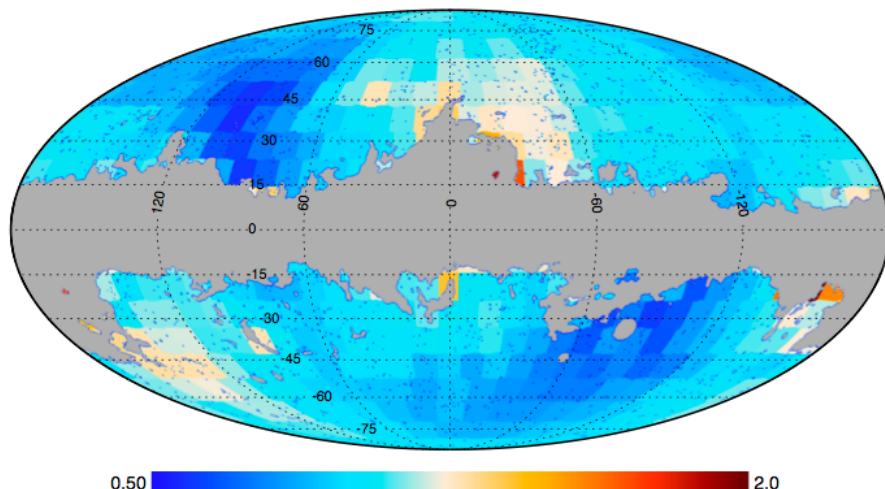
- identified counterpart (e.g., X-ray, optical)
- follow up observation (e.g., Telescope at Canary Island Observatory)

- **Masses:**

- identified counterpart (e.g., X-ray, optical)
- **scalings relations**

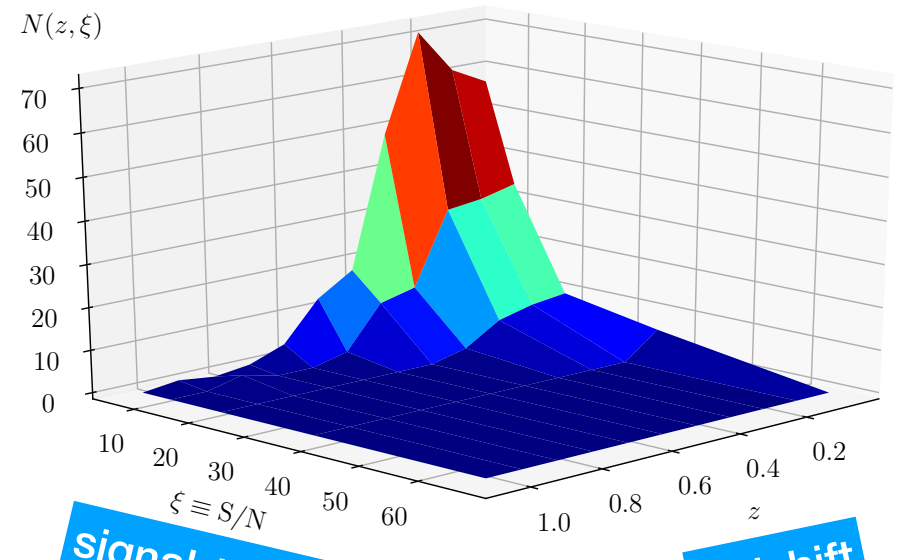
Crucial info of the cosmo sample:

- Signal-to-noise (MMF)
- Noise map
- redshifts (complementary or follow-up observations)



Noise map

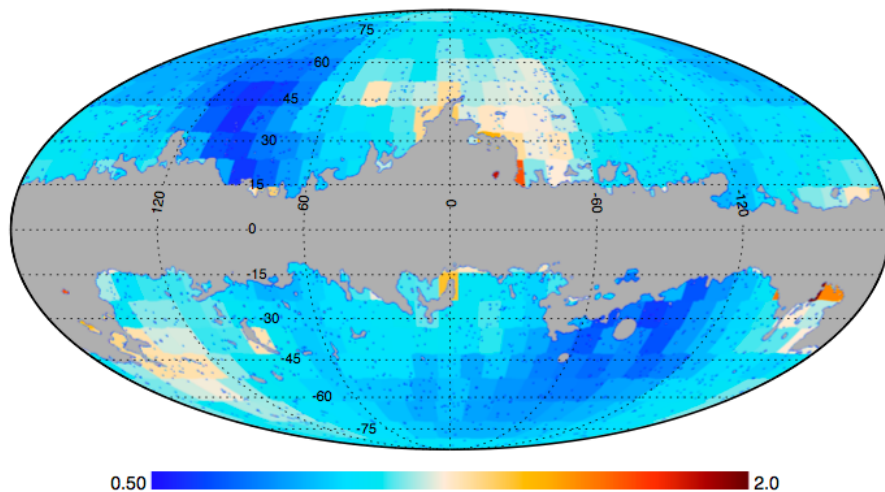
Figure from Planck XX paper



Observed cluster counts

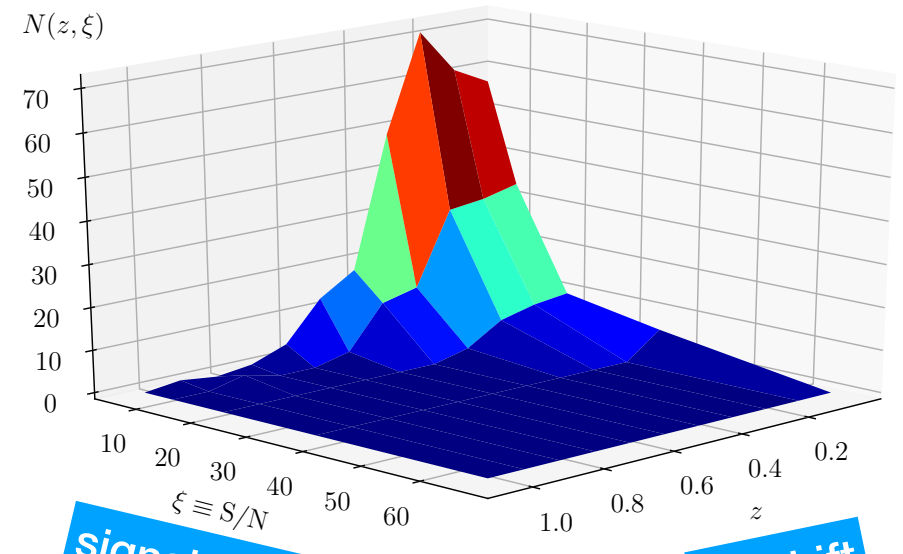
Crucial info of the cosmo sample:

- Signal-to-noise (MMF)
- Noise map
- redshifts (complementary or follow-up observations)
- completeness



Noise map

Figure from Planck XX



signal-to-noise

redshift

Observed cluster counts

Survey Completeness

Detection probability

$$\chi(\xi) = \frac{1}{2} \left[1 - \text{erf} \left(\frac{\xi - \xi_{\text{cut}}}{\sqrt{2}} \right) \right]$$

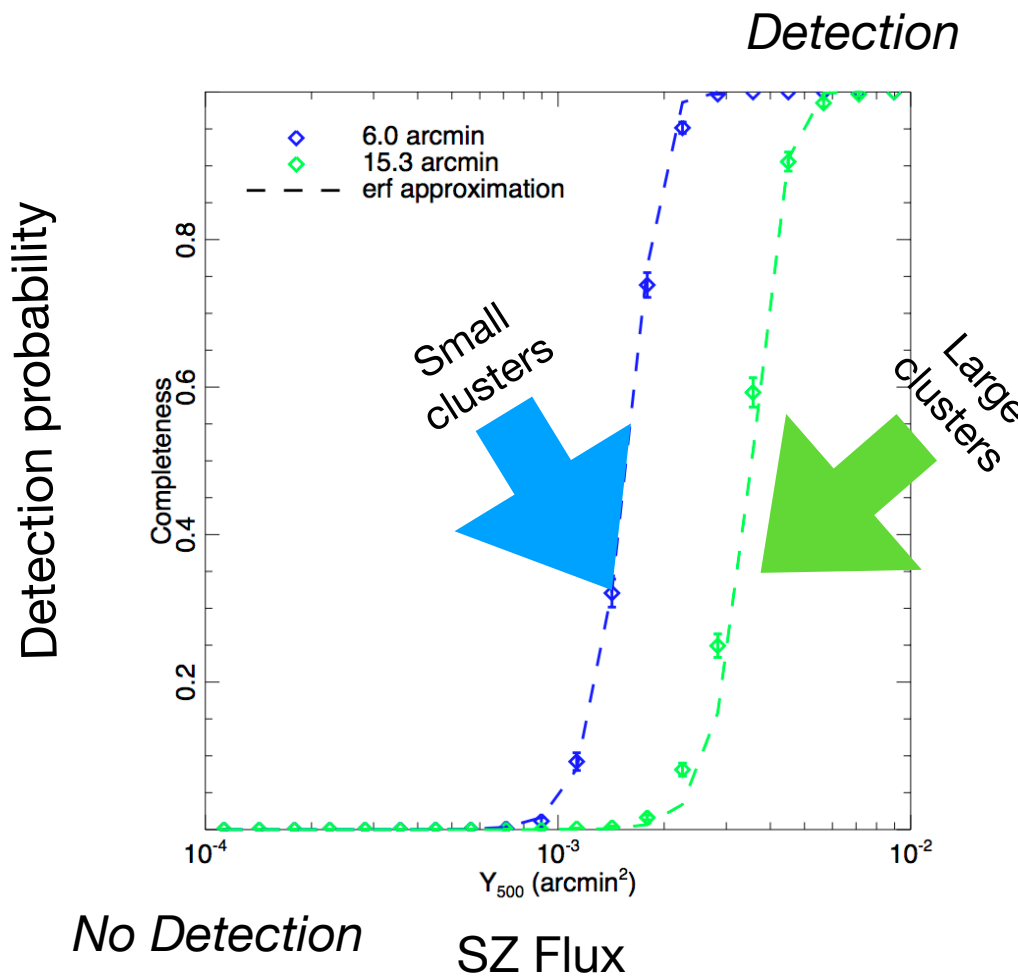
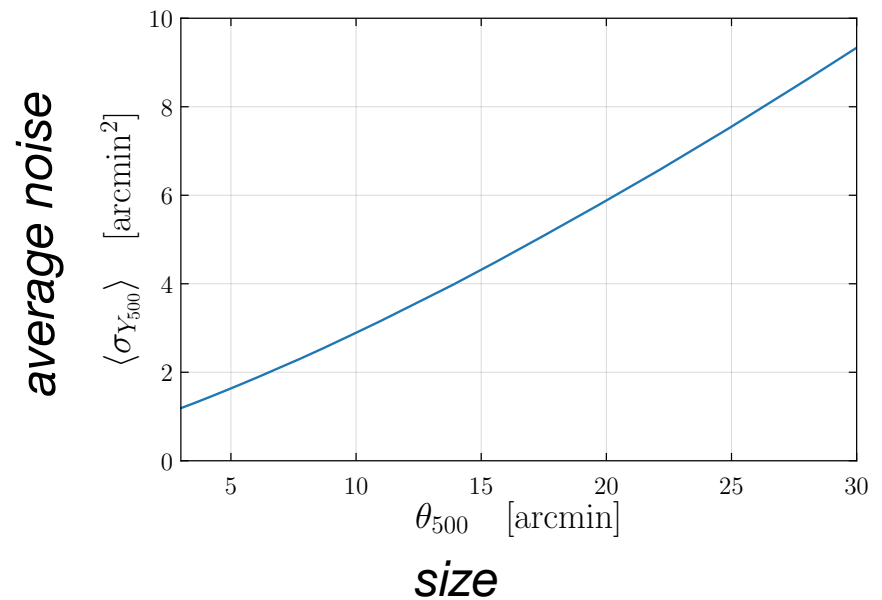
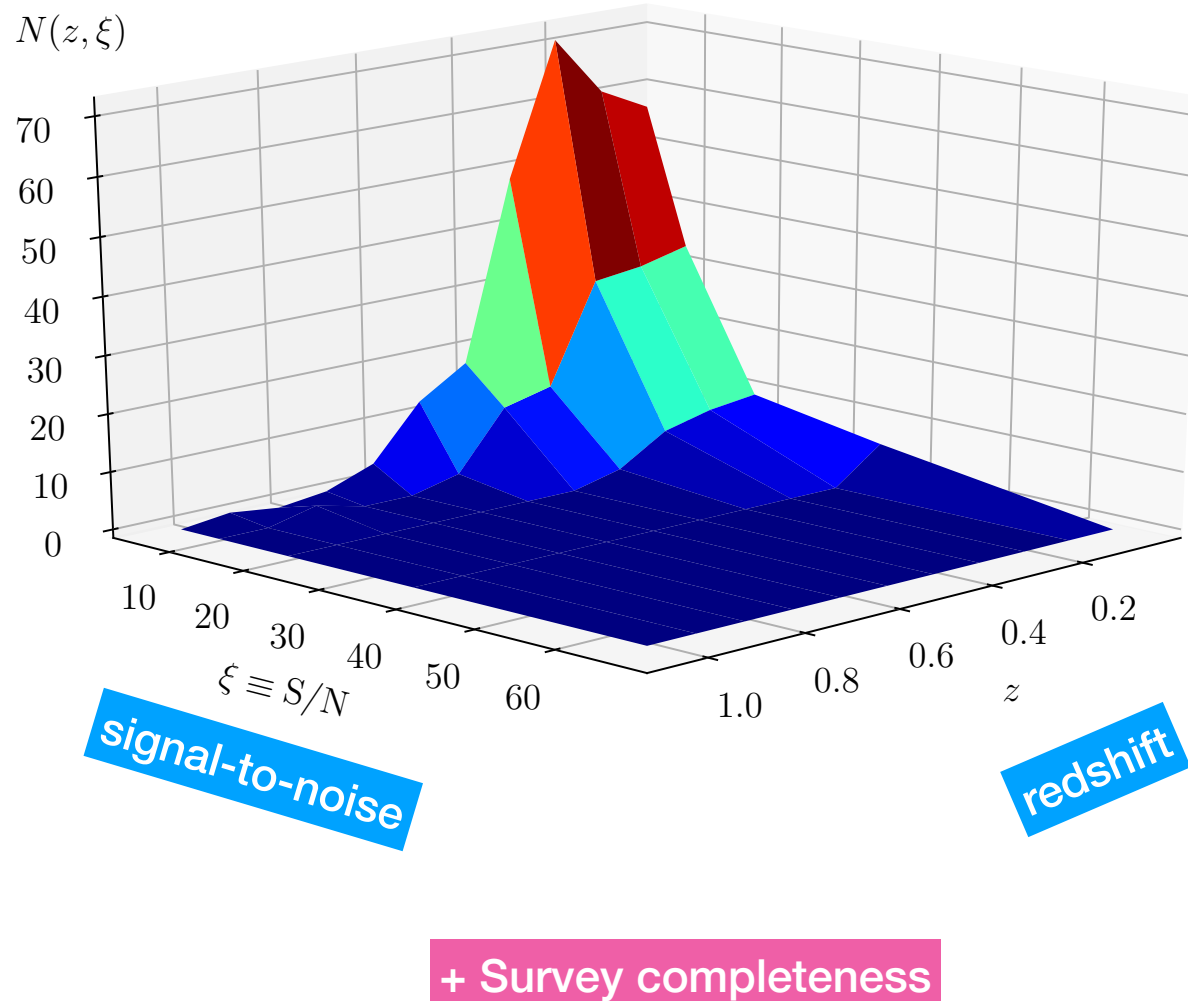


Figure from Planck XX



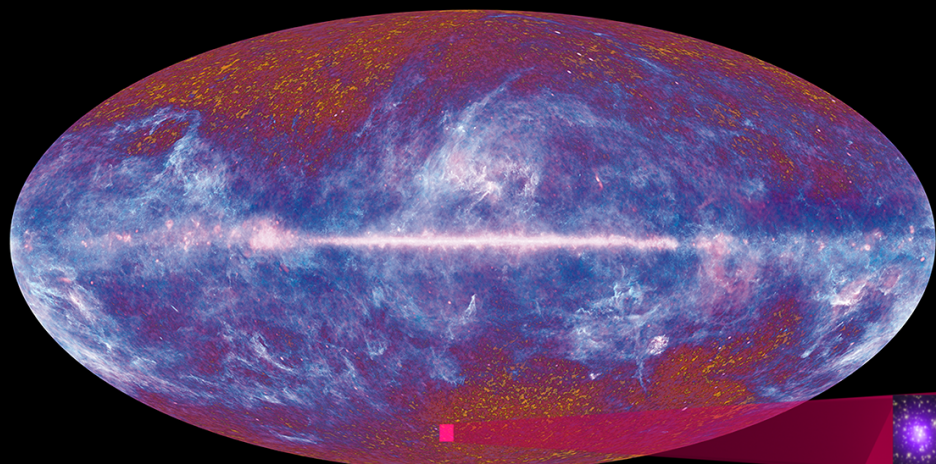
Noise proportional to size

Summary of Planck Cosmo sample

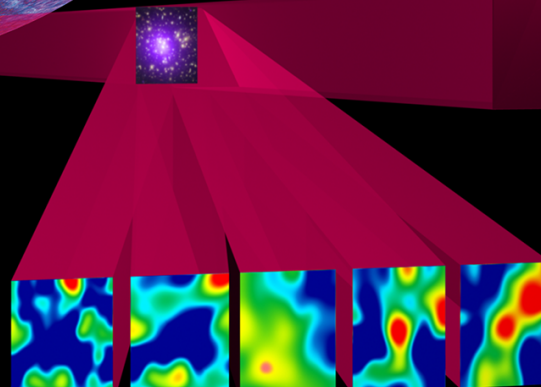
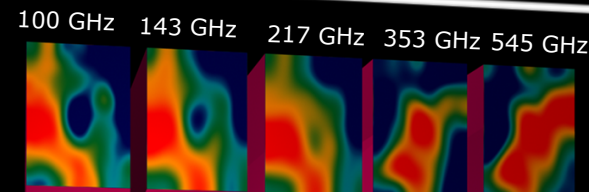


Planck Compton y-map

Planck all-sky Compton y-map



SZ + CMB + Galactic dust emission



100 GHz 143 GHz 217 GHz 353 GHz 545 GHz

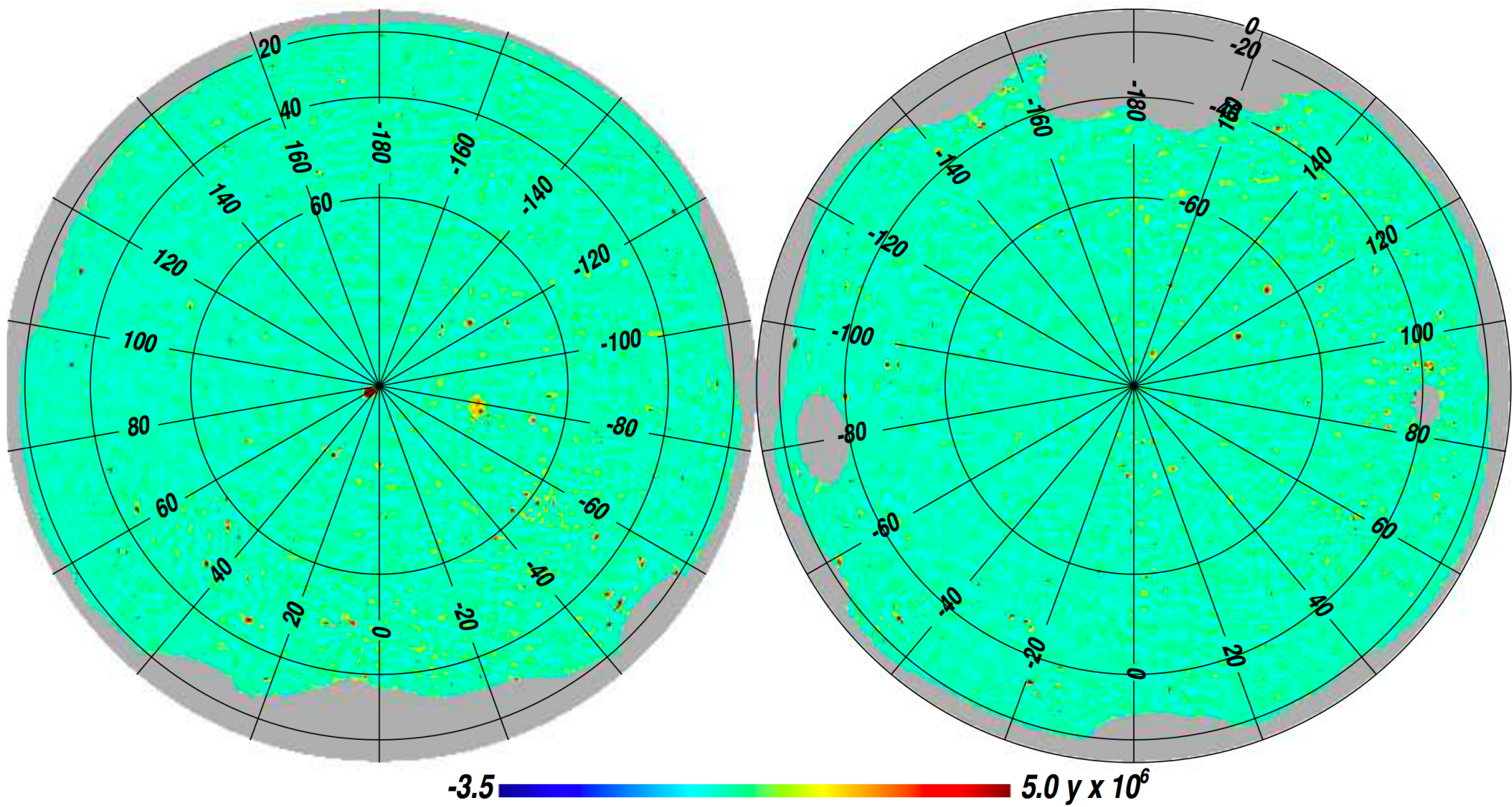
SZ only

**Component separation
NILC and MILCA**

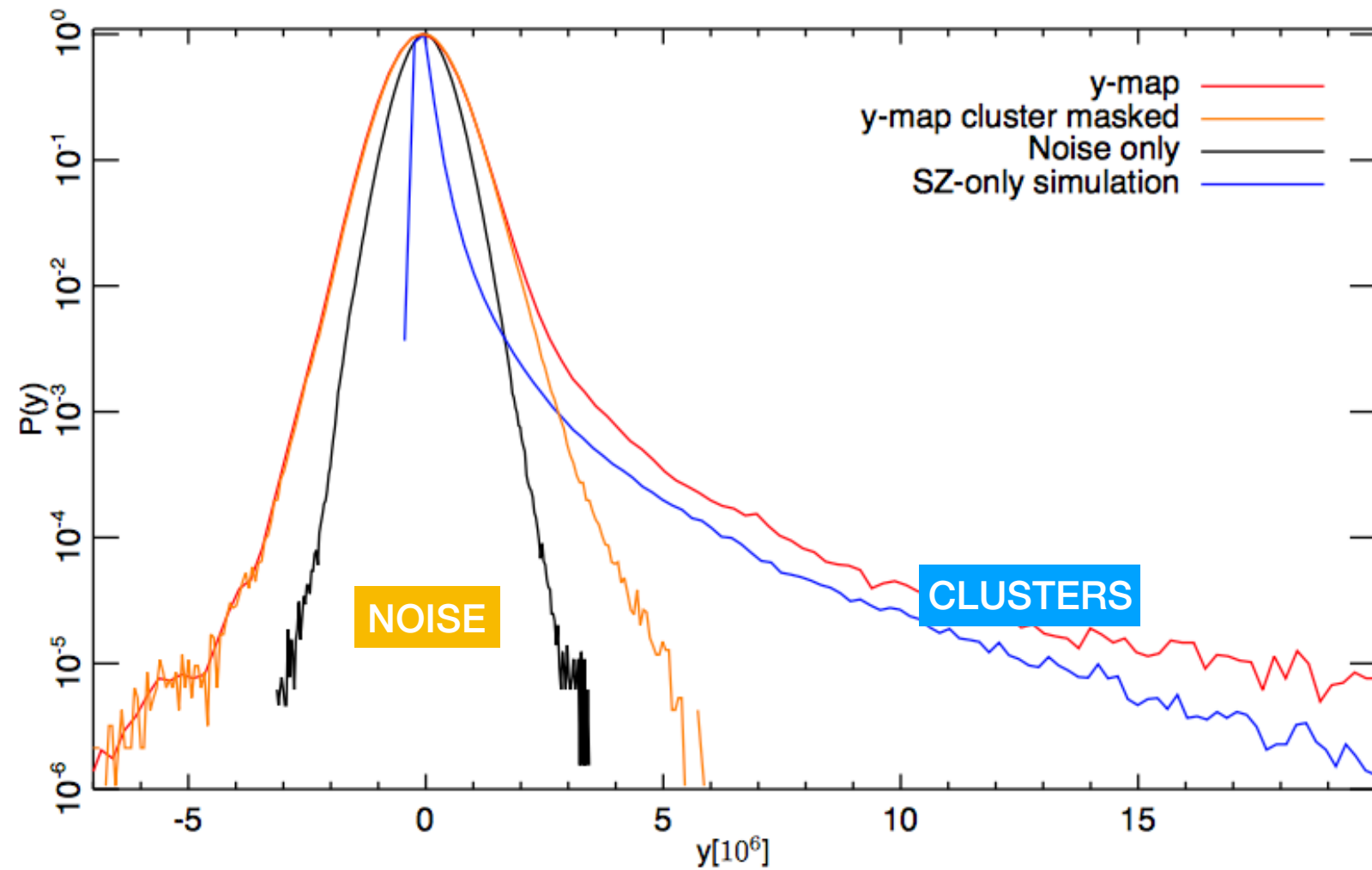


Planck Satellite

Planck all-sky Compton y-map



y-map 1D probability distribution



y-map power spectrum

- Spherical harmonics

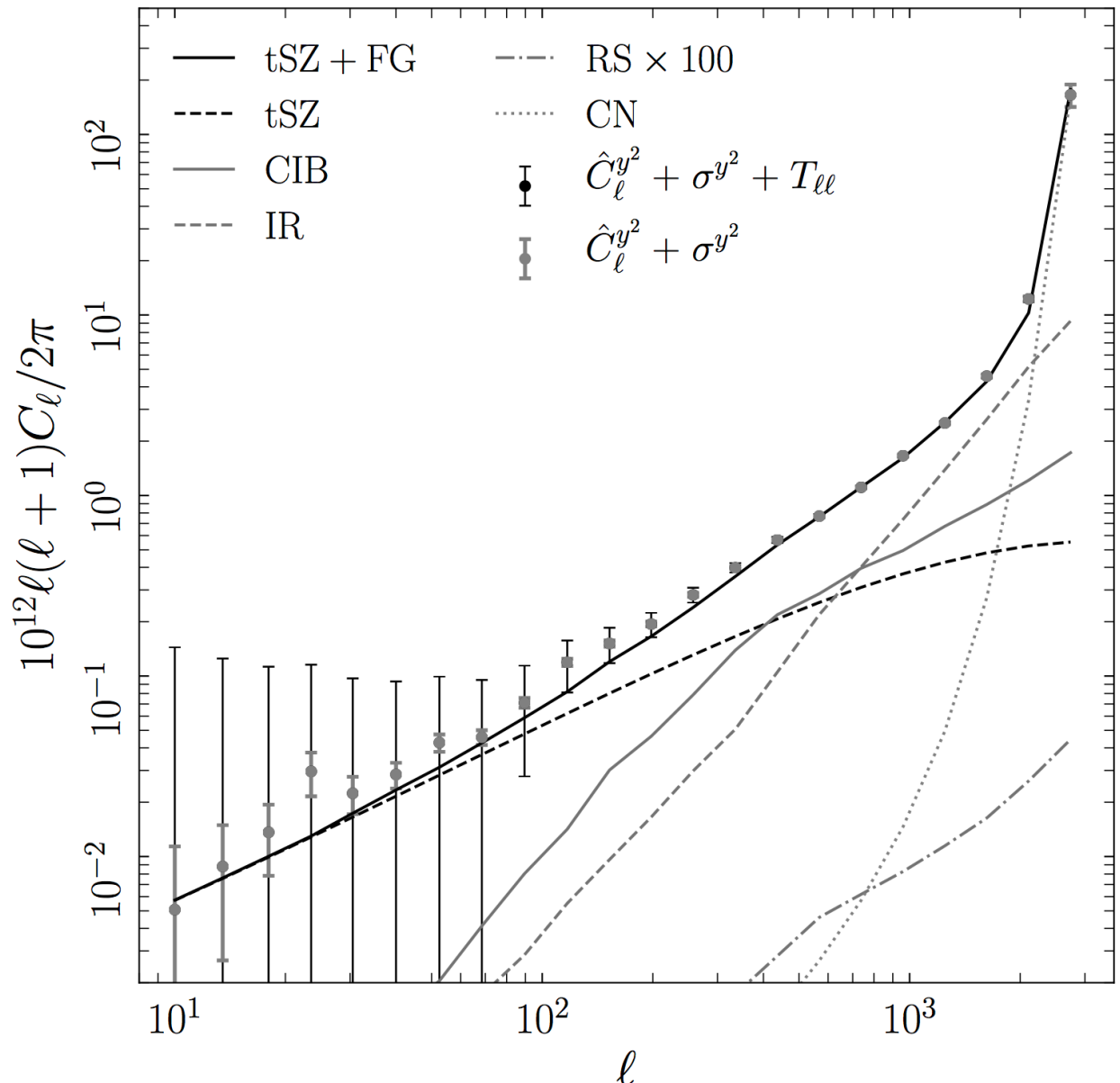
$$y = \sum_{\ell m} y_{\ell m} Y_{\ell m}$$

- Power spectrum

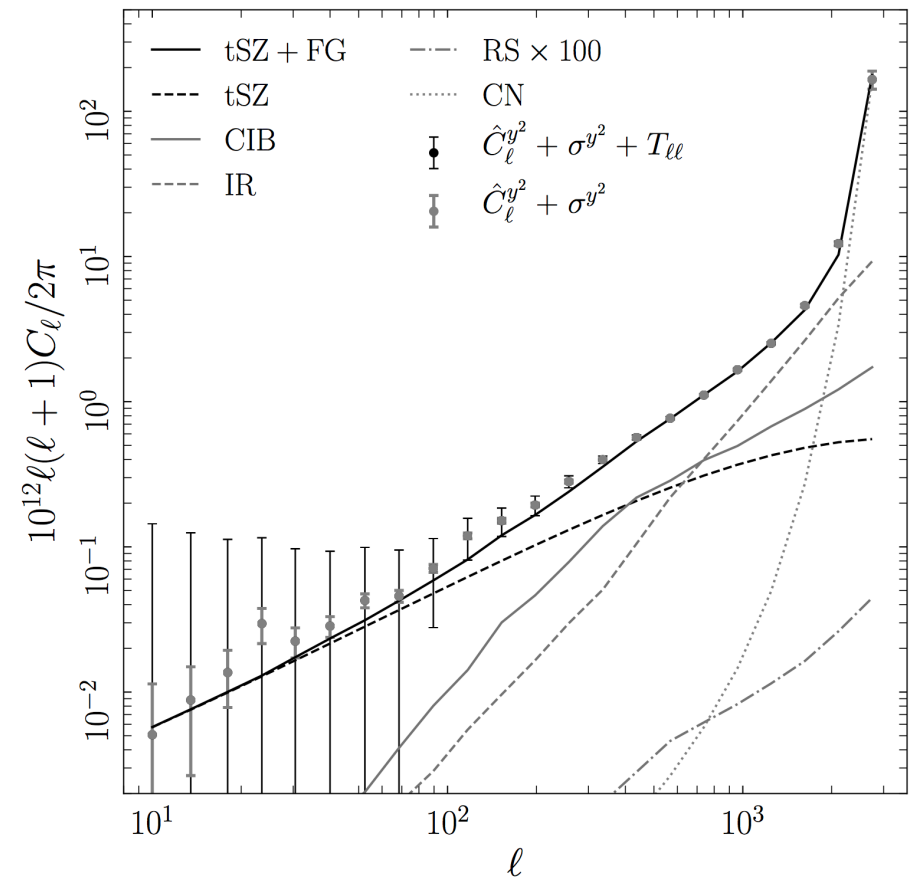
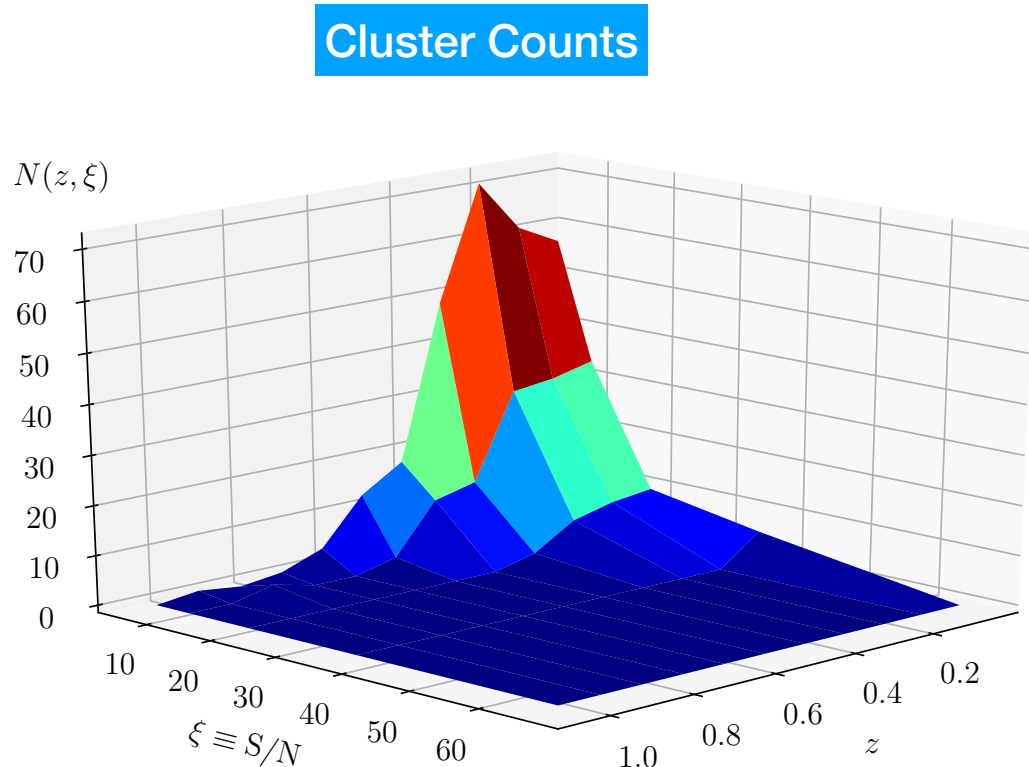
$$C_\ell = \frac{1}{2\ell + 1} \sum_m y_{\ell m} y_{\ell m}^*$$

- Variance

- Noise + foreground residuals



Summary of Planck SZ data



y-map power spectrum

- Clusters of Galaxies
- Thermal Sunyaev Zeldovich Effect
- Planck Cluster Catalogue
- Planck all-sky Compton y -map
- **Cluster Counts: Theory**
- **Cluster Counts: Likelihood**
- **SZ Power spectrum: Theory**
- **SZ Power spectrum: Likelihood**
- Cosmological Constraints
- Promising future directions for SZ

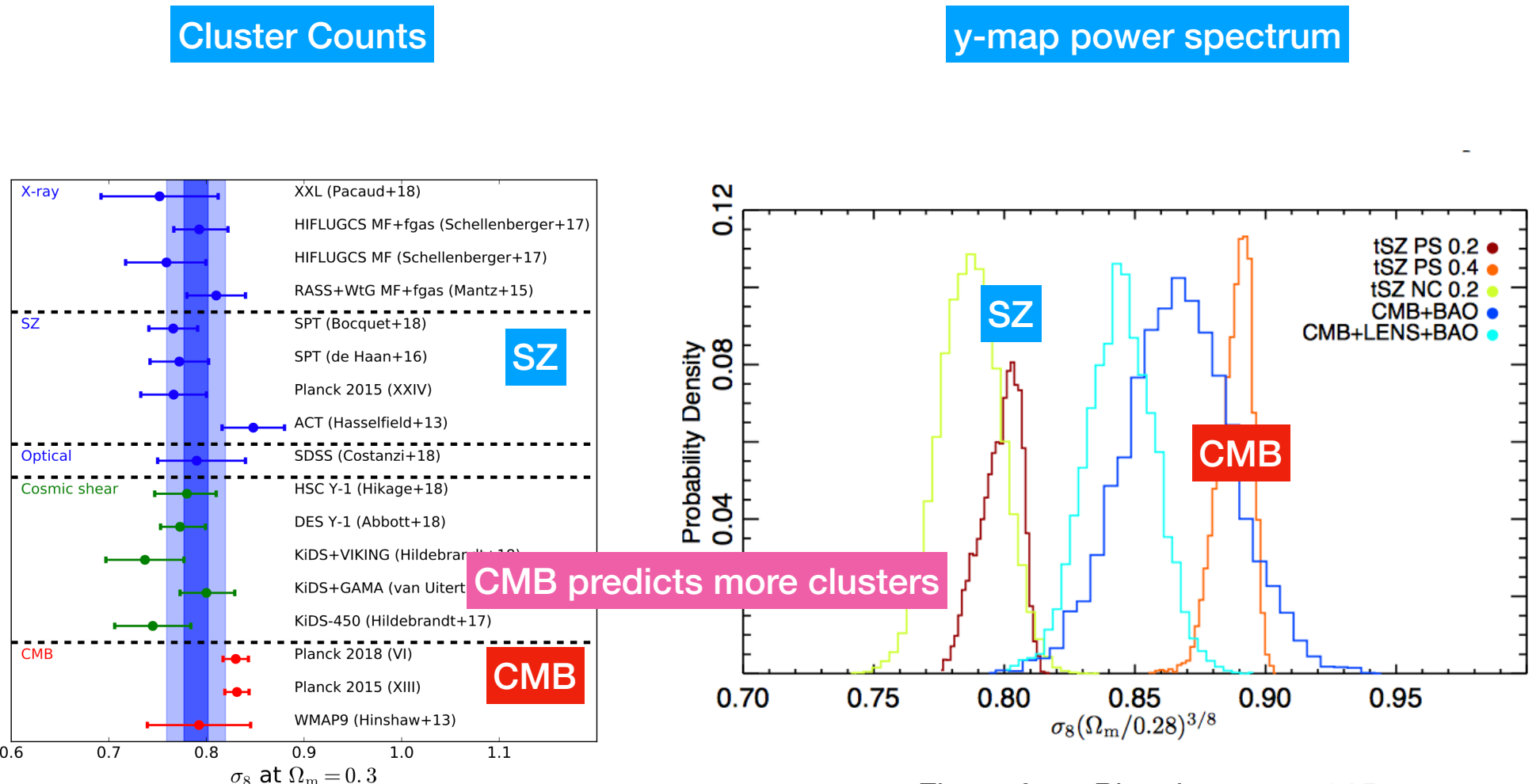


Fig. 17 Constraints on σ_8 at $\Omega_M = 0.3$ from the cluster mass function (sometimes combined with f_{gas} constraints) are shown with blue symbols. Standard deviation (≈ 0.033) and error (≈ 0.012) around the unweighted mean (≈ 0.789) of all seven independent cluster analyses are shown as light and dark blue shaded bands, respectively. Also shown are constraints from WL/cosmic shear/galaxy clustering (green symbols) and from CMB (red symbols). Details on all the constraints are provided in Sections 5.2 and 5.3. Note that analysis details differ for the various works. Adapted from Schellenberger & Reiprich (2017b).

Figure from Pratt et al [1902.10837]

Cluster Counts

How many clusters of mass M?

- key parameters: σ_8 Ω_m $h \equiv H_0/(100\text{km s}^{-1}\text{Mpc}^{-1})$
- definition of the mass

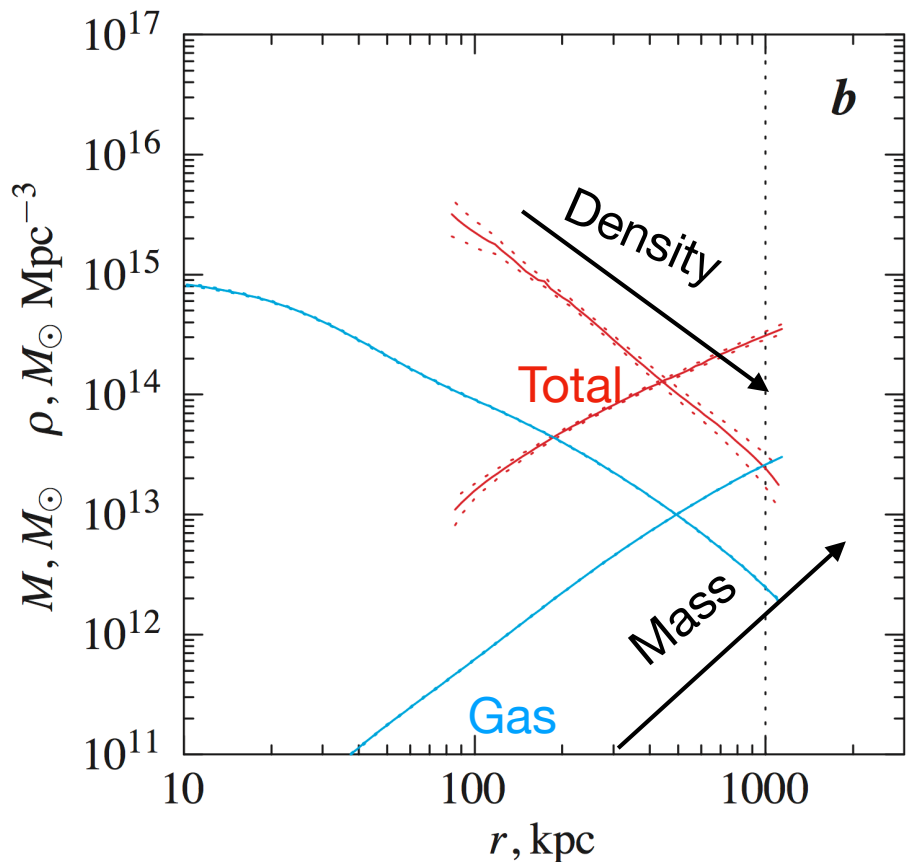


Figure from Vikhlinin et al [0507092]

Spherical over-density mass

M_{500} mass within r_{500}

$$\rho(r_{500}) = 500 \times \rho_{\text{crit}}(z)$$

$$M_{500} = 500\rho_{\text{crit}}(z) \times \frac{4}{3}\pi r_{500}^3$$

How many clusters of mass M?

Press and Schechter (1974):

$$\frac{dn}{dM} = \frac{\rho_{m0}}{M} \times \left| \frac{d\psi}{dM} \right| \quad \rho_m \equiv \rho_{\text{matter}}$$

$\psi(M)$: probability for collapse into halo of mass M or larger

Example: Gaussian density field

$$\sigma^2(M, z) \equiv \int_{k_{\min}}^{k_{\max}} \frac{dk}{k} \frac{k^3}{2\pi^2} P(k, z) W^2(kR)$$

$$\psi(M) = \frac{1}{2} \left[1 - \text{erf} \left(\frac{\delta_c}{\sqrt{2}\sigma(M, z)} \right) \right] \quad R \equiv [3M/4\pi\rho_{m0}]^{1/3}$$

See, e.g., Kravtsov NED level5 for details and references

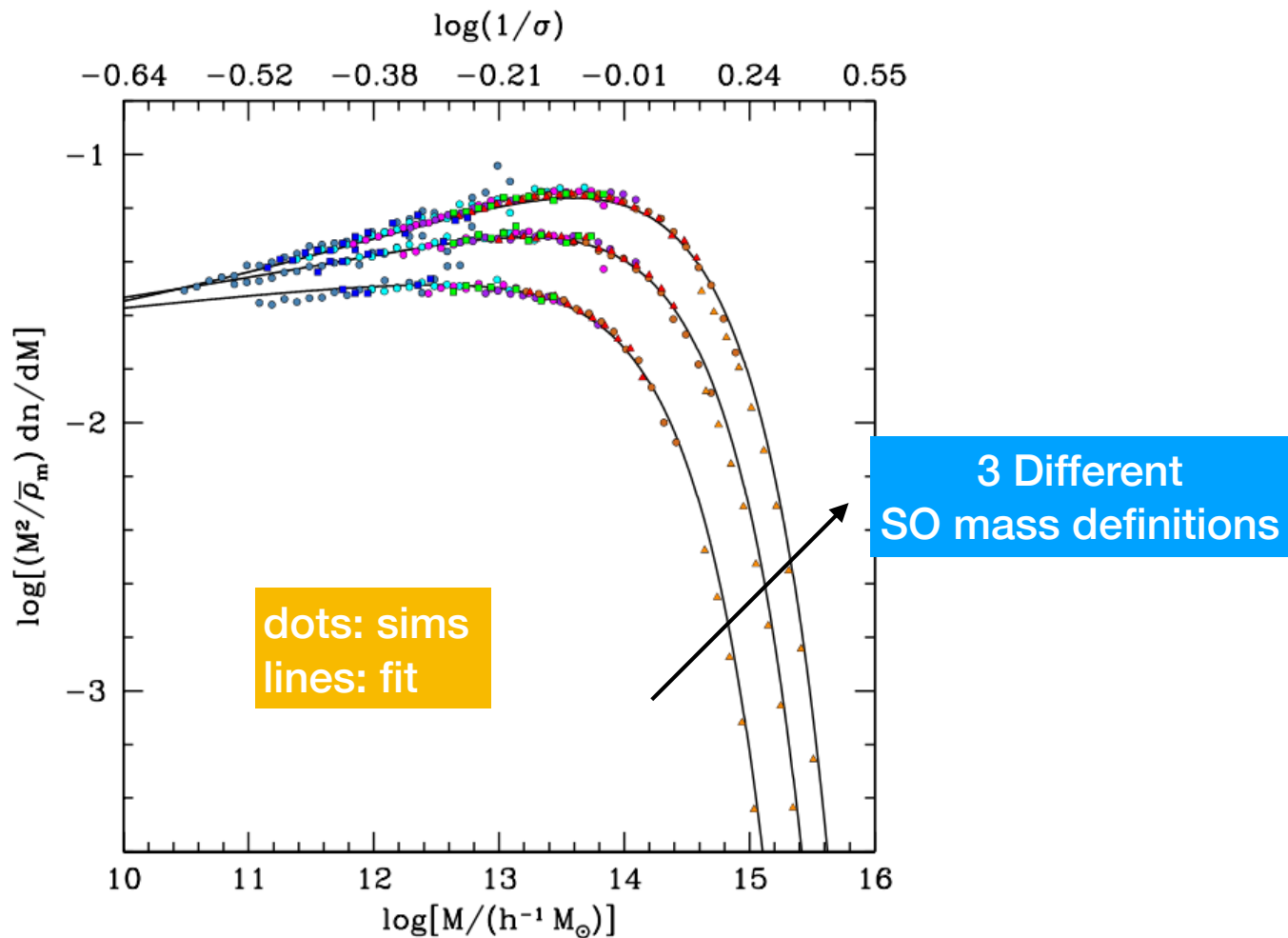


FIG. 5.— The measured mass functions for all WMAP1 simulations, plotted as $(M^2/\bar{\rho}_m)dn/dM$ against $\log M$. The solid curves are the best-fit functions from Table 2. The three sets of points show results for $\Delta = 200$, 800, and 3200 (from top to bottom). To provide a rough scaling between M and σ^{-1} , the top axis of the plot shows σ^{-1} for this mass range for the WMAP1 cosmology. The slight offset between the L1280 results and the solid curves is due to the slightly lower value of $\Omega_m = 0.27$.

Figure from Tinker et al 2008

Halo Mass Function

- Fitting formula to N-body sims

$$\frac{dn}{d \ln M} = -\frac{1}{2} f(\sigma, z) \frac{\rho_{m0}}{M} \frac{d \ln \sigma^2}{d \ln M}$$

$$f(\sigma, z) = A \left[\left(\frac{\sigma}{b} \right)^{-a} + 1 \right] \exp \left(-\frac{c}{\sigma^2} \right)$$

(e.g., Tinker et al 2008, Bocquet et al 2016)

- Values of params given at a specific SO mass
- Redshift dependent parameters

Scaling of total number of clusters

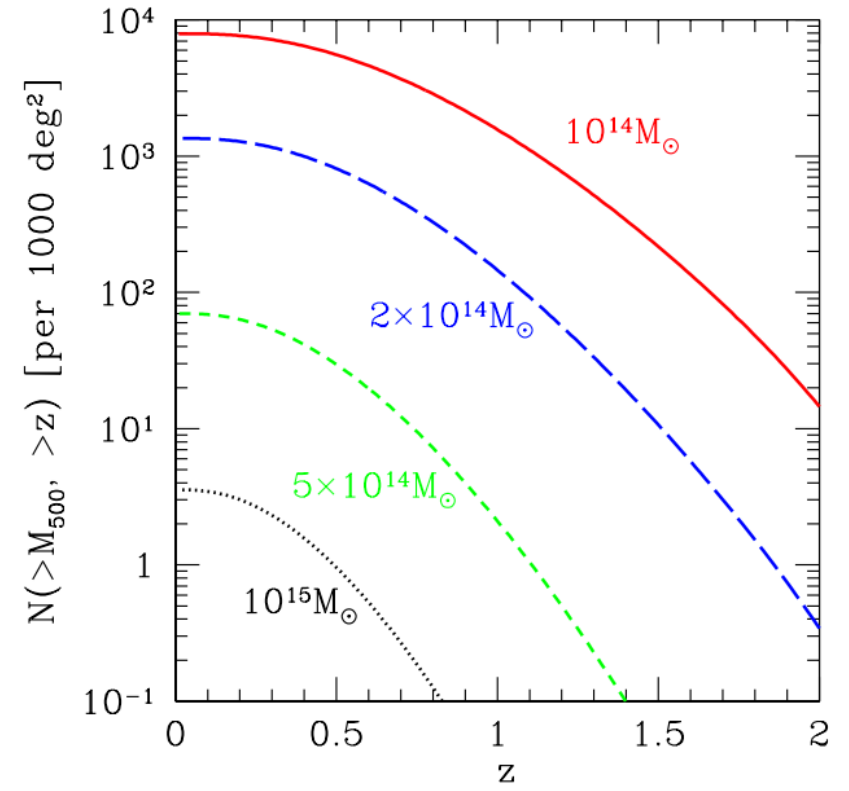
$$N_{\text{tot}} = \int d\Omega \int dz \int dM \frac{dV}{dz d\Omega} \frac{dN}{dM dV}$$

- Comoving volume

$$\frac{dV}{dz d\Omega} = \frac{c}{H_0} \frac{(1+z)^2 D_A(z)^2}{E(z)}$$

$$E(z) = \frac{H(z)}{H_0} \simeq \sqrt{\Omega_m(1+z)^3 + \Omega_\Lambda}$$

$$N_{\text{tot}} \propto \sigma_8^{4.3} \Omega_m^{1.5} h^{0.5}$$



Kitayama [1404.0870]

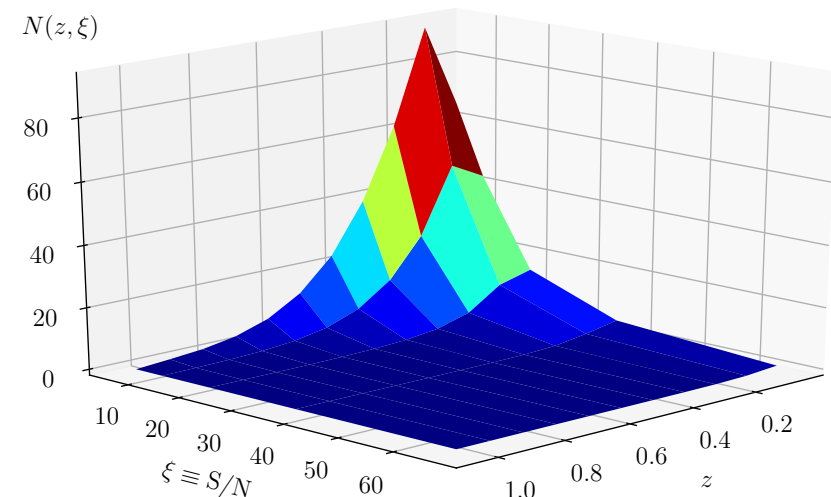
- To compare to observed Planck catalogue:
 - ➡ survey completeness
- Number of clusters in redshift and signal-to-noise bin: $\bar{N}_{ij} = \frac{dN}{dz d\xi} \Delta z_i \Delta \xi_j$

$$\frac{dN}{dz d\xi} = \int d\Omega \int dM \frac{dV}{dz d\Omega} \frac{dN}{dM dV} \mathcal{P}(\xi, \xi_j)$$

- Scaling: $N_{\text{tot}} = \sum_{ij} \bar{N}_{ij}$

$$N_{\text{tot}} \propto \sigma_8^{9.8} \Omega_m^{2.9} B^{-3.2} h^{-0.5}$$

strong sigma8 dependence



degeneracy with mass bias

Prediction of number of clusters in Planck

What is expected signal-to-noise for cluster of mass M at redshift z?

scaling relations: we need **θ-M** for the **noise** and **Y-M** for the **signal**

Scaling relations

- two relations: θ -M and Y-M, both refer to X-ray mass.
- θ -M is a simple “geometrical” relation

$$\left. \begin{array}{l} M_{500} = 500\rho_{\text{crit}}(z) \times \frac{4}{3}\pi r_{500}^3 \\ \theta_{500} = \frac{r_{500}}{D_A(z)} \end{array} \right\} \quad \begin{array}{l} \theta_{500} = \theta_\star h_{70}^{-2/3} \left[\frac{(M_{500}/B)}{3 \times 10^{14} M_\odot} \right]^{1/3} \frac{500 \text{ Mpc}}{D_A(z)} E(z)^{-2/3} \\ \theta_\star = 6.997 \text{ arcmin} \end{array}$$

- Y-M calibrated on X-ray data

B: X-ray mass bias

$$E(z)^{-2/3} \left[\frac{D_A(z)^2 Y_{500}}{10^{-4} \text{ Mpc}^2} \right] = Y_\star h_{70}^{-2+\alpha} \left[\frac{(M_{500}/B)}{6 \times 10^{14} M_\odot} \right]^\alpha$$

$$\log_{10} Y_\star = -0.19 \pm 0.02 \quad \alpha = 1.79 \pm 0.08$$

- Given M_{500} and z : compute θ_{500} and Y_{500}
- compute signal-to-noise: interpolate noise map

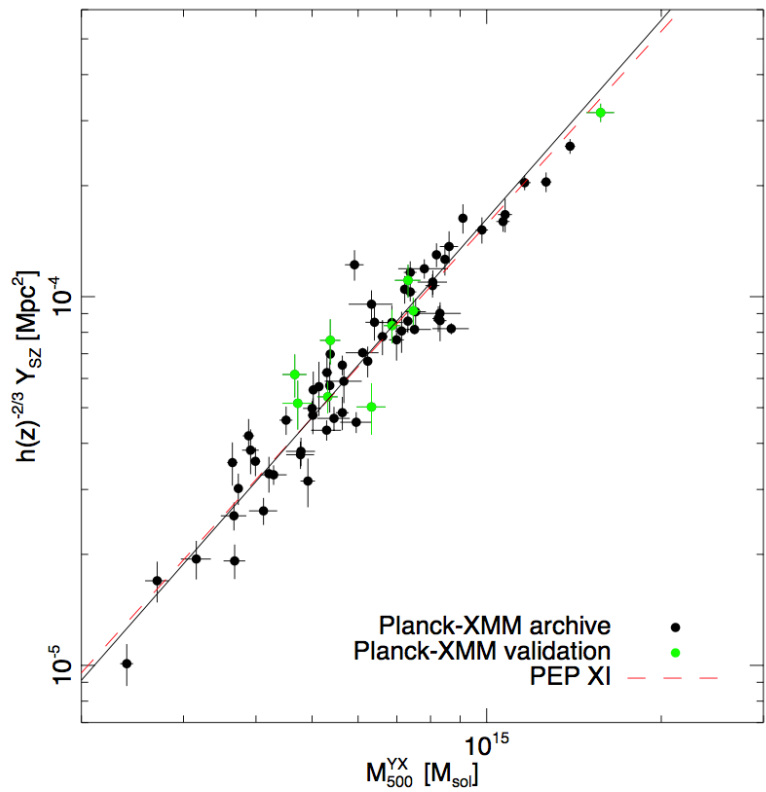
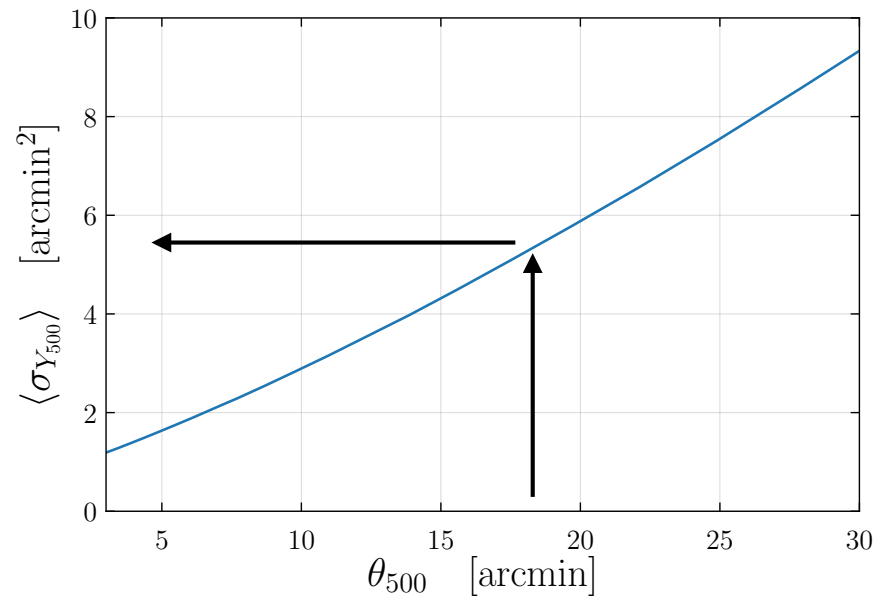


Fig. A.1. Best scaling relation between Y_{500} and M_{500} , and the data points utilized after correction of the Malmquist bias

Figure from Planck 2013 CC paper

$$\xi = \frac{Y_{500}}{\sigma_{Y_{500}}(\theta_{500})}$$



Detection probability:

$$\mathcal{P}(\xi, \xi_j) = \chi(\xi) \times \chi(\xi_j^{\min}) \times [1 - \chi(\xi_j^{\max})] \times \frac{1}{\sqrt{2\pi}\sigma_{\log_{10} Y}} \exp\left(-\frac{\log_{10} \xi - \log_{10} \xi_j}{\sqrt{2}\sigma_{\log_{10} Y}}\right)$$

$$\chi(\xi) = \frac{1}{2} \left[1 - \text{erf}\left(\frac{\xi - \xi_{\text{cut}}}{\sqrt{2}}\right) \right]$$

Intrinsic scatter:

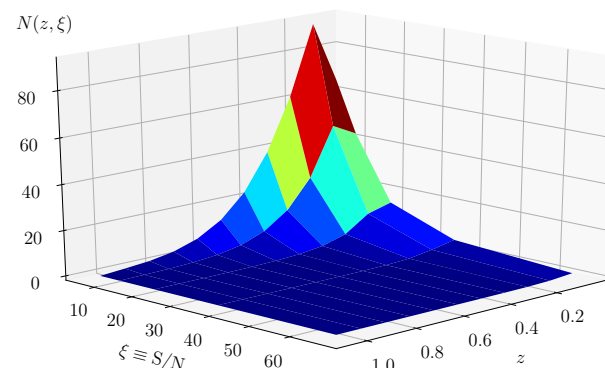


- independent of statistical scatter
- account for different cluster formation history

$$\frac{dN}{dz d\xi} = \int d\Omega \int dM \frac{dV}{dz d\Omega} \frac{dN}{dM dV} \mathcal{P}(\xi, \xi_j)$$

$$\sigma_{\log_{10} Y} = 0.075 \pm 0.01$$

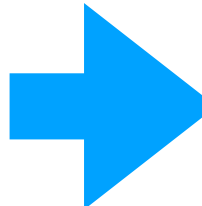
$$N_{\text{tot}} \propto \sigma_8^{9.8} \Omega_m^{2.9} B^{-3.2} h^{-0.5}$$



A word on the X-ray mass bias B

- X-ray mass estimates: hydrostatic equilibrium assumption
- X-ray mass estimates: neglects non-thermal pressure
- Hydrostatic mass:

$$M_{\text{tot}}(< r) = - \frac{r P_{\text{gas}}}{\mu m_{\text{u}} G n_{\text{gas}}} \frac{d \log P_{\text{gas}}}{d \log r}$$

$P_{\text{thermal}} < P_{\text{true}}$  $M^{\text{X-ray}} < M_{\text{true}}$

X-ray mass bias

$$M^{\text{HSE}} = M_{500}/B$$

$$B > 1$$

- Which cosmological model is preferred by Planck SZ data?

- Markov Chain Monte Carlo method
- Minimise -log L given data
- Likelihood function: Poisson log-likelihood (Cash 1979)

$$\bar{N}_{ij} = \frac{dN}{dz d\xi} \Delta z_i \Delta \xi_j$$

likelihood

$$\ln \mathcal{L} = \sum_{ij} [N_{ij} \ln \bar{N}_{ij} - \bar{N}_{ij} - \ln(N_{ij}!)]$$

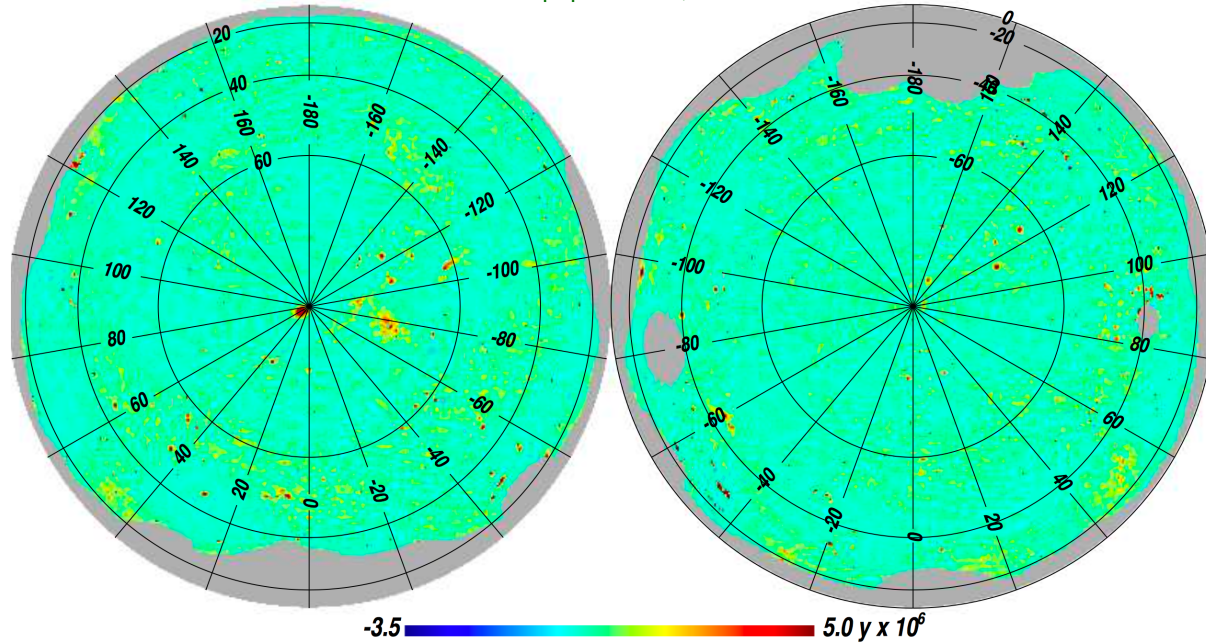
predicted

catalogue

- Clusters of Galaxies
- Thermal Sunyaev Zeldovich Effect
- Planck Cluster Catalogue
- Planck all-sky Compton y -map
- Cluster Counts: Theory
- Cluster Counts: Likelihood
- **SZ Power spectrum: Theory**
- **SZ Power spectrum: Likelihood**
- Cosmological Constraints
- Promising future directions for SZ

Planck "y-map"

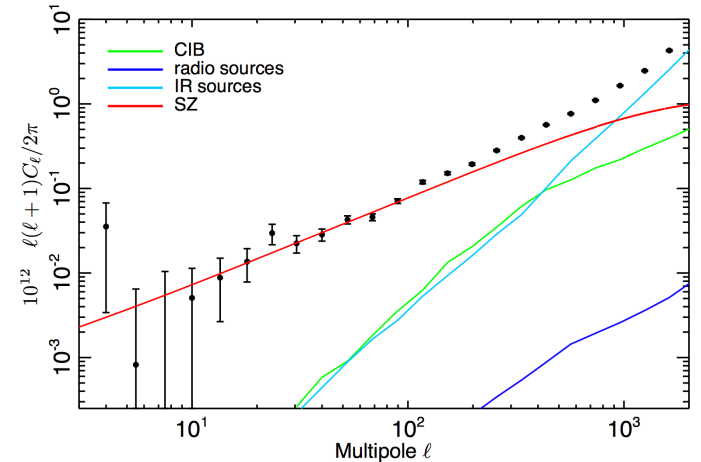
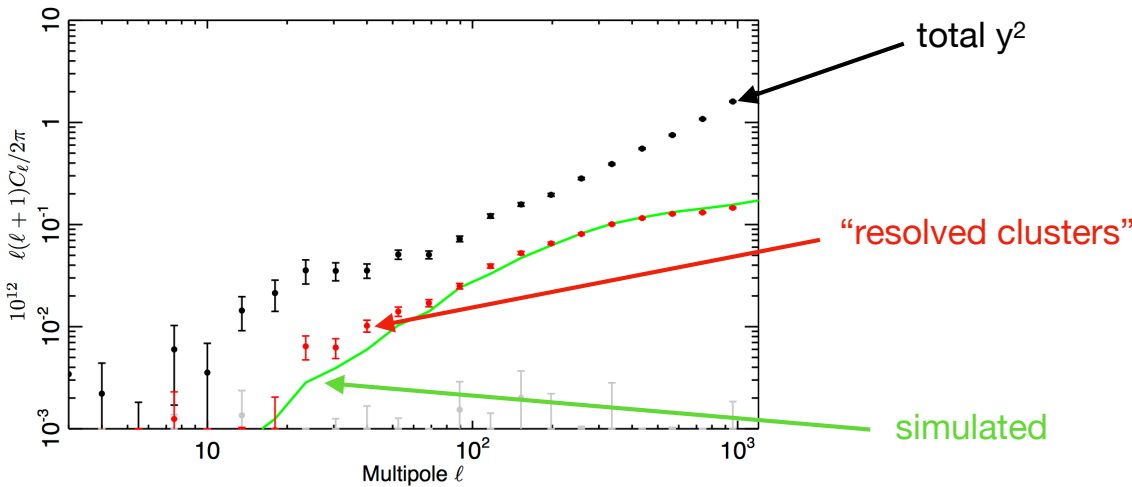
Planck papers 2013, 2015



contains foreground residuals

$$y^2 = t\text{SZ} + \text{CIB} + \text{RS} + \text{IR}$$

Power spectrum of the Compton y-map



See Hurier & Lacasa 2017 for an alternative method

Model for y-map power spectrum

- Compton y-map power spectrum has 5 ingredients:

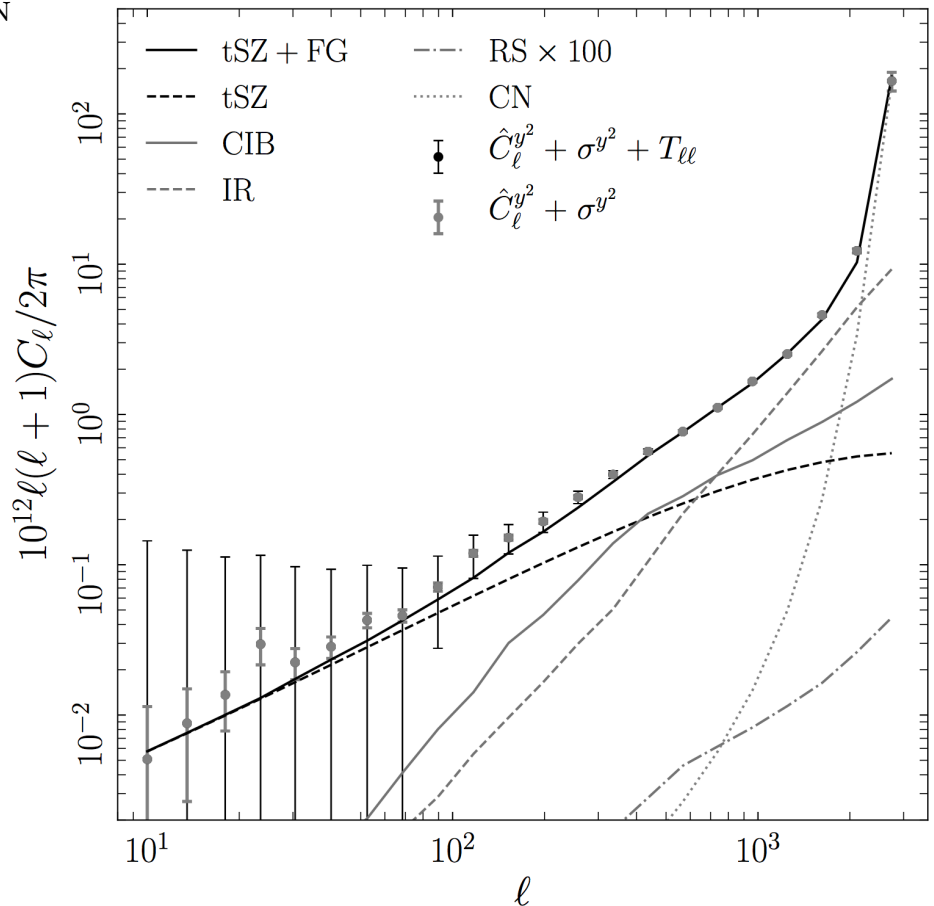
$$C_\ell^{y^2} = C_\ell^{\text{tSZ}} + A_{\text{CIB}} \hat{C}_\ell^{\text{CIB}} + A_{\text{IR}} \hat{C}_\ell^{\text{IR}} + A_{\text{RS}} \hat{C}_\ell^{\text{RS}} + A_{\text{CN}} \hat{C}_\ell^{\text{CN}}$$

- + the variance (i.e., uncertainty)

- Residual power spectra of foregrounds

Noise can be determined by looking at high ell:

$$A_{\text{CN}} = \hat{C}_{2742}^{y^2} / \hat{C}_{2742}^{\text{CN}} = 0.903$$



How do we compute tSZ?

Theoretical model for the tSZ power spectrum

$$C_\ell^{y^2} = C_\ell^{\text{tSZ}} + A_{\text{CIB}} \hat{C}_\ell^{\text{CIB}} + A_{\text{IR}} \hat{C}_\ell^{\text{IR}} + A_{\text{RS}} \hat{C}_\ell^{\text{RS}} + A_{\text{CN}} \hat{C}_\ell^{\text{CN}}$$

Computed with
CLASS_SZ

$$C_\ell^{\text{tSZ}} = \int_{z_{\min}}^{z_{\max}} dz \frac{dV}{dz d\Omega} \int_{\ln M_{\min}}^{\ln M_{\max}} d \ln M \frac{dn}{d \ln M} |y_\ell(M, z)|^2$$

Komatsu & Kitayama 1999, Komatsu & Seljak 2002

$$z_{\min} = 0$$

$$z_{\max} = 4$$

$$M_{\min} = 10^{11} \text{M}_\odot/h$$

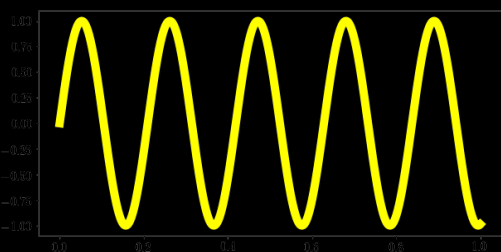
$$M_{\max} = 5 \times 10^{15} \text{M}_\odot/h$$

Tinker et al 2008 HMF
at M_{500}

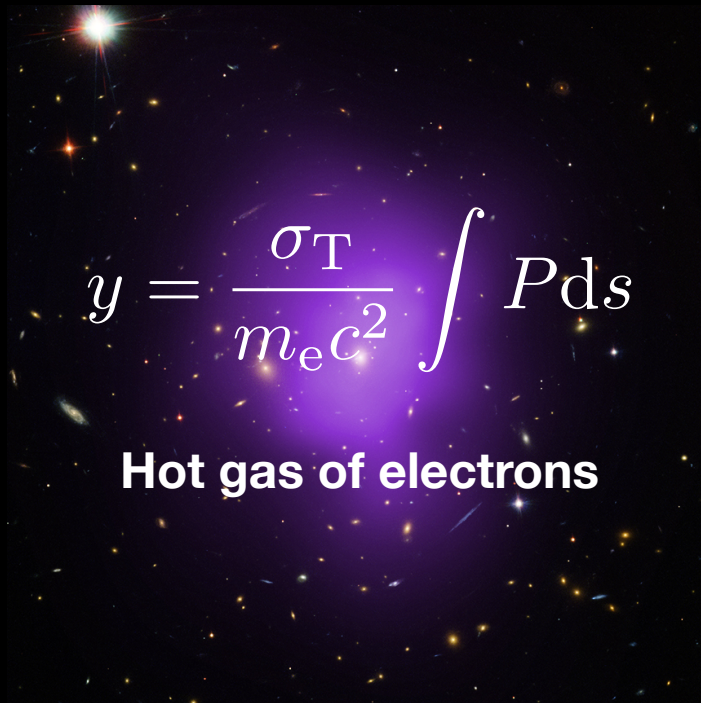
Inverse Compton Scattering

Electron give energy to photon

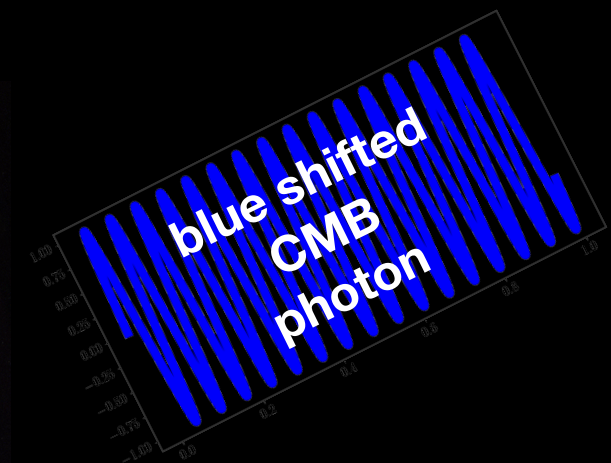
CMB
photon



Galaxy Cluster



Hot gas of electrons

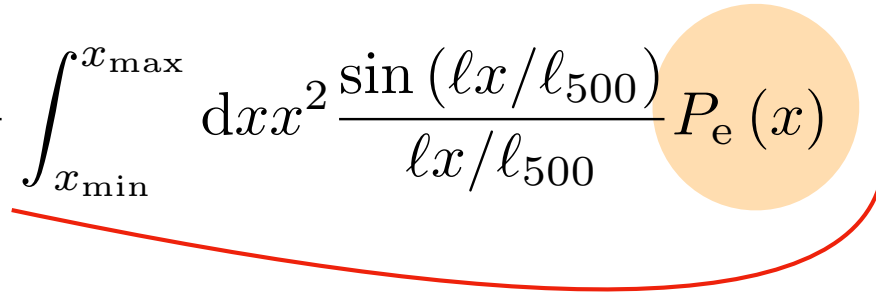


THERMAL SUNYAEV ZELDOVICH EFFECT

Theoretical model for the tSZ power spectrum

$$C_\ell^{\text{tSZ}} = \int_{z_{\min}}^{z_{\max}} dz \frac{dV}{dz d\Omega} \int_{\ln M_{\min}}^{\ln M_{\max}} d \ln M \frac{dn}{d \ln M} |y_\ell(M, z)|^2$$

Thomson cross section

$$y_\ell = \frac{\sigma_T}{m_e c^2} \frac{4\pi r_{500}}{\ell_{500}^2} \int_{x_{\min}}^{x_{\max}} dx x^2 \frac{\sin(\ell x / \ell_{500})}{\ell x / \ell_{500}} P_e(x)$$


Projected pressure profile

$$x \equiv r/r_{500}$$

$$\ell_{500} \equiv d_A/r_{500}$$

Pressure profile

$$y_\ell = \frac{\sigma_{\text{T}}}{m_{\text{e}} c^2} \frac{4\pi r_{500}}{\ell_{500}^2} \int_{x_{\min}}^{x_{\max}} dx x^2 \frac{\sin(\ell x / \ell_{500})}{\ell x / \ell_{500}} P_{\text{e}}(x)$$

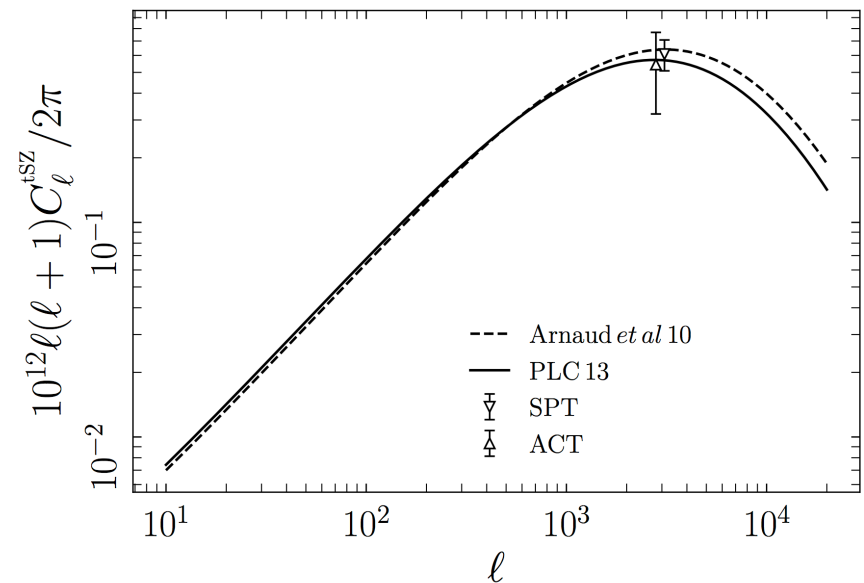
Generalised Navarro-Frenk-White parameterisation (Nagai et al 2007):

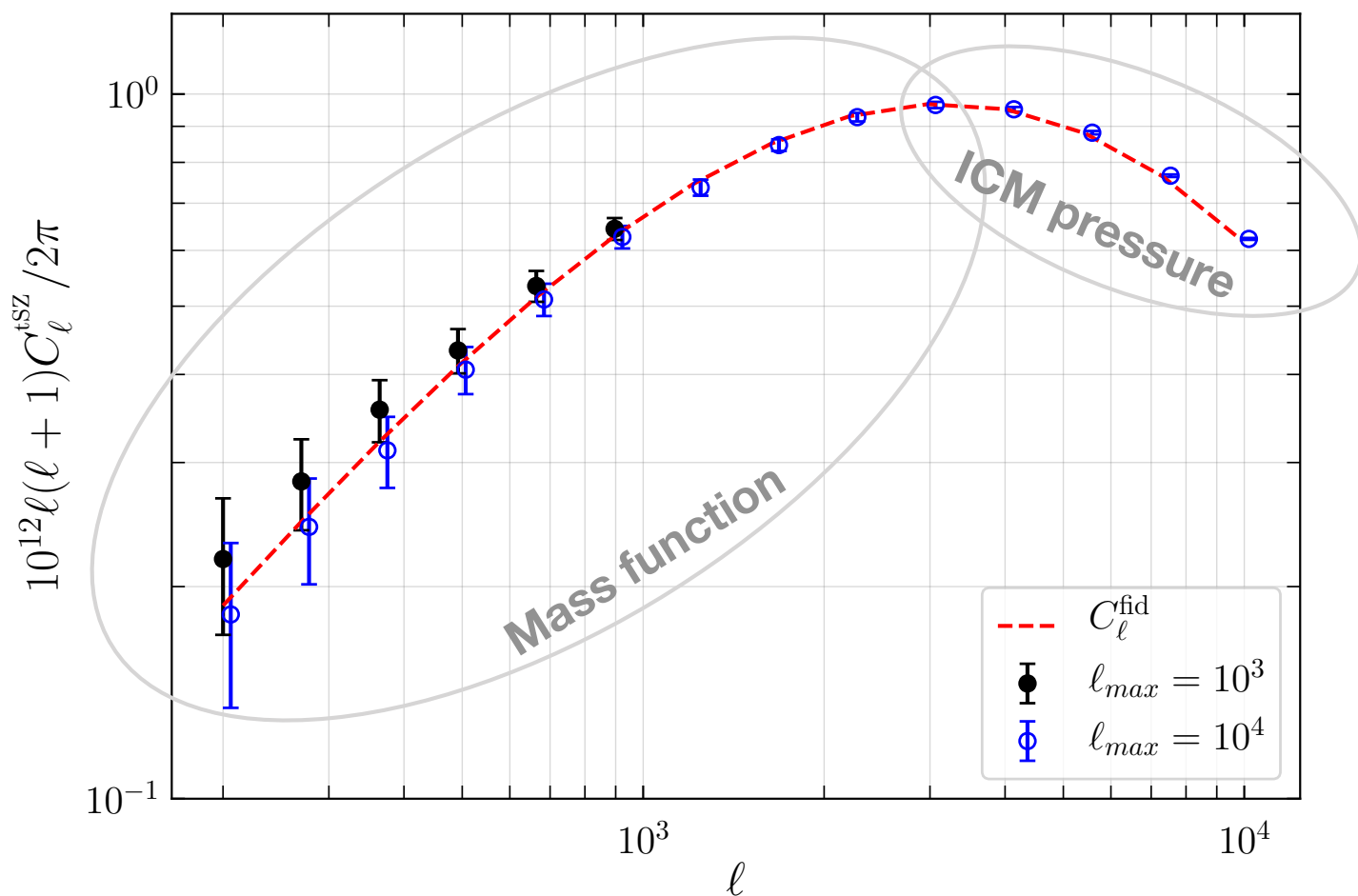
$$P_{\text{e}}(x) = C \times P_0 (c_{500} x)^{-\gamma} [1 + (c_{500} x)^\alpha]^{(\gamma - \beta)/\alpha}$$

*Normalisation is set from the “Y-M” relations derived from **X-ray** measurements:*

$$C = 1.65 \left(\frac{h}{0.7} \right)^2 \left(\frac{H}{H_0} \right)^{\frac{8}{3}} \left[\frac{(h/0.7) \tilde{M}_{500c}}{3 \times 10^{14} M_\odot} \right]^{\frac{2}{3} + 0.12} \text{ eV cm}^{-3}$$

	P_0	c_{500}	γ	α	β
PLC 13	6.41	1.81	0.31	1.33	4.13
Arnaud et al. 2010	8.13	1.16	0.33	1.06	5.48





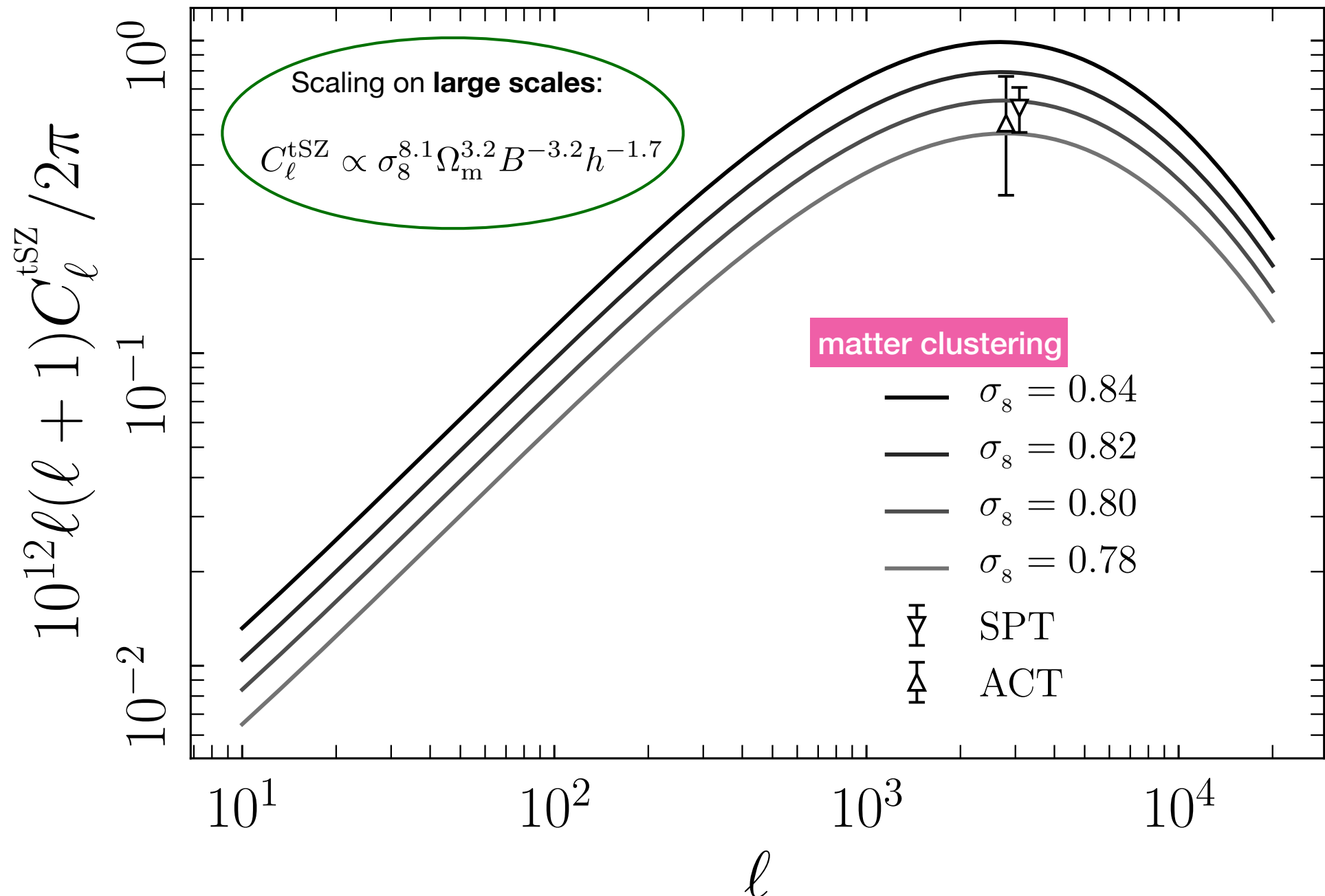
Statistical uncertainty for the SZ power spectrum

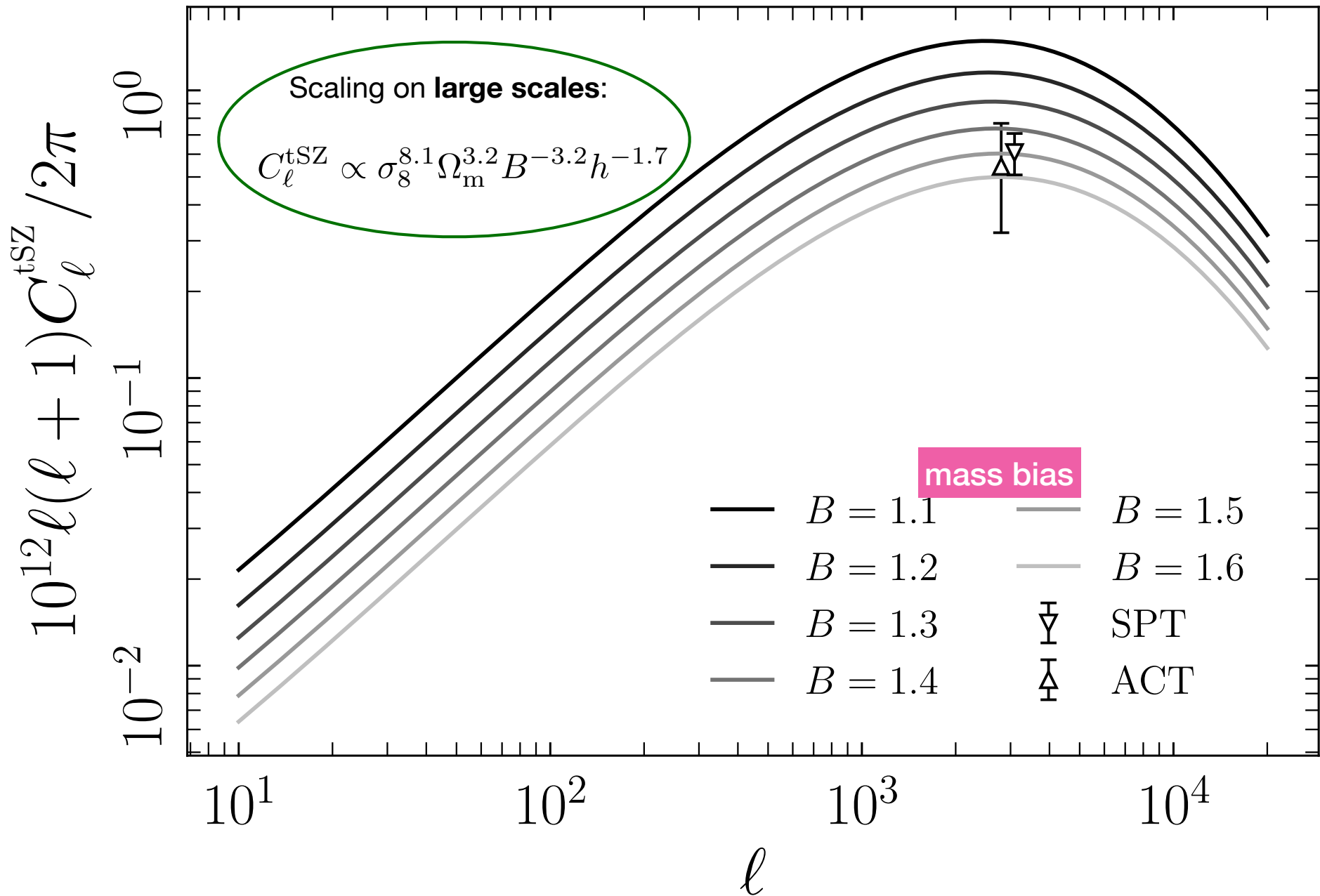
- Clusters: Poisson statistics, not gaussian
- 4pt-function does not vanish
- Cosmic variance : Gaussian + trispectrum (4pt-function)

(see, e.g., Komatsu and Seljak 2002, Hill and Pajer, 2013)

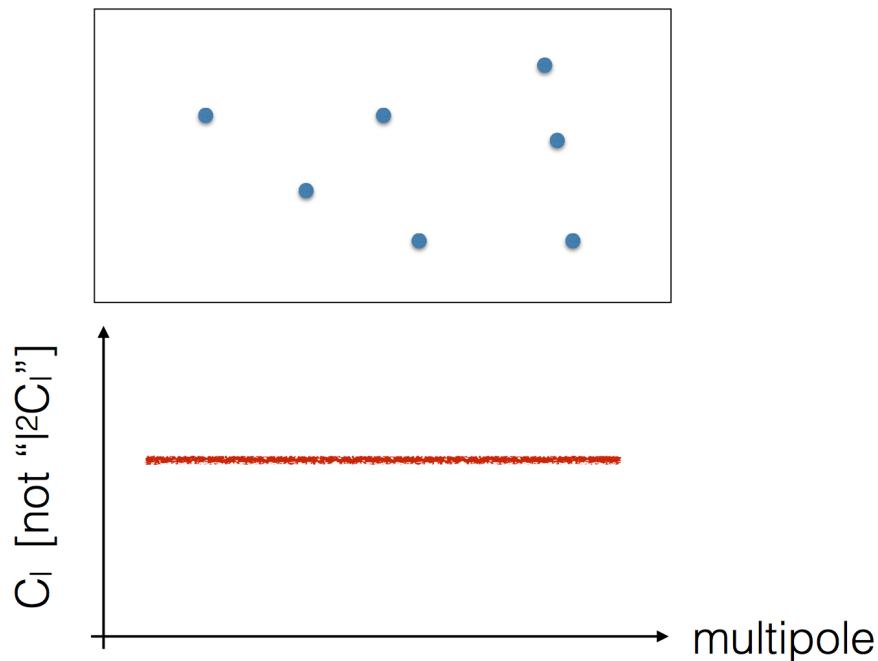
$$T_{\ell\ell'} = \int dz \frac{dV}{dz d\Omega} \int d \ln M \frac{dn}{d \ln M} |y_\ell(M, z)|^2 |y_{\ell'}(M, z)|^2$$

➡ correlations between multipoles



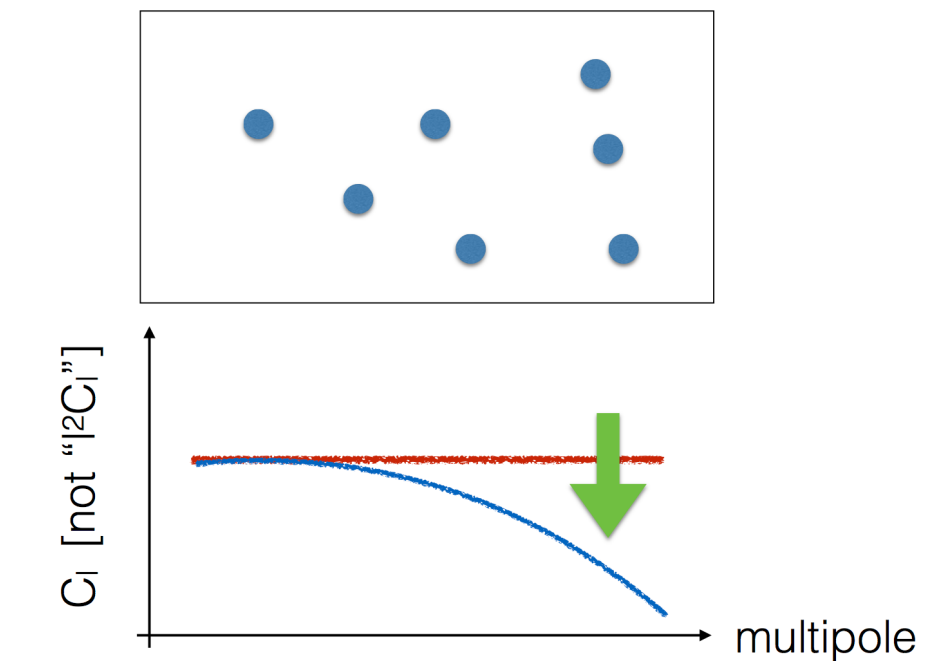


- Shape of the tSZ spectrum



- Randomly-distributed point sources
= Poisson spectrum = $\sum_i (\text{flux}_i)^2 / 4\pi$

²⁸

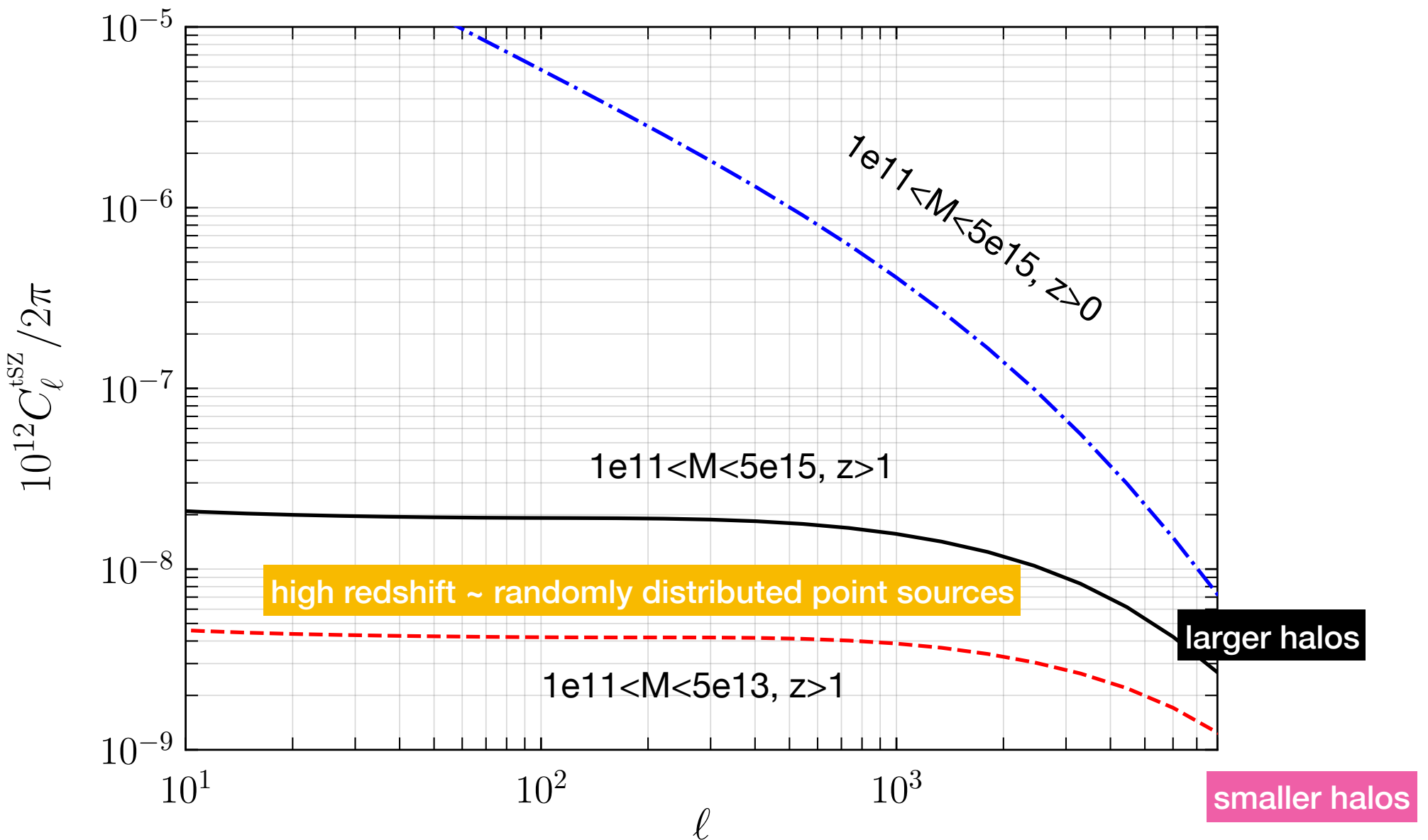


- Extended sources = the power spectrum reflects intensity profiles

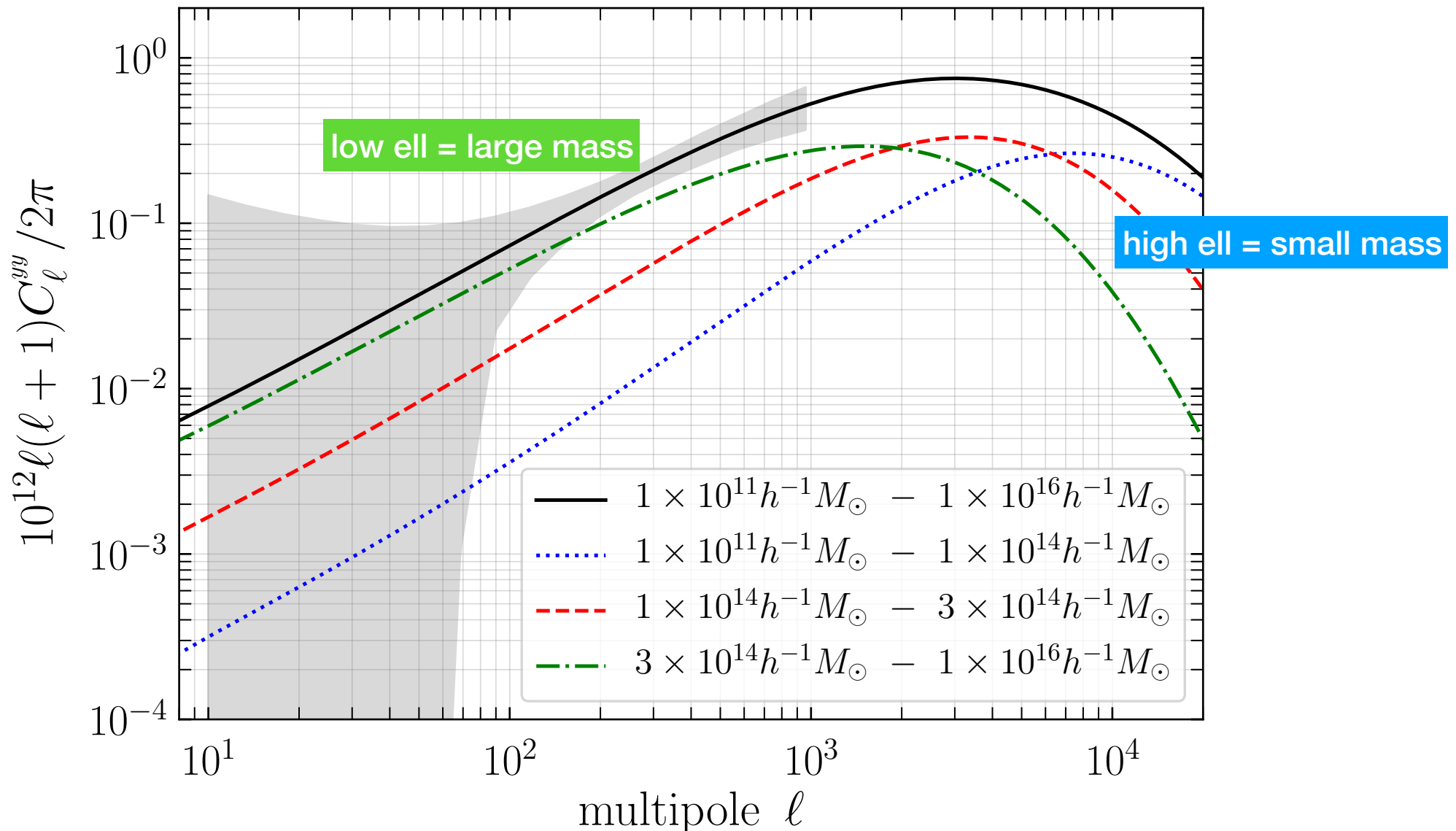
²⁹

Figures from Komatsu's talks

- Shape of the tSZ spectrum



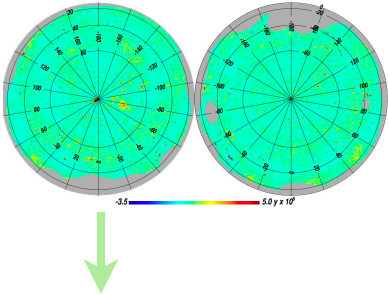
- Which masses contribute more to tSZ power spectrum?



Remazeilles, Bolliet, Rotti, Chluba [1809.09666]

Maximum likelihood analysis

Given the Compton-y data, search for the cosmological parameters and foreground amplitudes that minimise:



$$-2 \ln \mathcal{L} = \chi^2 + \ln |M| + \text{const.}$$

We used MontePython, Audren et al 2013

$$C_\ell^{y^2} = C_\ell^{\text{tSZ}} + A_{\text{CIB}} \hat{C}_\ell^{\text{CIB}} + A_{\text{IR}} \hat{C}_\ell^{\text{IR}} + A_{\text{RS}} \hat{C}_\ell^{\text{RS}} + A_{\text{CN}} \hat{C}_\ell^{\text{CN}}$$

$$\chi^2 \equiv \sum_{a \leq a'} \left(C_{\ell_{\text{eff}}^a}^{y^2} - \hat{C}_{\ell_{\text{eff}}^a}^{y^2} \right) [M^{-1}]_{aa'} \left(C_{\ell_{\text{eff}}^{a'}}^{y^2} - \hat{C}_{\ell_{\text{eff}}^{a'}}^{y^2} \right)$$

Covariance matrix

$$M_{aa'} = \left(\sigma_{\ell_{\text{eff}}^a}^{y^2} \right)^2 \delta_{aa'} + \frac{\ell_{\text{eff}}^a (\ell_{\text{eff}}^a + 1) \ell_{\text{eff}}^{a'} (\ell_{\text{eff}}^{a'} + 1)}{4\pi^2} \frac{T_{aa'}}{4\pi f_{\text{sky}}}$$

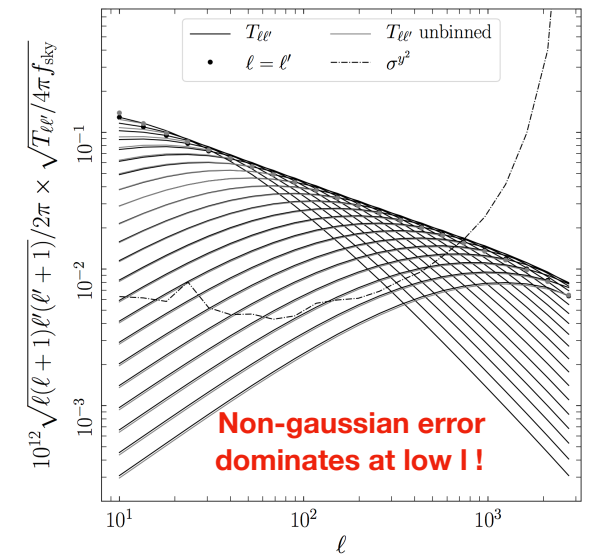
ℓ_{eff}	$\hat{C}_\ell^{y^2}$	$\sigma_\ell^{y^2}$	\hat{C}_ℓ^{RC}	σ_ℓ^{RC}	$\hat{C}_\ell^{\text{CIB}}$	\hat{C}_ℓ^{RS}	\hat{C}_ℓ^{IR}	\hat{C}_ℓ^{CN}
10	0.00508	0.00629	0.000421	0.000160	0.000000	0.000043	0.000007	0.000001
13.5	0.00881	0.00615	0.000710	0.000192	0.000000	0.000142	0.000024	0.000001
18	0.01363	0.00579	0.001251	0.000254	0.000000	0.000296	0.000048	0.000002
23.5	0.02961	0.00805	0.002837	0.000446	0.000000	0.000400	0.000073	0.000004
30.5	0.02241	0.00521	0.003933	0.000460	0.000902	0.000541	0.000111	0.000006
40	0.02849	0.00464	0.005969	0.000510	0.002010	0.001056	0.000224	0.000010
52.5	0.04276	0.00468	0.010318	0.000672	0.003119	0.001647	0.000449	0.000018
68.5	0.04580	0.00429	0.014045	0.000699	0.006278	0.002787	0.000837	0.000030
89.5	0.07104	0.00454	0.024061	0.000896	0.012242	0.004306	0.001400	0.000052
117	0.11914	0.00562	0.032976	0.000936	0.021584	0.006842	0.002701	0.000089
152.5	0.15150	0.00594	0.047100	0.001020	0.045915	0.011264	0.004721	0.000153
198	0.19390	0.00611	0.062380	0.001040	0.070582	0.016744	0.008115	0.000262
257.5	0.28175	0.00687	0.081730	0.001030	0.119786	0.027345	0.014618	0.000456
335.5	0.39837	0.00824	0.101911	0.000978	0.211686	0.043275	0.024893	0.000815
436.5	0.56743	0.00958	0.117412	0.000860	0.332863	0.070587	0.051570	0.001503
567.5	0.76866	0.01242	0.132234	0.000769	0.434931	0.115356	0.107293	0.002934
738	1.11010	0.01650	0.143214	0.000642	0.602030	0.154926	0.197053	0.006334
959.5	1.66140	0.02400	0.156202	0.000544	0.754733	0.207200	0.361713	0.016171
1247.5	2.52170	0.04170	0.175341	0.000492	1.029014	0.287652	0.681036	0.054883
1622	4.58510	0.09870	0.283969	0.000900	1.357567	0.410274	1.295272	0.301480
2109	12.2690	0.40100	1.363680	0.003650	1.850146	0.657659	2.534448	3.738250
2742	165.600	23.6000	54.69000	2.310000	2.629002	1.117189	4.545315	183.2673

Trispectrum

$$T_{aa'} = \sum_{\ell \in a} \sum_{\ell' \in a'} \frac{T_{\ell\ell'}}{N_a N_{a'}}$$

$$T_{\ell\ell'} = \int dz \frac{dV}{dz d\Omega} \int d\ln M \frac{dn}{d\ln M} |y_\ell(M, z)|^2 |y_{\ell'}(M, z)|^2$$

Komatsu & Seljak 2002



Use the condition: “*foregrounds can not be too large!*”

$$A_{\text{CIB}} \hat{C}_\ell^{\text{CIB}} + A_{\text{IR}} \hat{C}_\ell^{\text{IR}} + A_{\text{RS}} \hat{C}_\ell^{\text{RS}} + A_{\text{CN}} \hat{C}_\ell^{\text{CN}} < \hat{C}_\ell^{y^2} - \hat{C}_\ell^{\text{RC}}$$

Split between slow and fast parameters

$$\underbrace{A_s, n_s, \tau_{\text{reio}}, \theta_s, \Omega_b h^2, \Omega_c h^2, w, B}_{C_\ell^{\text{tSZ}}: \text{slow param.}} \underbrace{A_{\text{CIB}}, A_{\text{IR}}, A_{\text{RS}}}_{C_\ell^{\text{FG}}: \text{fast param.}}$$

- Clusters of Galaxies
- Thermal Sunyaev Zeldovich Effect
- Planck Cluster Catalogue
- Planck all-sky Compton y -map
- Cluster Counts: Theory
- Cluster Counts: Likelihood
- SZ Power spectrum: Theory
- SZ Power spectrum: Likelihood
- **Cosmological Constraints**
- Promising future directions for SZ

Planck y-map power spectrum analysis

- Planck 2015: Low sigma8 and tight constraints

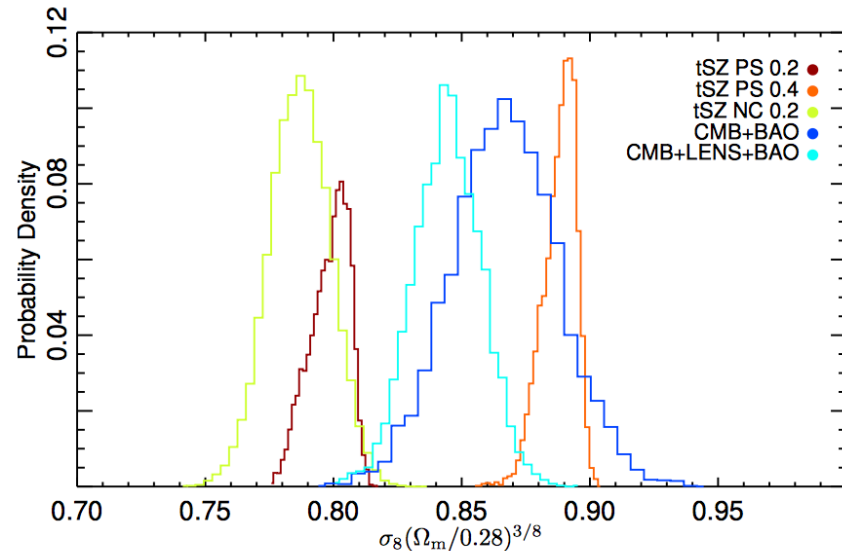


Fig. 19. Marginalized likelihood distribution for $\sigma_8(\Omega_m/0.28)^{3/8}$ for tSZ- and CMB-based analyses. We represent the tSZ power spectrum analysis results assuming a mass bias, b , of 0.2 (red) and 0.4 (orange), the cluster number count analysis results (green; Planck Collaboration XXIV 2016), and the combined *Planck* CMB and BAO analysis (Planck Collaboration XIII 2016) with (cyan) and without (blue) extra lensing constraints.

➡ Reanalysis of Planck data **with trispectrum**

(see, e.g., Horowitz and Seljak 2017, Salvati et al 2018, Bolliet et al 2018)

=> wider confidence level interval

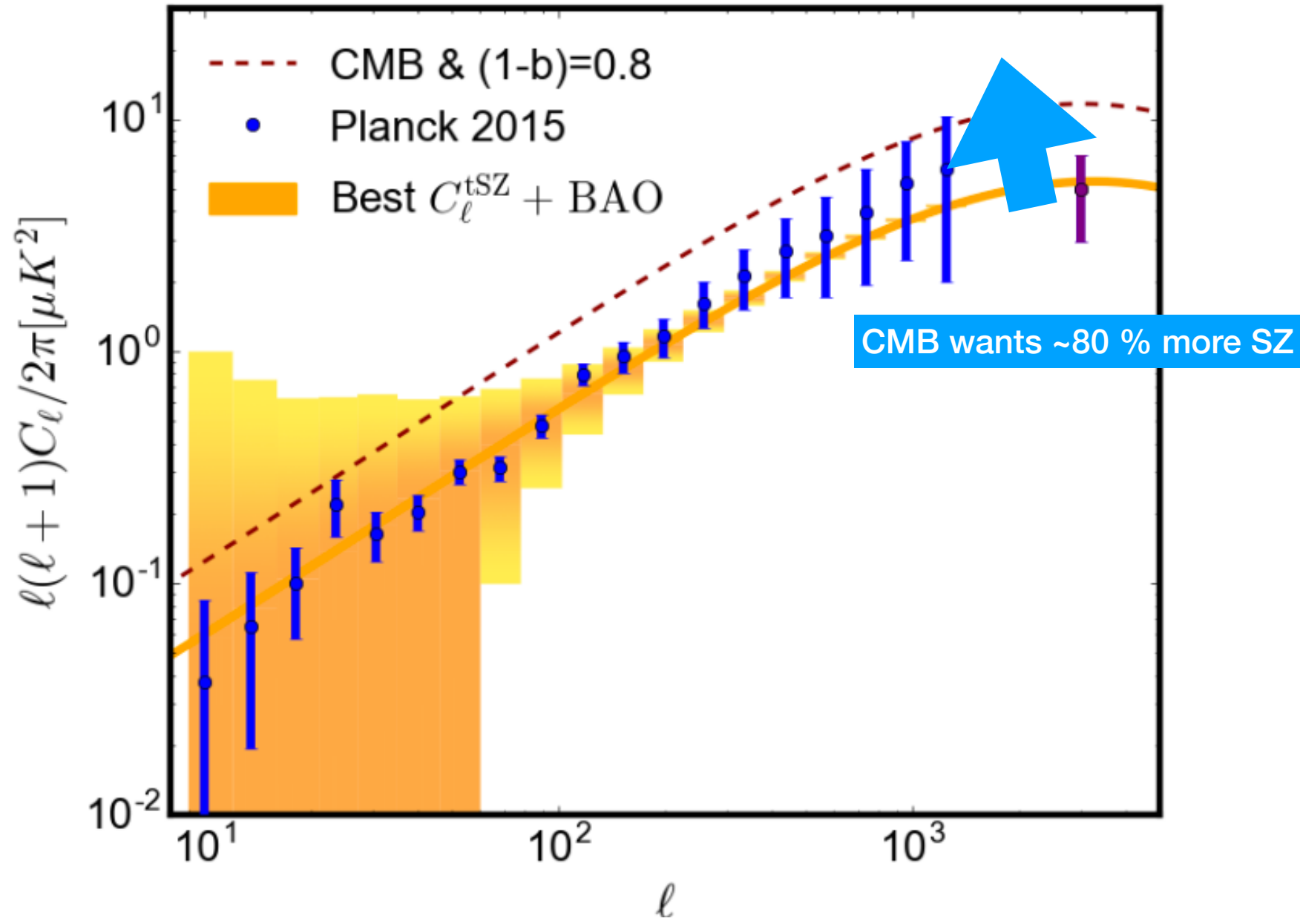
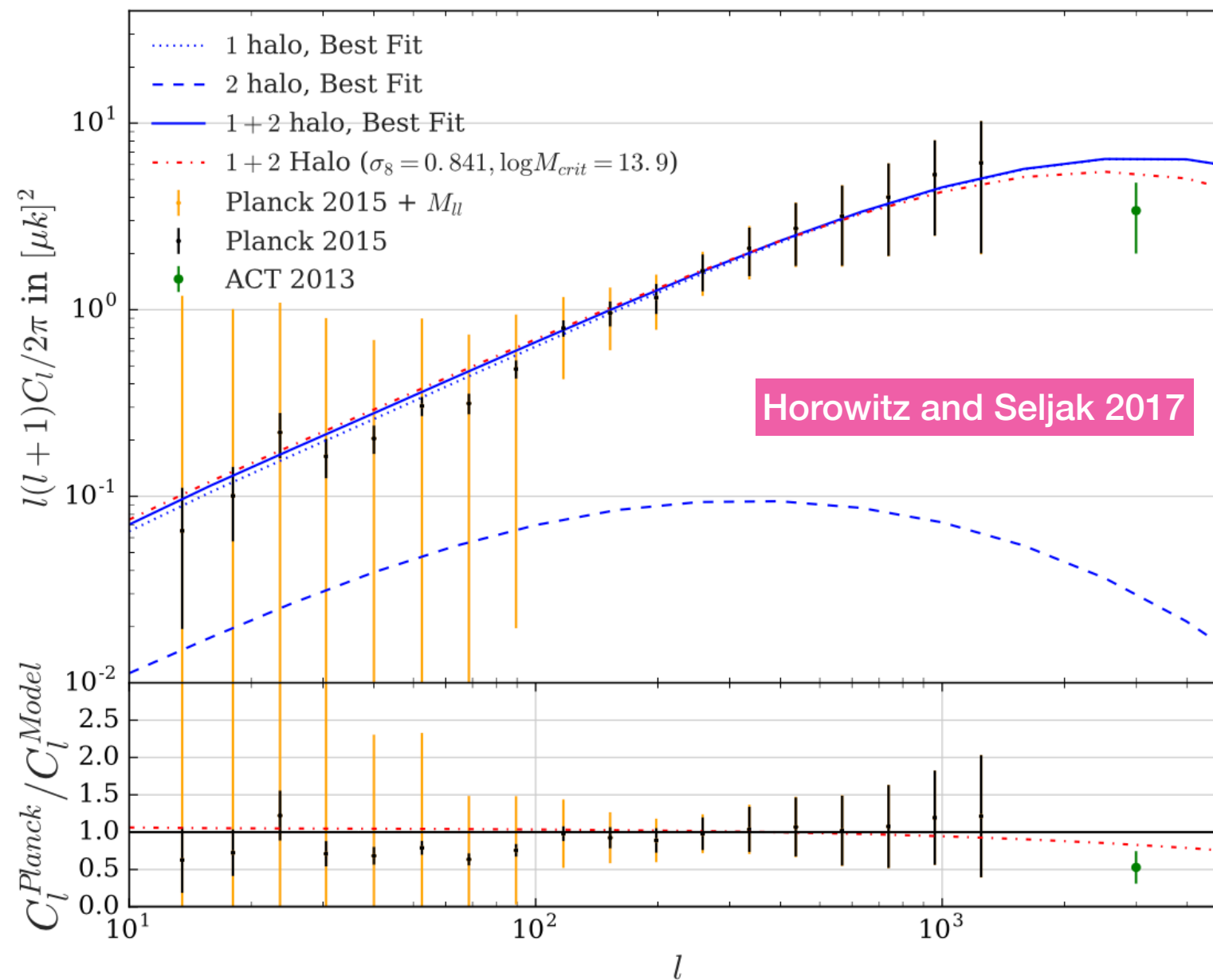
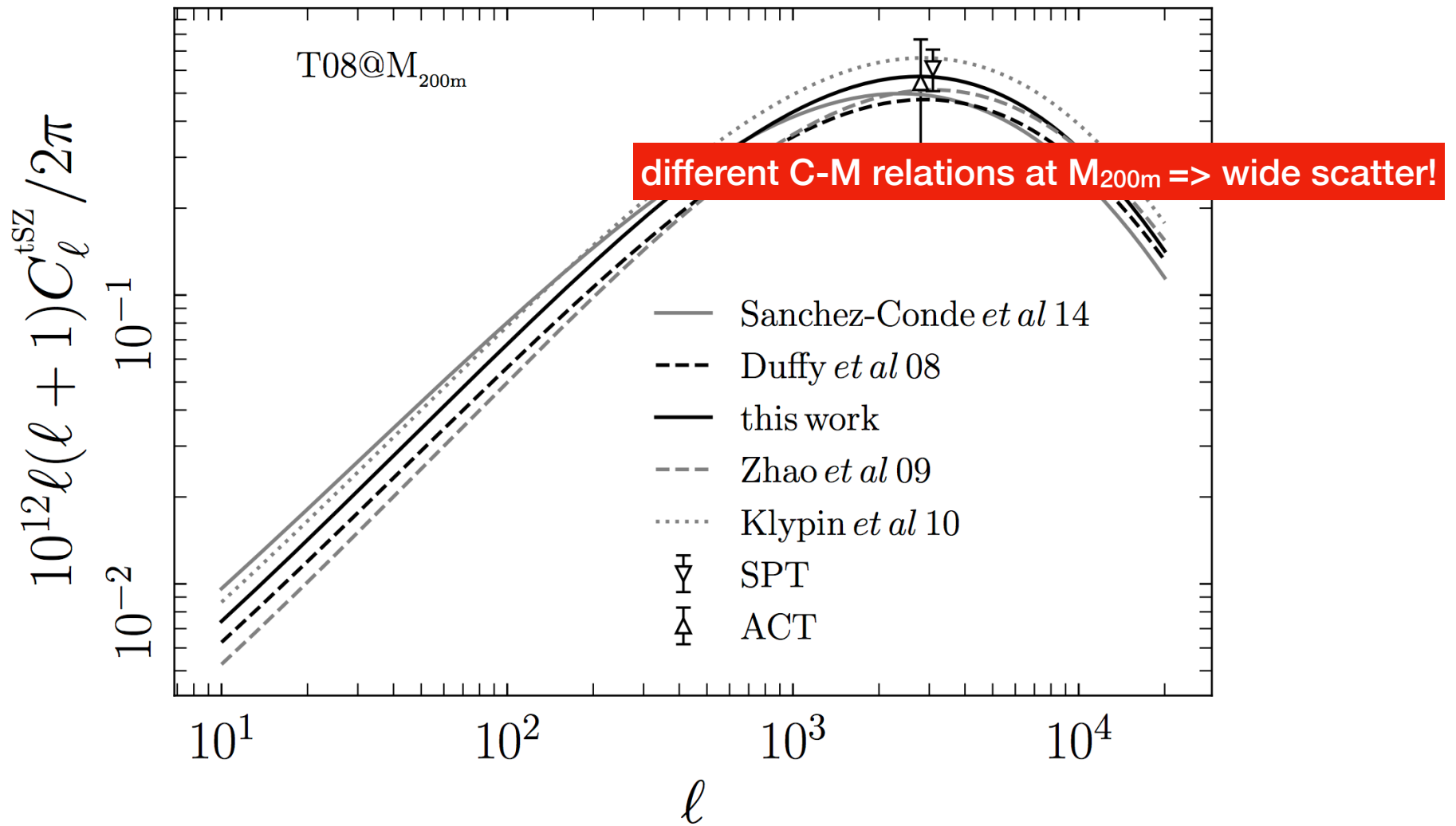


Figure from Salvati et al 2018



- Horowitz and Seljak 2017: no tension?
- uses Tinker et al 2008 at M_{200m} => needs mass conversion => needs C-M relation

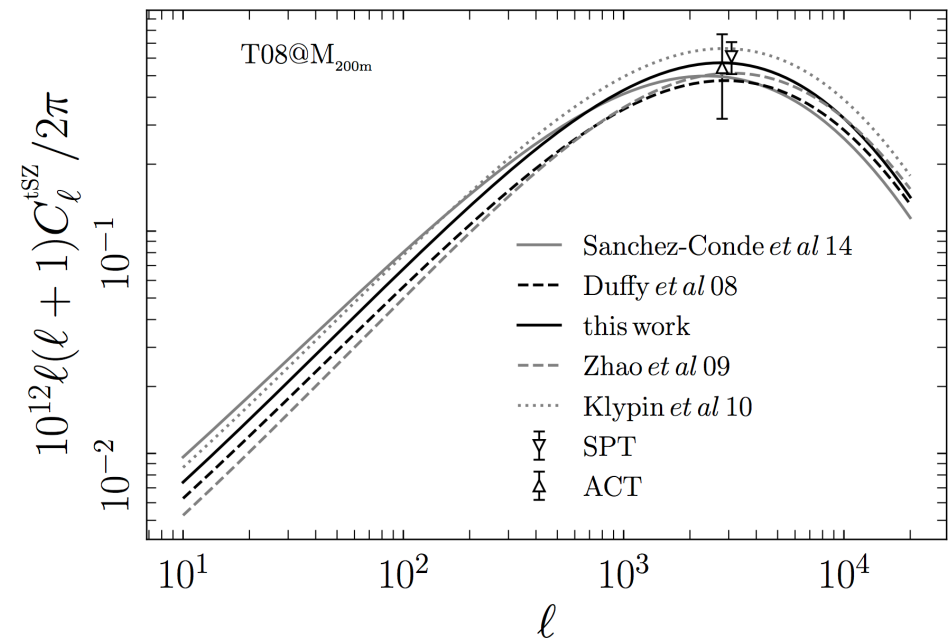
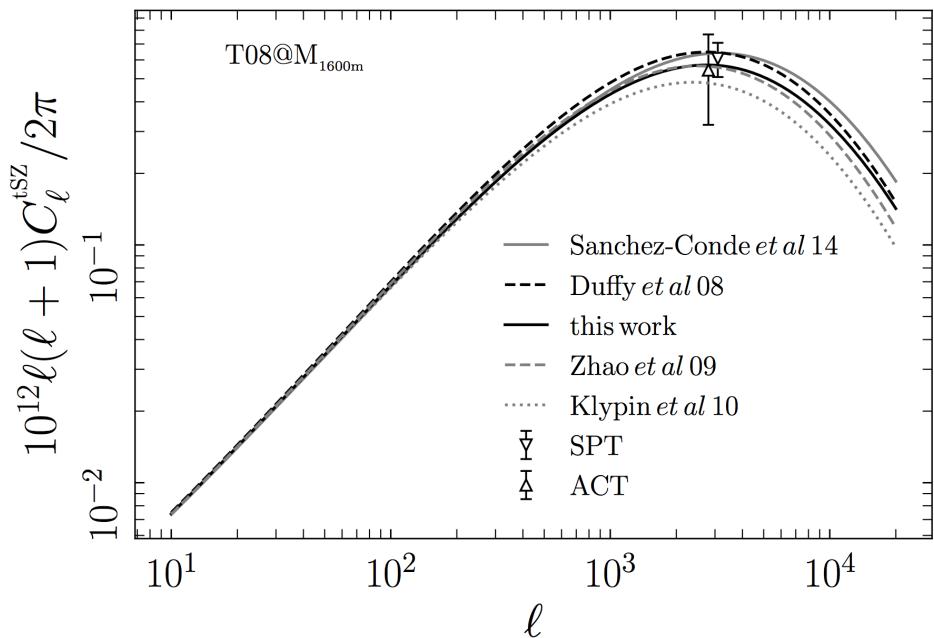


- T08 200m: lower SZ than T08 M500 => higher sigma8

- Why use T08 at M500?

→ Because pressure profile is calibrated at M500

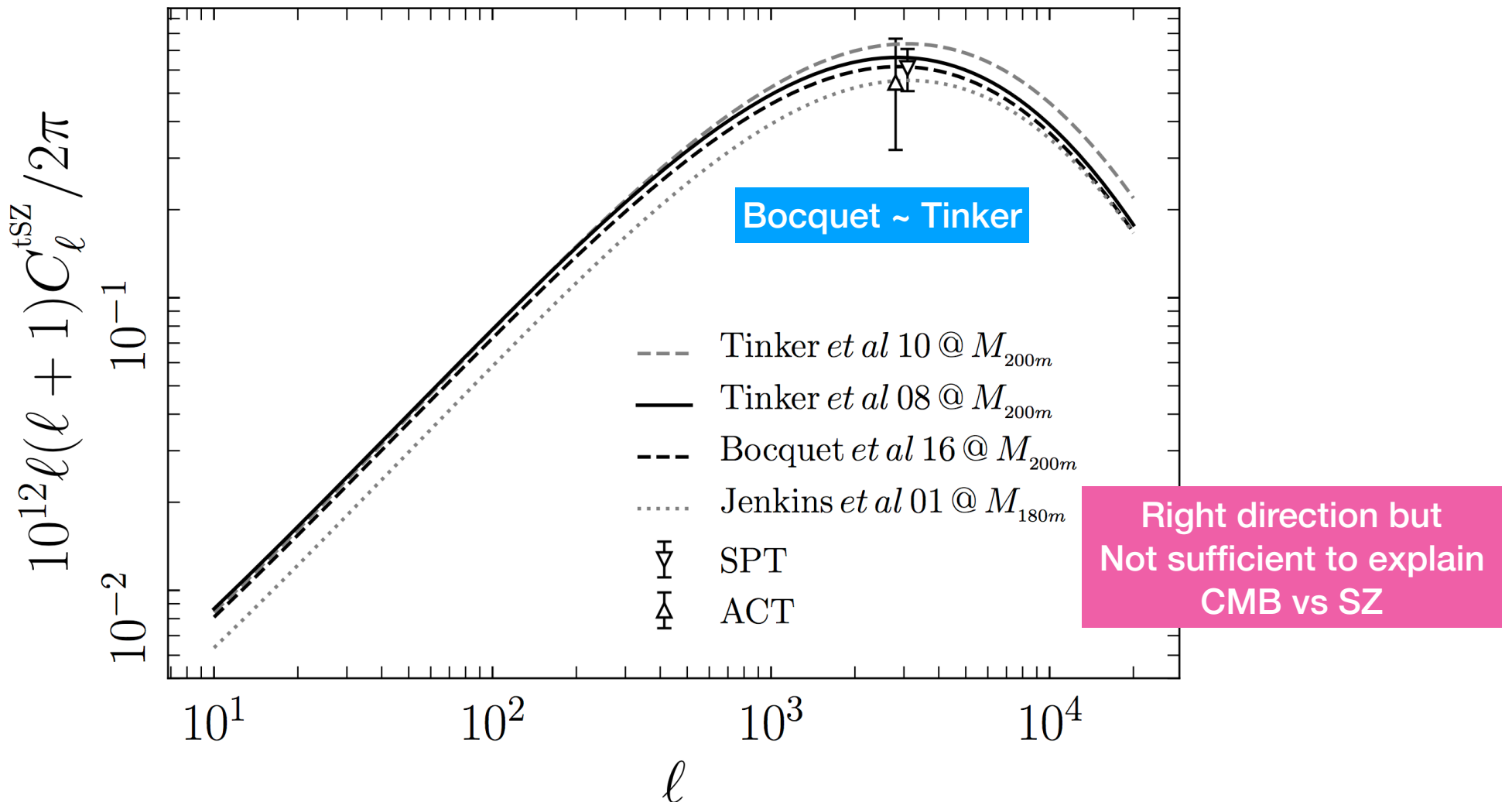
C-M relations agree at small radii but disagree at large radii



- C-M relations agree at small radii but disagree at large radii

→ Avoid mass conversion

- Bocquet et al [1502.07357]: New mass function with baryonic physics
- Compare tSZ for different mass functions



Consistent analysis of Planck y-map

With Barbara Comis, Eiichiro Komatsu, Juan Macias-Perez (2017) :

- Start from the Compton y-map 2015

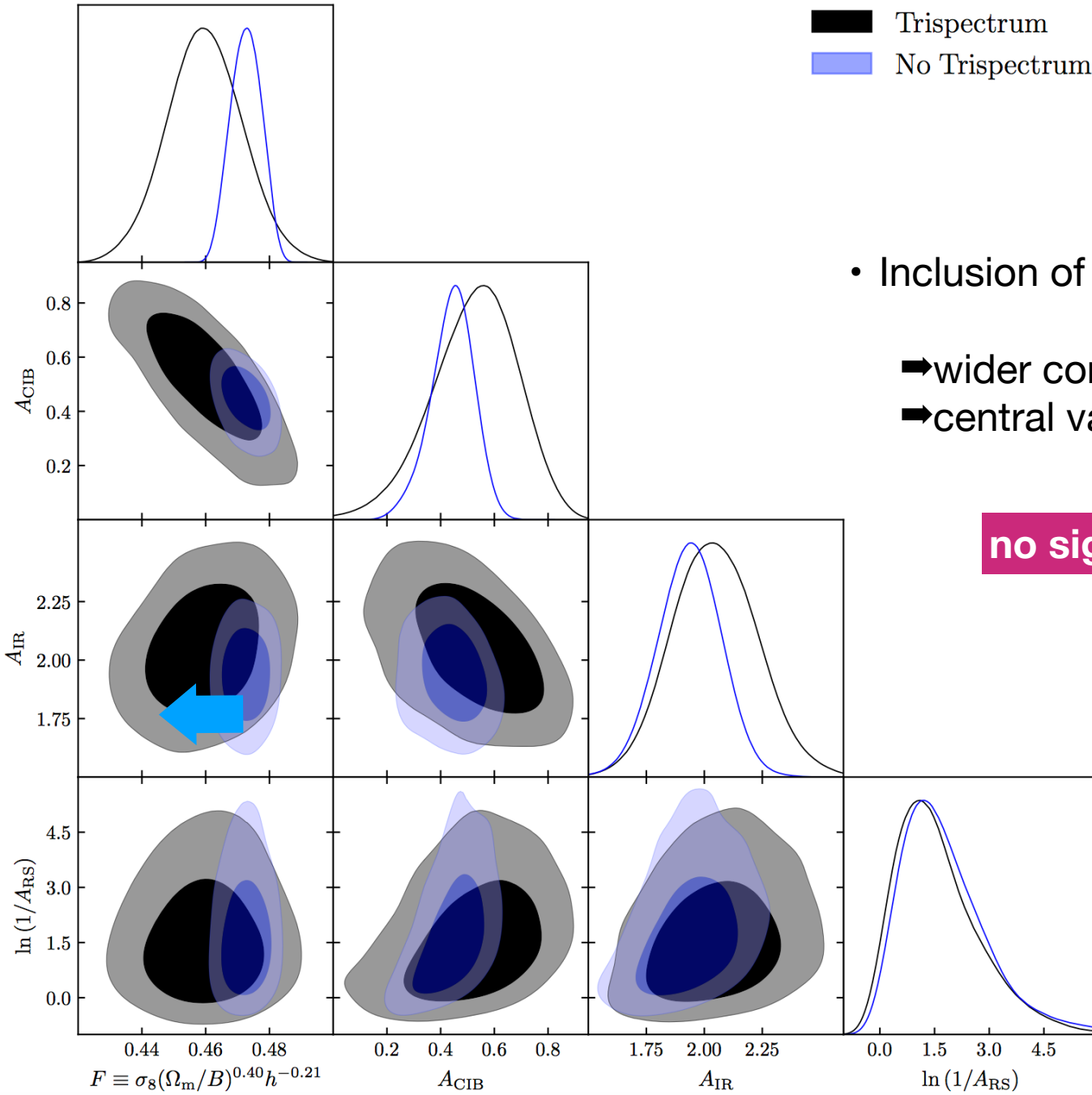
(diff. from Salvati et al 2018: fitted the marginalised Planck 2015 tSZ)

- No mass conversion

- Trispectrum

$$M_{aa'} = \left(\sigma_{\ell_{\text{eff}}^a}^{y^2} \right)^2 \delta_{aa'} + \frac{\ell_{\text{eff}}^a (\ell_{\text{eff}}^a + 1) \ell_{\text{eff}}^{a'} (\ell_{\text{eff}}^{a'} + 1)}{4\pi^2} \frac{T_{aa'}}{4\pi f_{\text{sky}}}$$

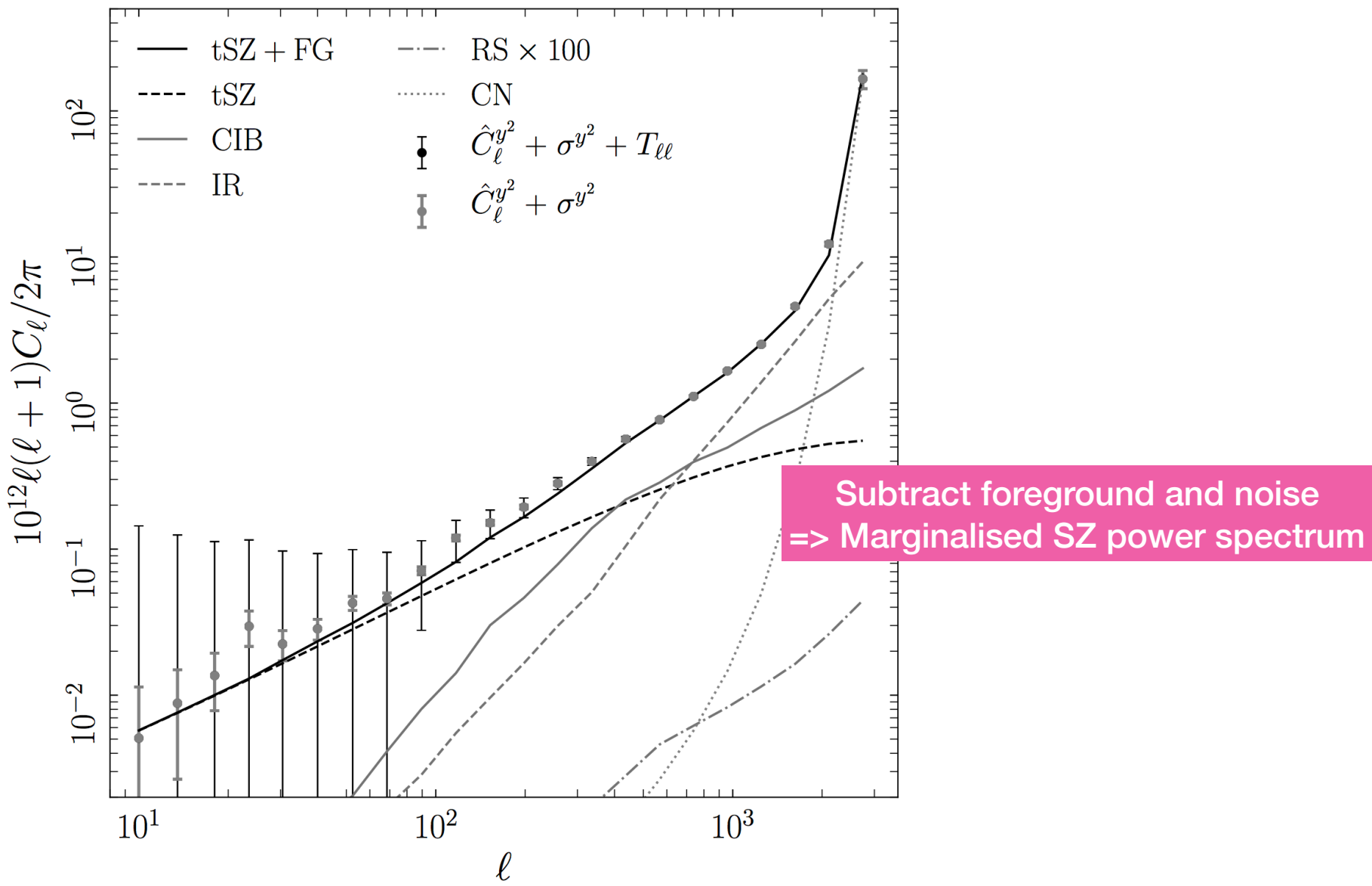
$$T_{\ell\ell'} = \int dz \frac{dV}{dz d\Omega} \int d\ln M \frac{dn}{d\ln M} |y_\ell(M, z)|^2 |y_{\ell'}(M, z)|^2$$



- Inclusion of trispectrum:
 - wider confidence level interval
 - central value shifts downward

no sign of larger sigma8

$\sim \sigma_8$



Planck 2015 marginalised power spectrum

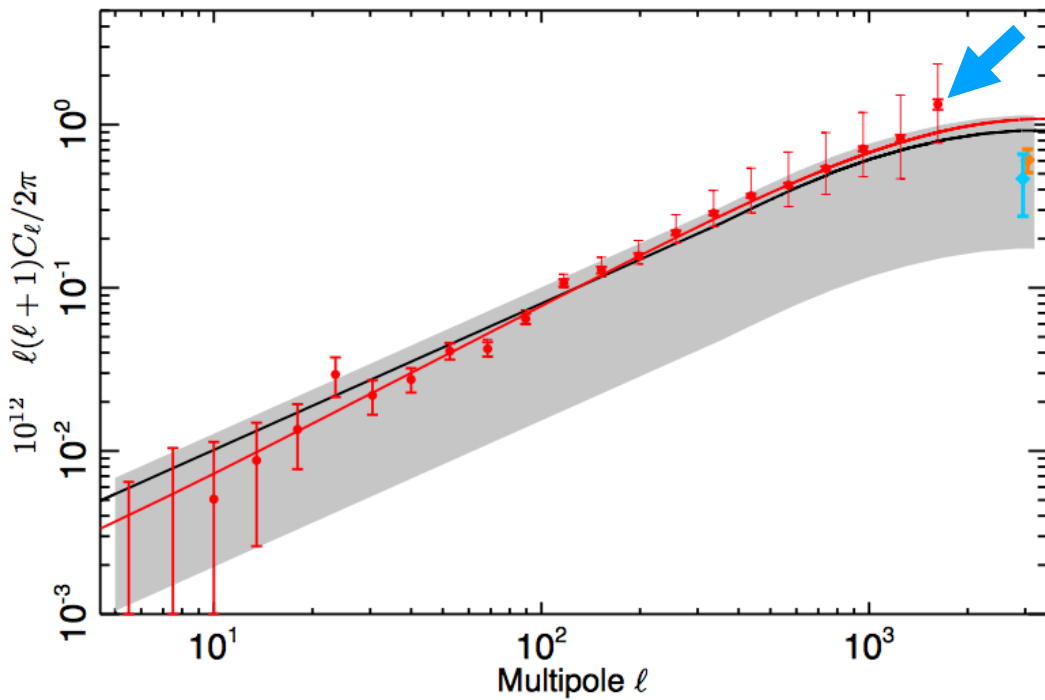


Fig. 17: NILC - MILCA F/L cross-power spectrum after foreground subtraction (red points), compared to the Atacama Cosmology Telescope (ACT; cyan dot) and the South Pole Telescope (SPT; orange, [George et al., 2014](#)) power spectrum estimates. The black line shows the tSZ power spectrum template (EM12 [Efstathiou & Migliaccio, 2012](#)) used in the *Planck* CMB cosmological analysis ([Planck Collaboration XVI, 2014](#); [Planck Collaboration XI, 2015](#)) with its best fit amplitude $A_{t\text{SZ}}$ ([Planck Collaboration XI, 2015](#)), the grey region allows comparison with the 2σ interval.

Note: we don't use this point in our analysis

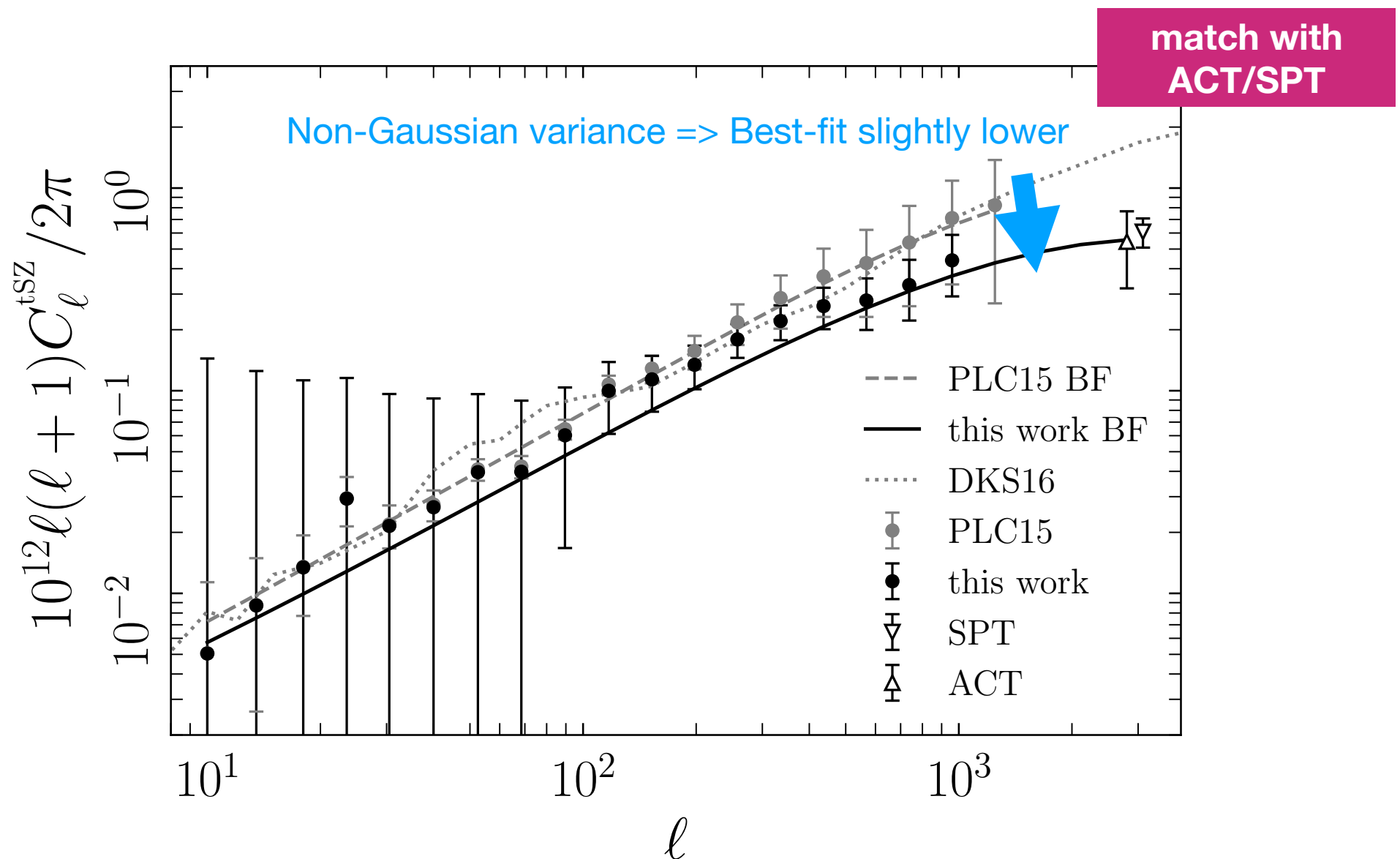
The Planck CMB likelihood has three ‘nuisance’ parameters related to the SZ effect ([Planck Collaboration 2014, 2016a](#)): $\xi^{\text{tSZ} \times \text{CIB}}$ to account for the correlation between SZ and CIB foregrounds; A^{kSZ} for the amplitude of the kinetic SZ power spectrum; and A^{tSZ} for the amplitude of the thermal SZ power spectrum in μK^2 at $\ell = 3000$. The template for the SZ power spectrum used in the Planck CMB likelihood is the model of [Efstathiou & Migliaccio \(2012\)](#) (with pressure profile evolution parameter $\epsilon = 0.5$) rescaled to unity at $\ell = 3000$ ². Motivated by a SPT measurement ([Reichardt et al. 2012](#)), the Planck CMB likelihood has a conservative Gaussian prior on the linear combination

$$A^{\text{kSZ}} + 1.6A^{\text{tSZ}} = (9.5 \pm 3)\mu\text{K}^2 \quad (13)$$

([Planck Collaboration 2016b](#)) as well as a uniform prior on $\xi^{\text{tSZ} \times \text{CIB}}$ between 0 and 1 (justified by the constraint of [George et al. 2015](#)). In this work, we use the same settings

² The amplitude of the [Efstathiou & Migliaccio \(2012\)](#) model is $\mathcal{D}_{3000} = 4.796 \mu\text{K}^2$ at 143 GHz.

Updated marginalised SZ power spectrum



Consistency between Planck y-map power spectrum and cluster analyses

Parameter combinations

Given data, there is a combination that **minimises fractional error**

- SPT-SZ (Bocquet et al 2018):

$$S_8^{0.2} \equiv \sigma_8(\Omega_m/0.3)^{0.2} \quad \rightarrow \quad 3\%$$

- Planck SZ **clusters** with varying bias:

$$F^* \equiv \sigma_8(\Omega_m/B)^{0.35} \quad \rightarrow \quad 1.5\%$$

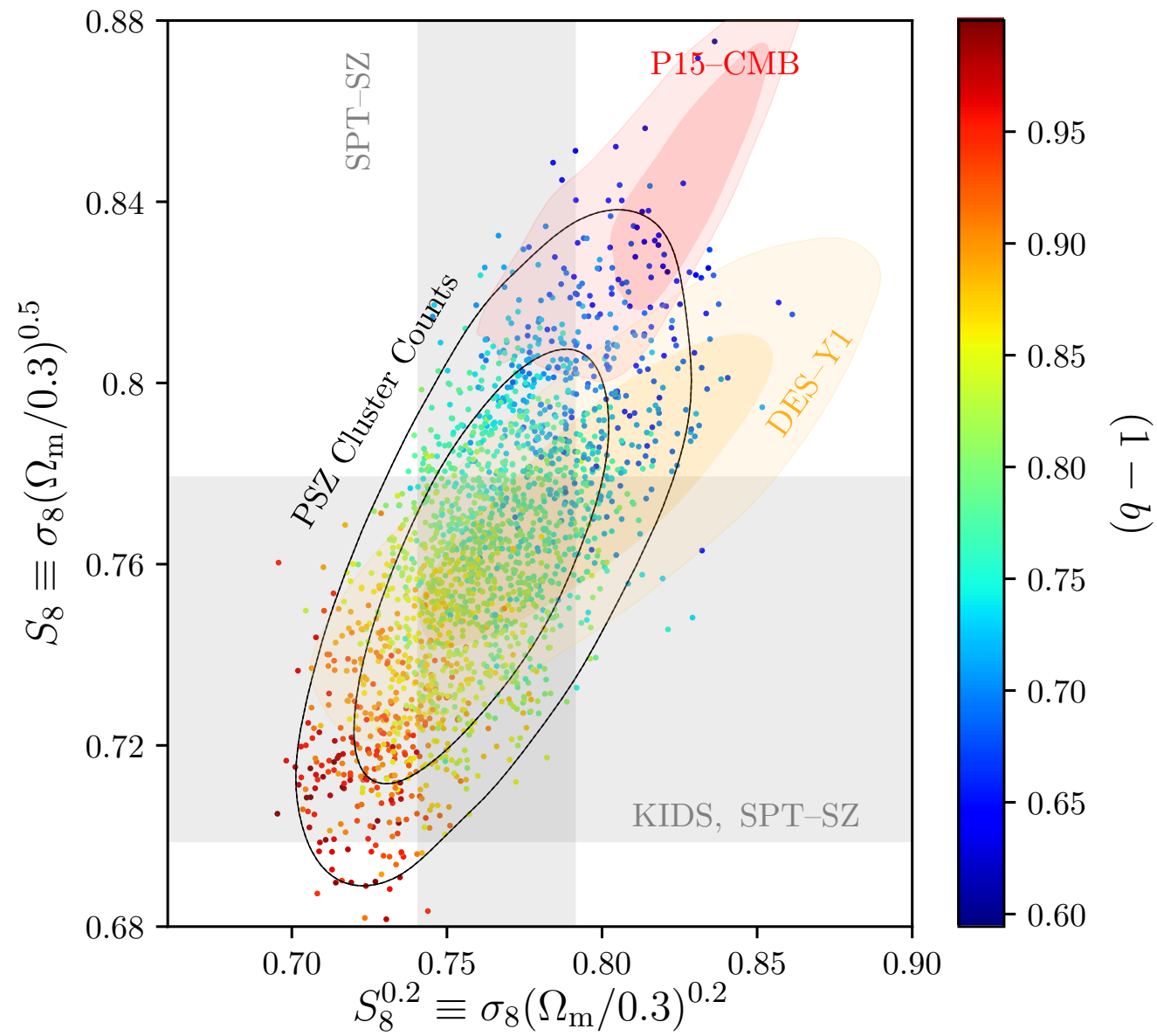
- Planck SZ **y-map** power spectrum:

$$F \equiv \sigma_8(\Omega_m/B)^{0.4} h^{-0.2} \quad \rightarrow \quad 3\%$$

- LSS:

$$S_8 \equiv \sigma_8(\Omega_m/0.3)^{0.5}$$

Planck Cluster Counts



Planck SZ power spectrum = Planck SZ cluster counts

With this prior, our analysis of Planck SZ cluster counts yields

$$S_8^{0.2} = 0.763 \pm 0.025 \text{ (68%CL)}, \quad (16)$$

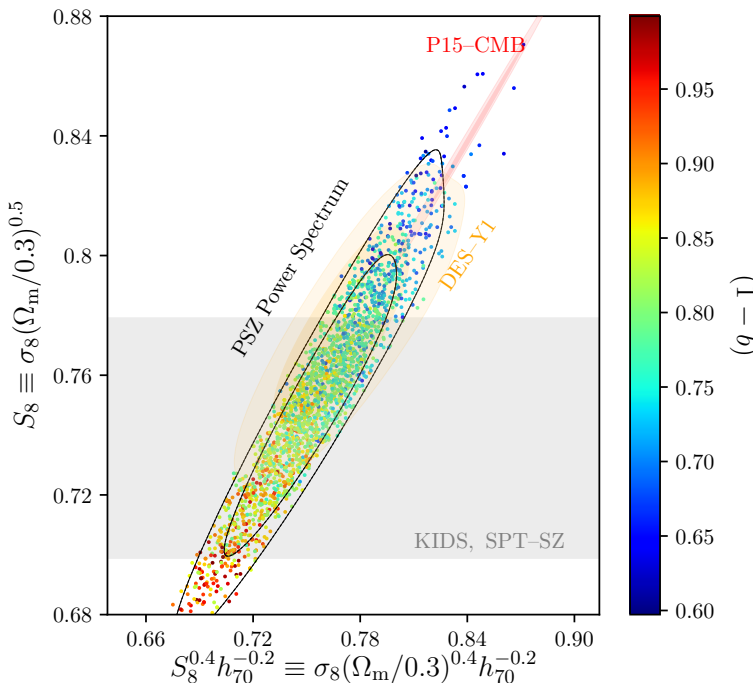
$$S_8 = 0.764 \pm 0.029 \text{ (68%CL)}. \quad (17)$$

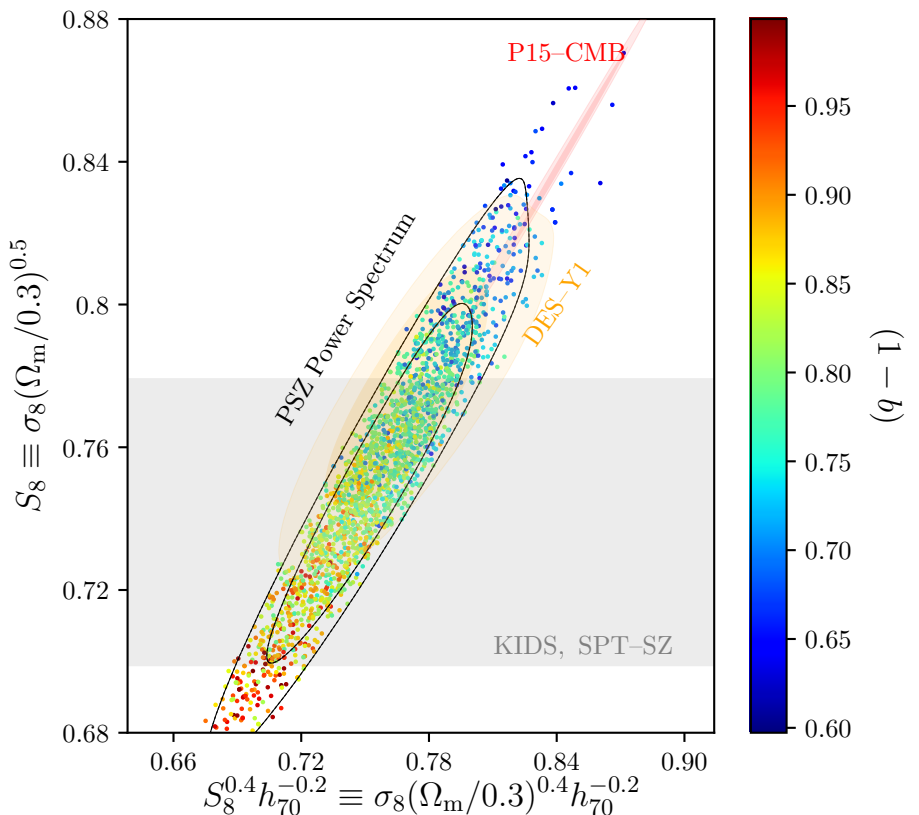
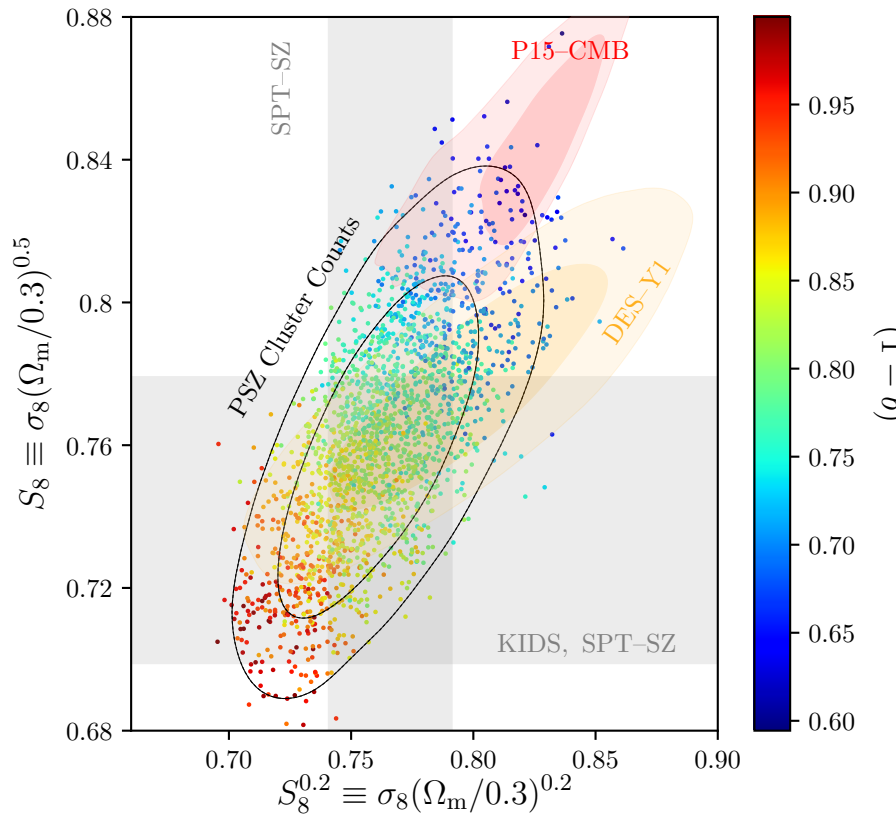
Our analysis of Planck y -map power spectrum yields

$$S_8^{0.4} h_{70}^{-0.2} = 0.756 \pm 0.033 \text{ (68%CL)}, \quad (18)$$

$$S_8 = 0.752 \pm 0.034 \text{ (68%CL)}. \quad (19)$$

[Bolliet, Brinckmann, Lesgourgues, Chluba (to appear)]





Planck SZ cluster and y-map + $(1-b)=0.80\pm0.08$ ~ SPT ~ DES ~ KIDS
 \neq
Primary CMB

SUMMARY

Planck SZ data ~ small tension with Planck primary CMB

SZ
(Planck, SPT)

$$\sigma_8 = 0.76 \pm 0.03$$

CMB

$$\sigma_8 = 0.811 \pm 0.006$$

(PLC18 [1807.06209])

$$\sigma_8 = 0.84 \pm 0.02$$

(PLC15 high-ell TT-TE-EE, low ell TT, tau prior)

CMB ~ 10% larger sigma8 =>

90% more clusters

80% more SZ power

But our SZ constraint is degenerate with bias...

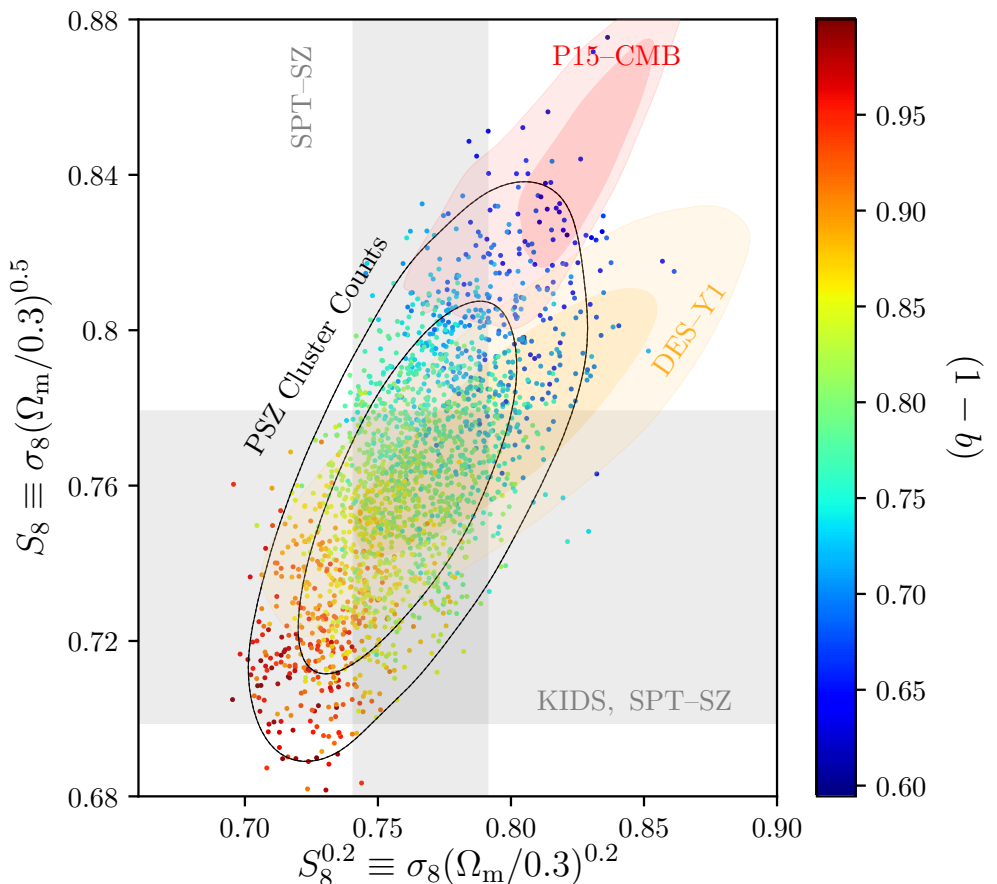
Assume cosmo fixed by CMB:

Which bias is required to explain SZ data?

all analyses agree >30-40% mass bias

(see e.g., Planck, Salvati, Bolliet, Makya,++)

Can we understand 30-40% bias?



$$M^{\text{X-ray}} = (1 - b)M^{\text{true}}$$

Bias = Hydrostatic + Calibration

CCCP The Canadian Cluster Comparison Project

Hoekstra [1502.01883]

Hydrostatic bias $\sim 20\%$ on average (10% to 30% depending on cluster)

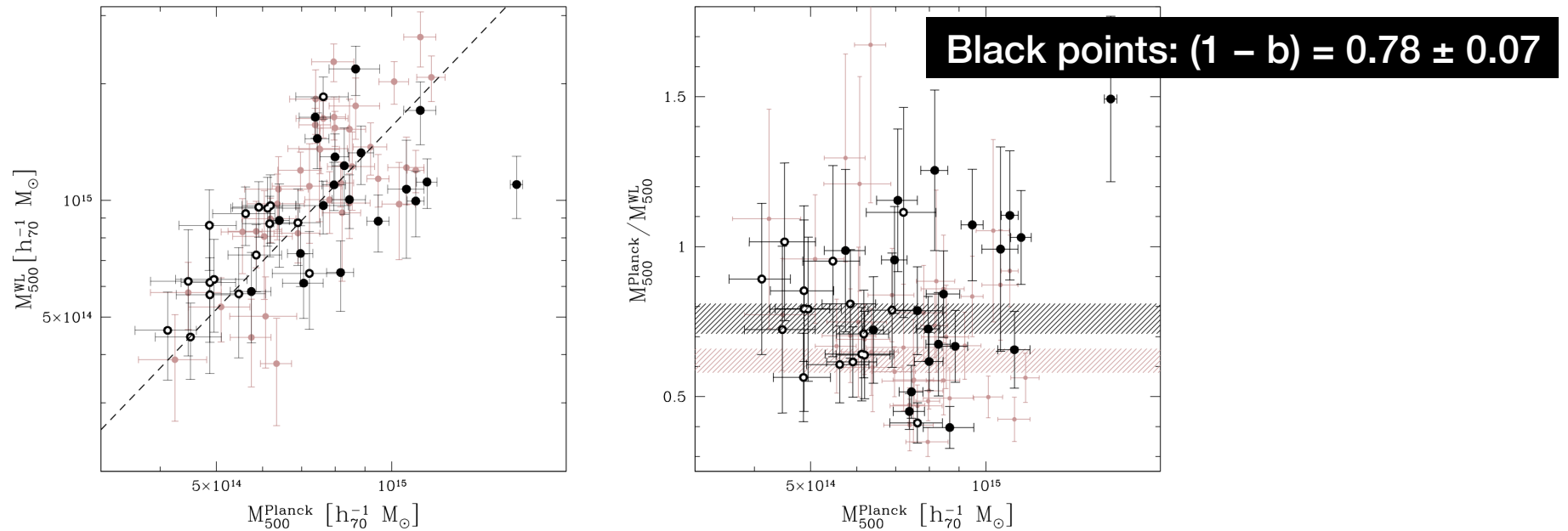


Figure 21. *Left panel:* the deprojected aperture mass M_{500} from weak lensing as a function of the hydrostatic mass from Planck Collaboration et al. (2014a). Note that M_{500}^{Planck} is measured using r_{500} from the estimate of Y_X , and M_{500}^{WL} is determined using the lensing derived value for r_{500} . The black points show our CCCP measurements, with the filled symbols indicating the clusters detected by *Planck* with a signal-to-noise ratio $SNR > 7$ and the open points the remainder of the sample. The dashed line shows the best-fit power law model. The WtG results are shown as rosy brown colored points. *Right panel:* ratio of the hydrostatic and the weak lensing mass as a function of mass. The dark hatched area indicates the average value of 0.76 ± 0.05 for the CCCP sample, whereas the rosy brown colored hatched region is the average for the published WtG measurements, for which we find 0.62 ± 0.04 .

Hyper Suprime-Cam Weak Lensing: $(1 - b) = 0.80 \pm 0.14$

Medezinski et al [1706.00434]

X-ray calibration and systematics

- assumption of spherical symmetry few %
- hydrostatic mass bias < 10 - 30%
- gas temperature inhomogeneities few - 10-15%
- gas clumping few %
- absolute X-ray temperature calibration 15-20%

Pratt et al [1902.10837]

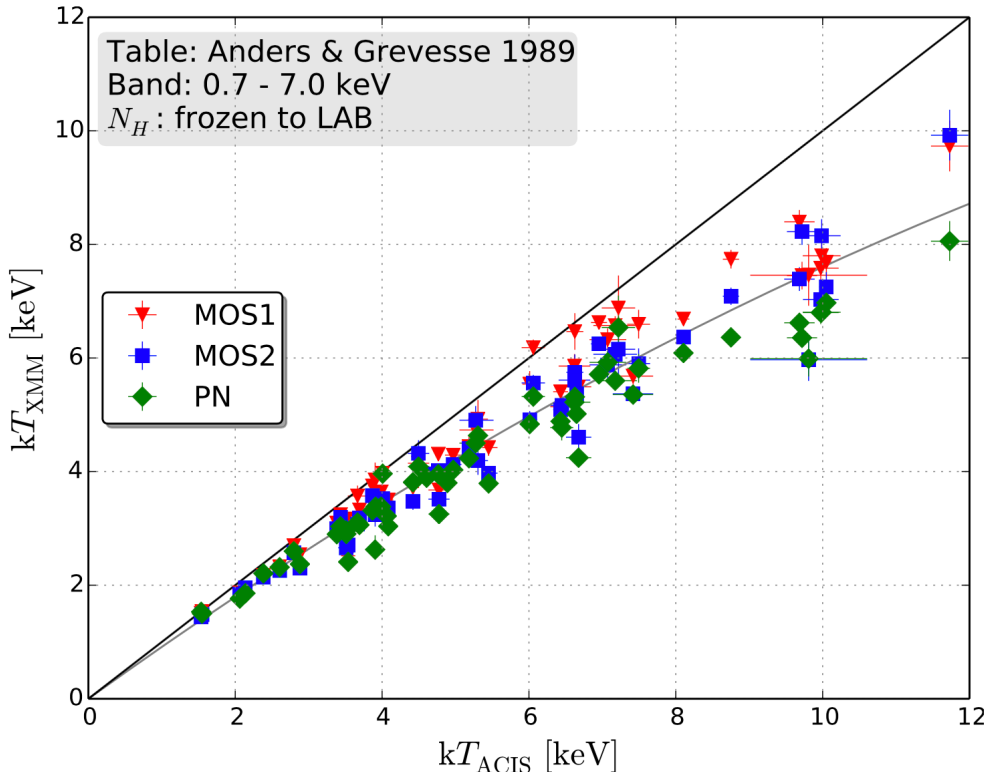
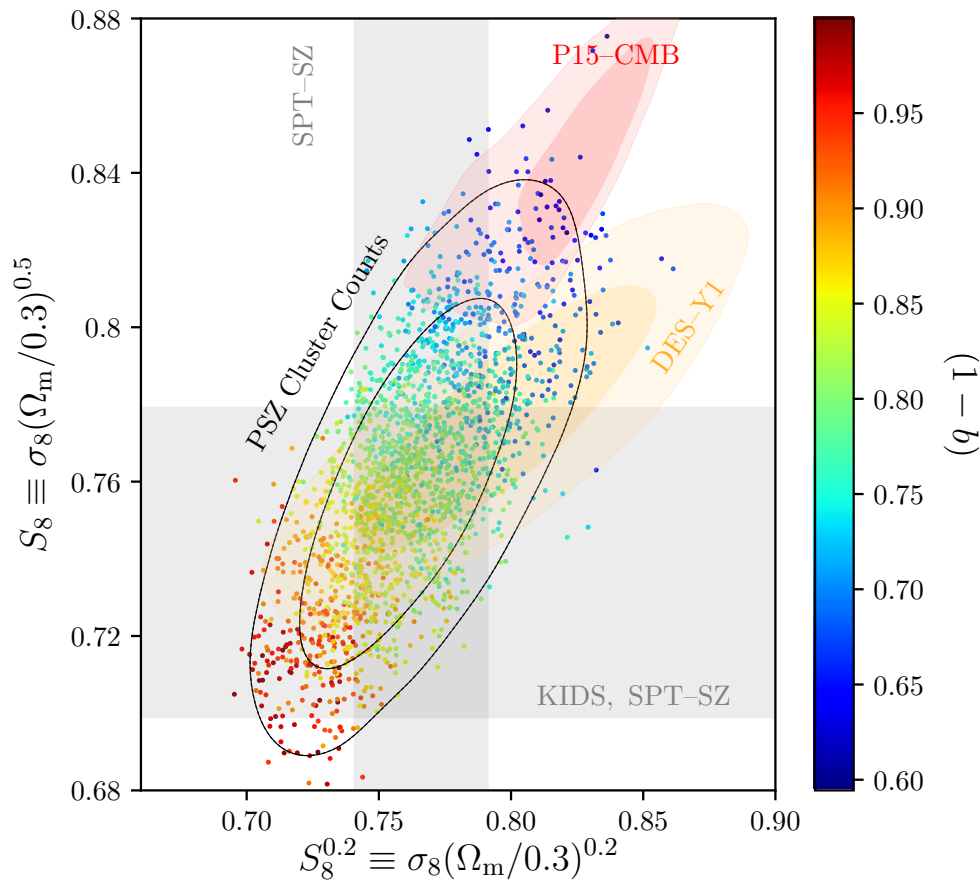


Fig. 7 ICM gas temperatures measured with the three XMM-*Newton* instruments (MOS1, MOS2, and PN) plotted against temperatures measured with *Chandra*/ACIS for the same regions. The black line is the one-to-one relation. Reproduced from Schellenberger et al. (2015).

Bias = 20 % Hydrostatic + 15% Calibration = 35%

- Solution to tension: Bias = 20 % Hydrostatic + 15% Calibration = 35%
- Solution = changing X-ray mass => works only for Planck SZ



- Other solutions:
 - less-Dark energy
 - more-Massive neutrino
- > smaller sigma8 inferred from CMB

Less-Dark Energy

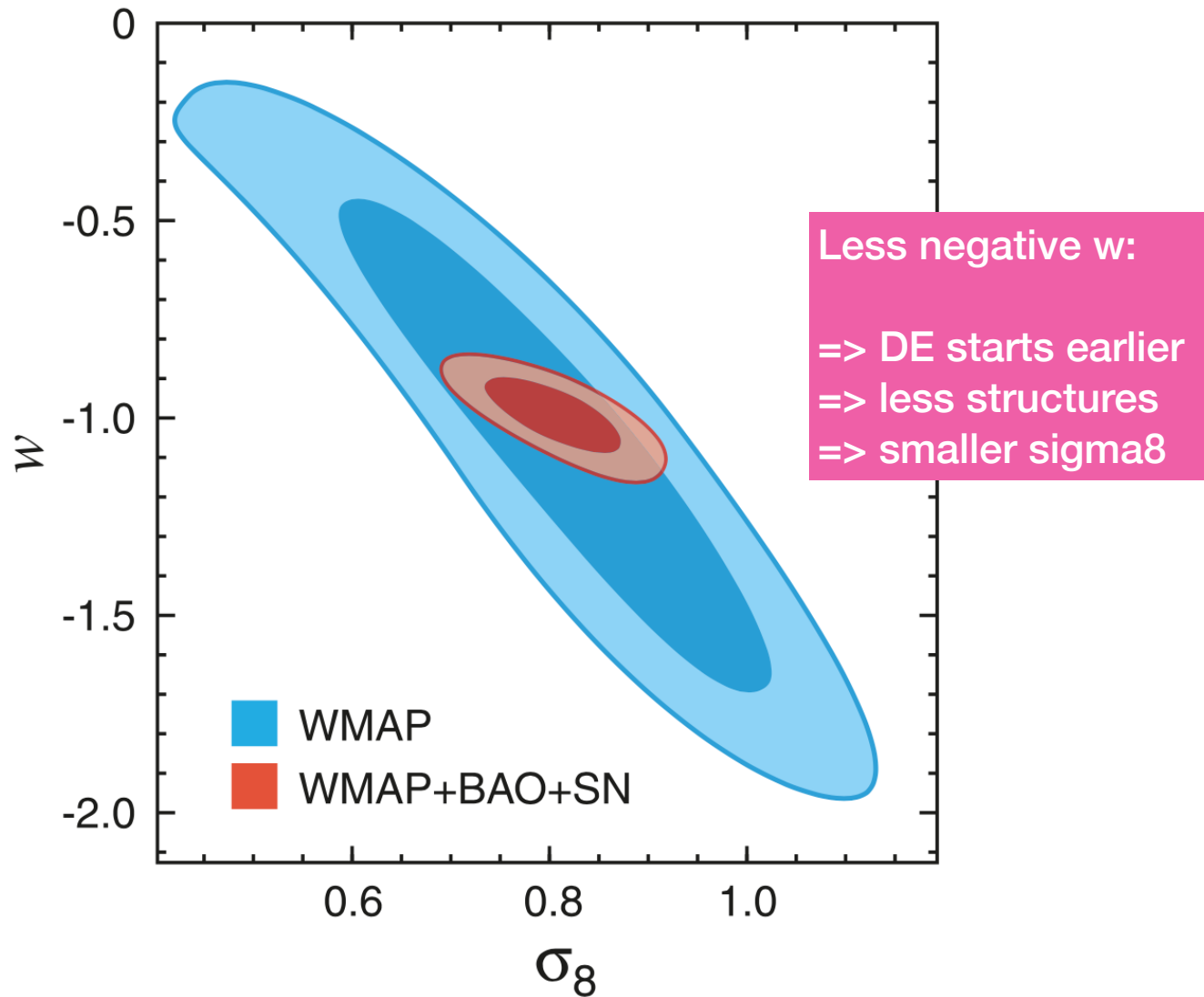


Figure from WMAP 5-years [0803.0547]

More-Massive neutrinos

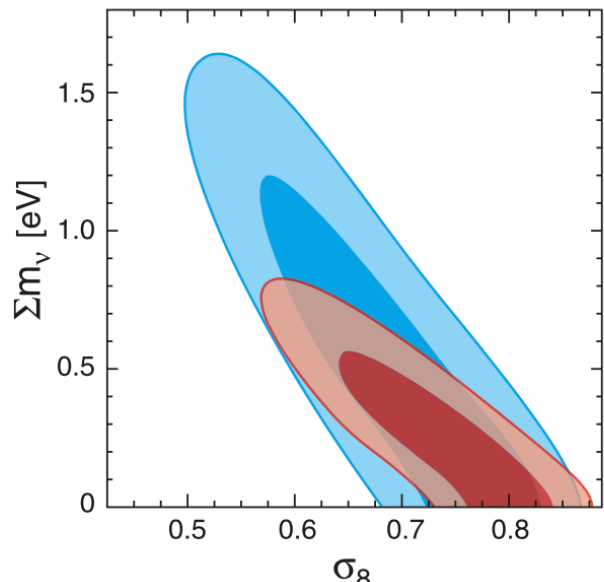
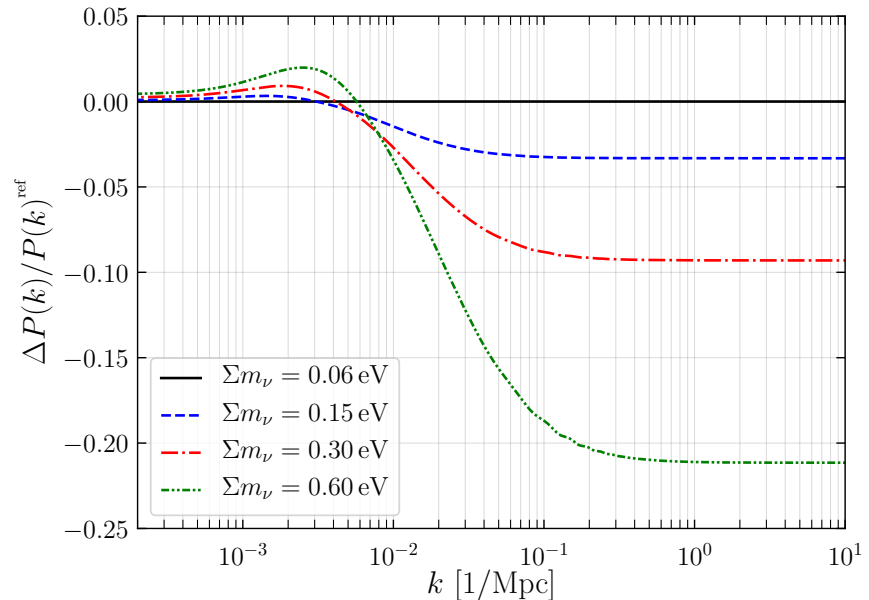


Figure from WMAP 5-years [0803.0547]



Massive neutrinos:

- => warm DM
- => thermal velocity
- => free-streaming
- => damp small-scale power

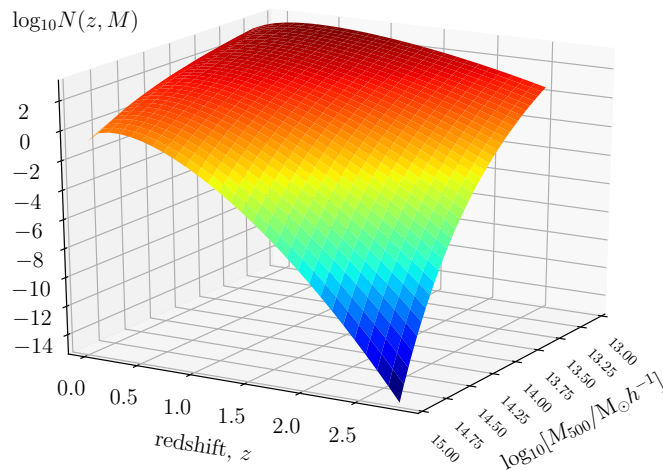
more-massive neutrinos = more damping

$$\Delta\sigma_8/\sigma_8 \approx -4f_\nu$$

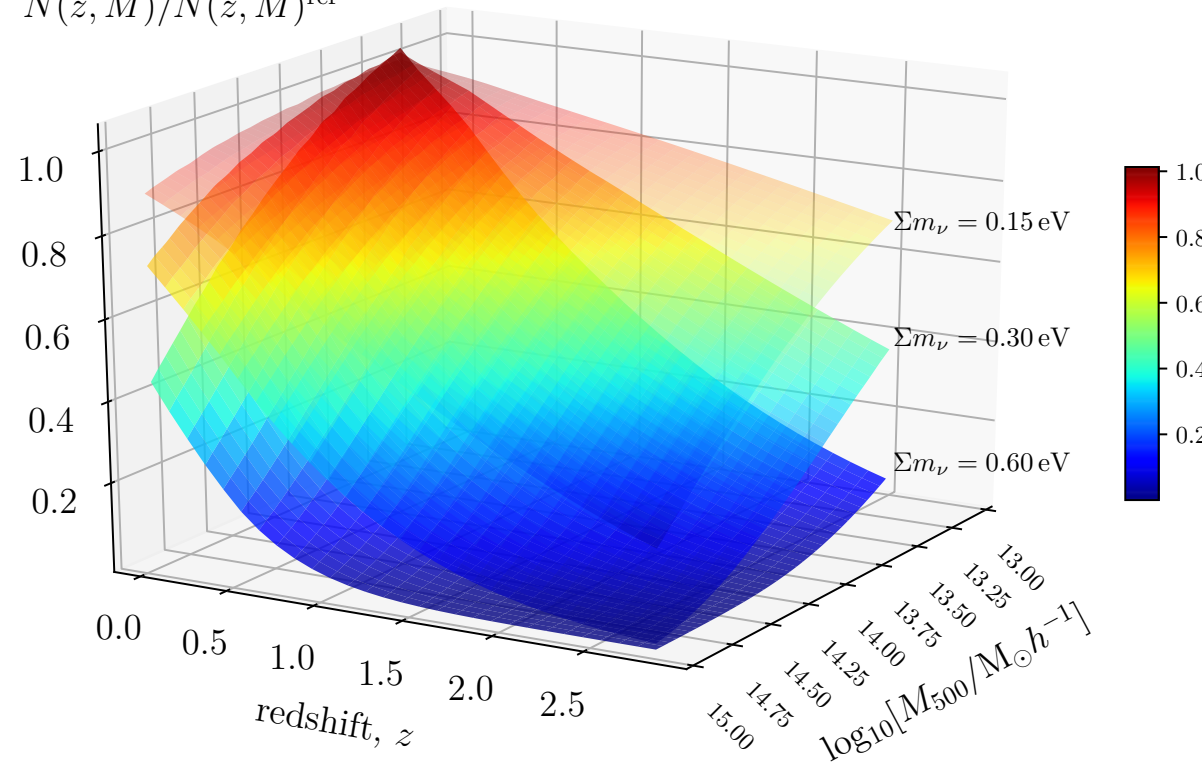
$$f_\nu \equiv \frac{\Omega_\nu}{\Omega_m}$$

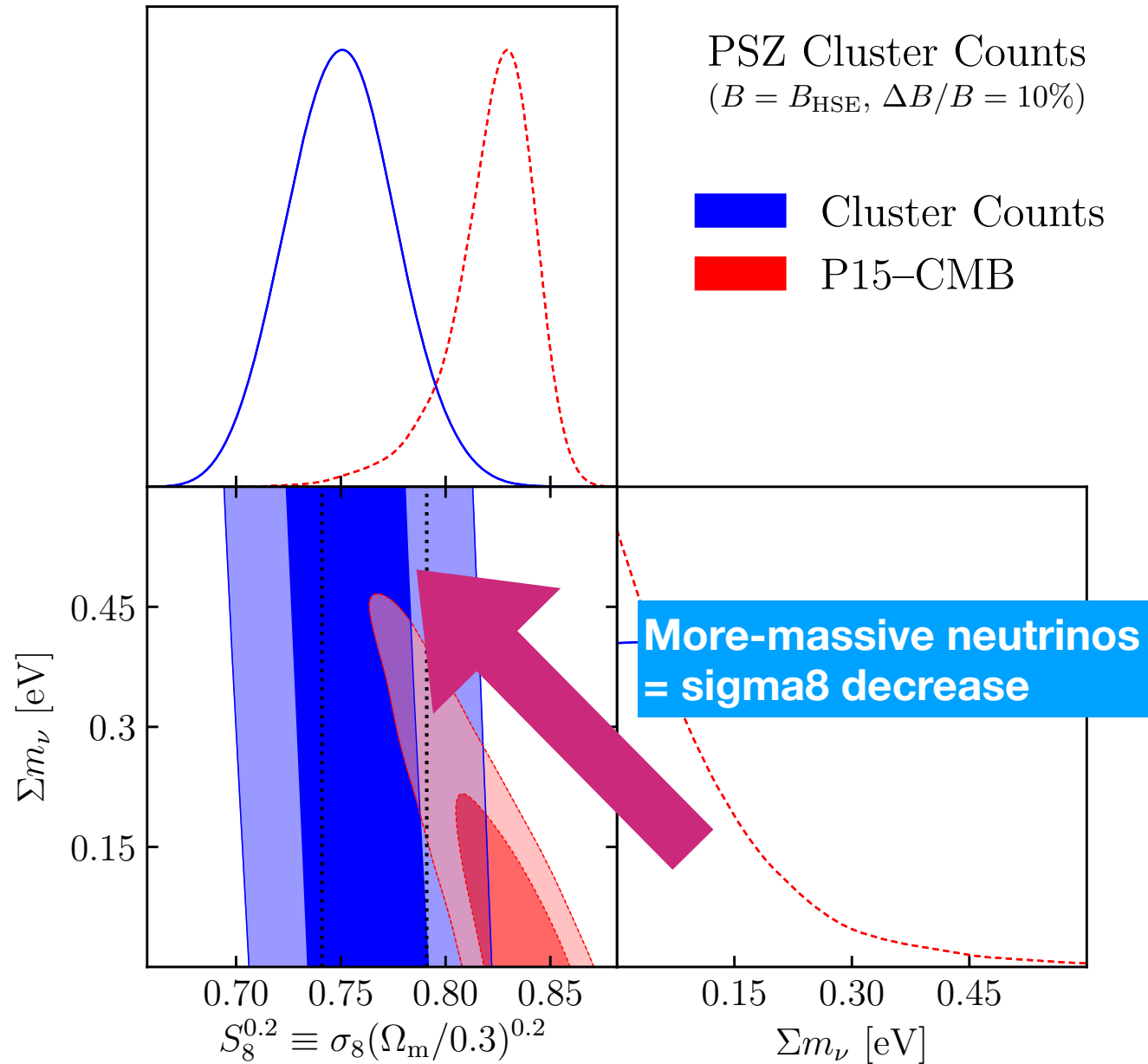
$$\Omega_\nu = \frac{\rho_\nu^0}{\rho_{\text{crit}}^0} = \frac{\sum m_\nu}{93.14 h^2 \text{ eV}},$$

More-Massive neutrinos



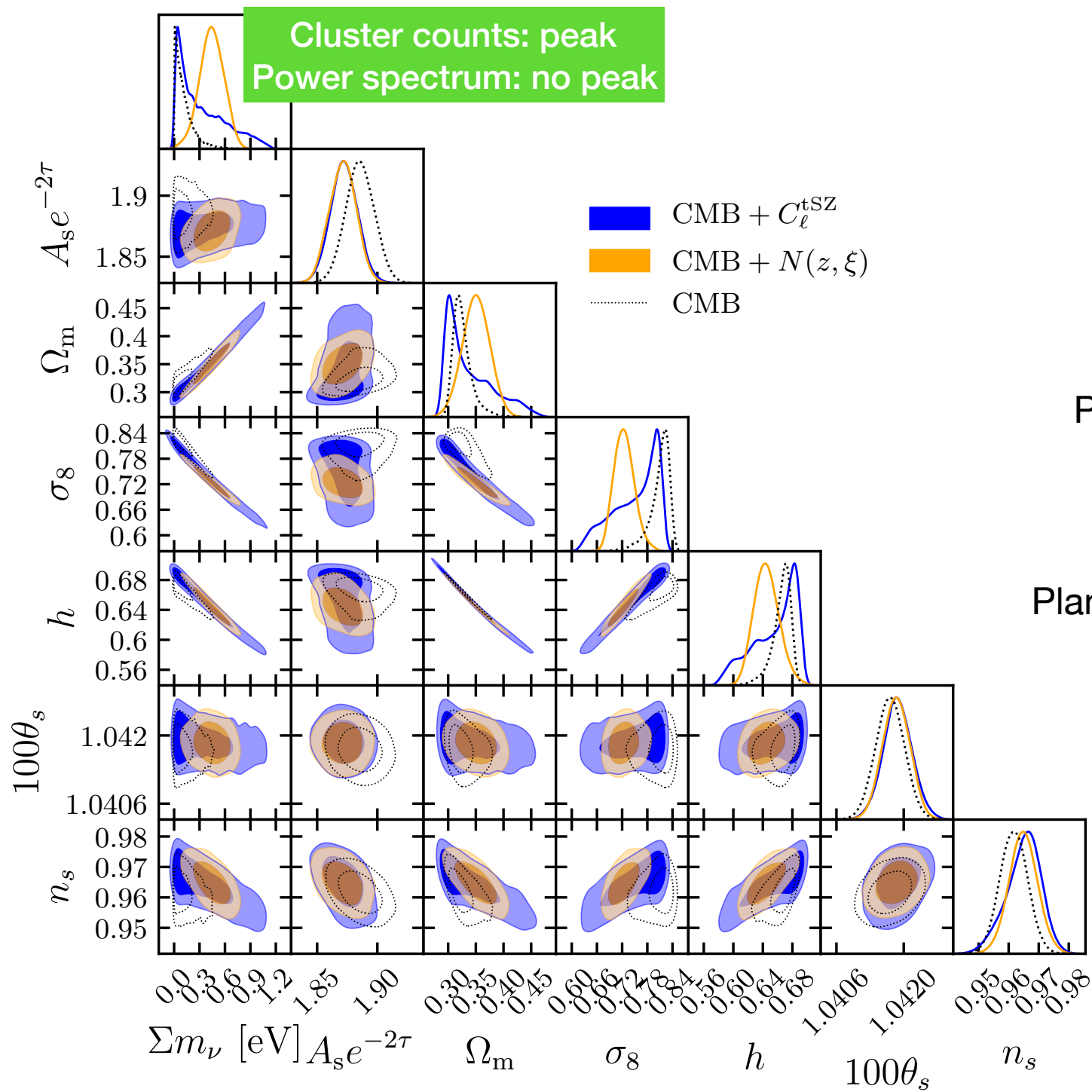
$$N(z, M)/N(z, M)^{\text{ref}}$$





SZ + CMB
in nuLCDM?

$M_{\nu} \sim 0.4\text{eV}$



Planck SZ clusters:

$$F^* \equiv \sigma_8(\Omega_m/B)^{0.35}$$

Planck SZ power spectrum:

$$F \equiv \sigma_8(\Omega_m/B)^{0.4} h^{-0.2}$$

In reality mass bias is not fixed: scatter + uncertainties = $\sim 10\%$ precision

SZ + CMB with 10% precision on bias, i.e., $(1-b)=0.80\pm0.08$

for Primary CMB combined with SZ cluster counts we find

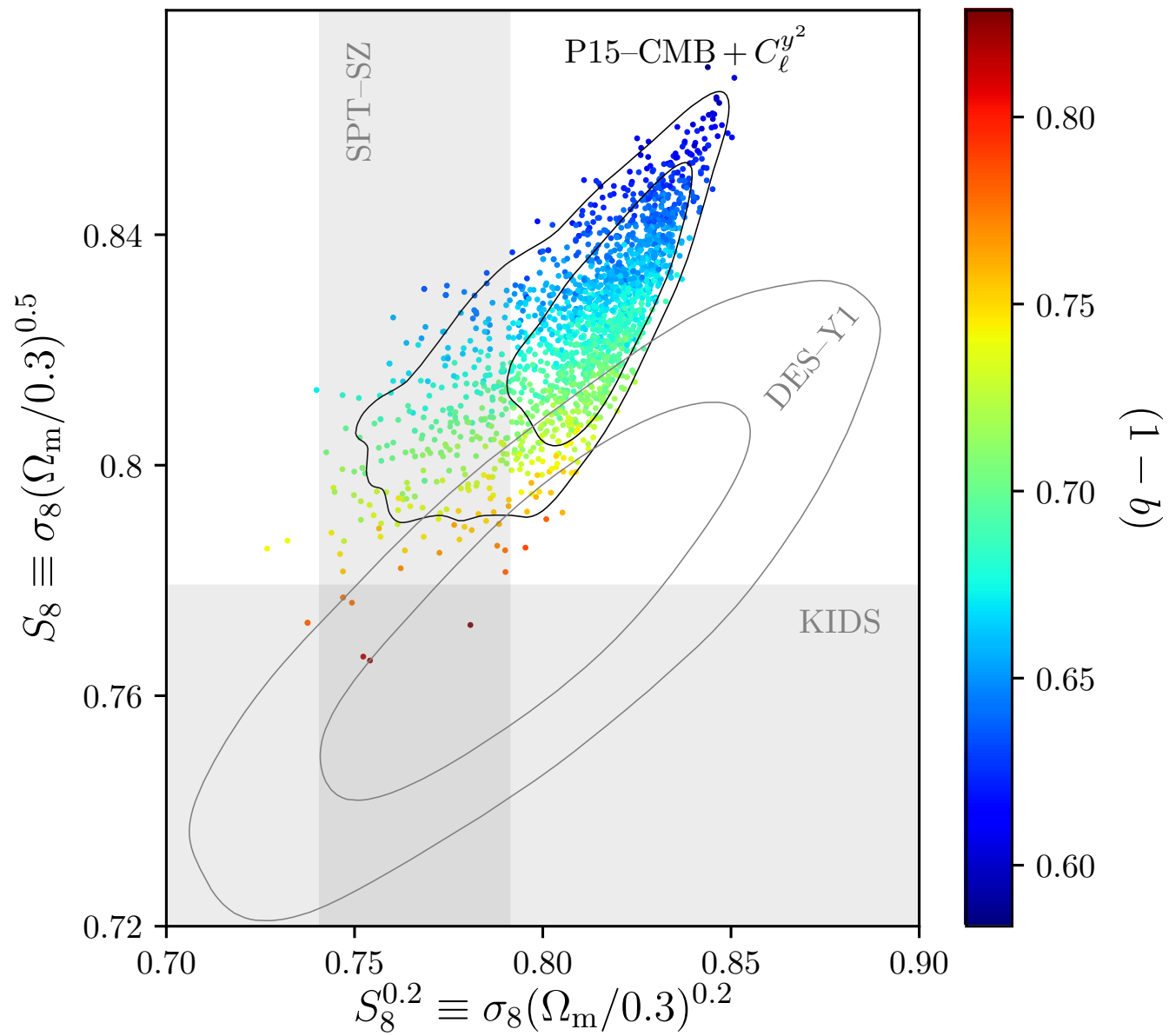
$$(1 - b) = 0.68^{+0.03}_{-0.04} \text{ (68\%CL)},$$
$$\Sigma m_\nu < 0.37 \text{ eV} \quad (95\%CL).$$

And with Planck y -map power spectrum we find

$$(1 - b) = 0.69 \pm 0.03 \text{ (68\%CL)},$$
$$\Sigma m_\nu < 0.39 \text{ eV} \quad (95\%CL).$$

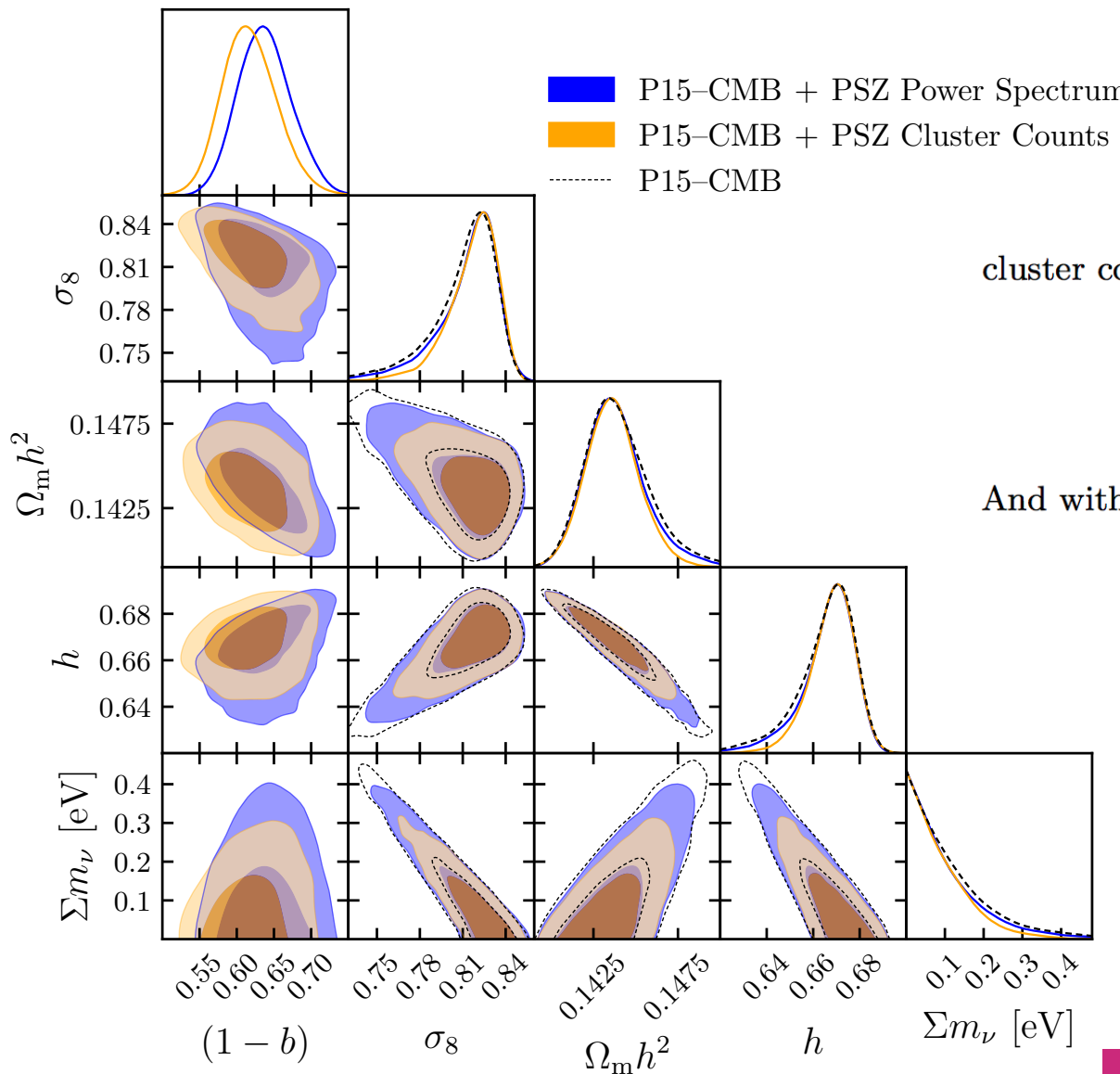
Data prefers to increase bias
(i.e., reduce $1-b$),
rather than increasing neutrino mass

No preferred value of neutrino mass for both cluster counts and power spectrum
(same conclusion as Salvati et al 2018)



Analysis with free mass-bias

Mass bias in LCDM with massive neutrinos



For Primary CMB combined with SZ cluster counts we find

$$\begin{aligned} F^* &= 0.464 \pm 0.006 & (68\% \text{CL}), \\ (1 - b) &= 0.62^{+0.03}_{-0.04} & (68\% \text{CL}), \\ \Sigma m_\nu &< 0.24 \text{ eV} & (95\% \text{CL}). \end{aligned}$$

And with Planck y -map power spectrum we find

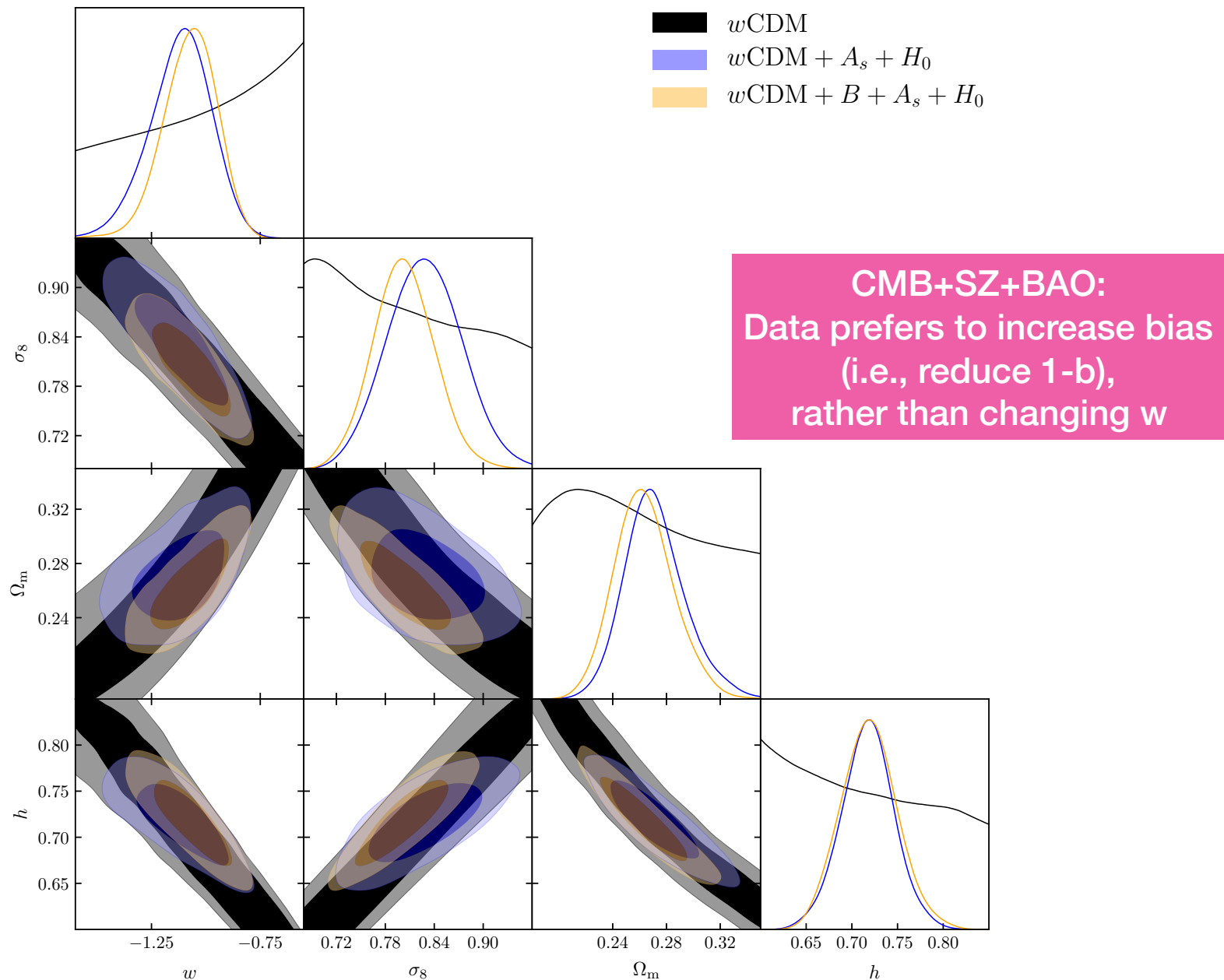
$$\begin{aligned} F &= 0.469^{+0.004}_{-0.003} & (68\% \text{CL}), \\ (1 - b) &= 0.64^{+0.03}_{-0.04} & (68\% \text{CL}), \\ \Sigma m_\nu &< 0.32 \text{ eV} & (95\% \text{CL}). \end{aligned}$$

[Bolliet, Brinckmann, Lesgourgues, Chluba (to appear)]

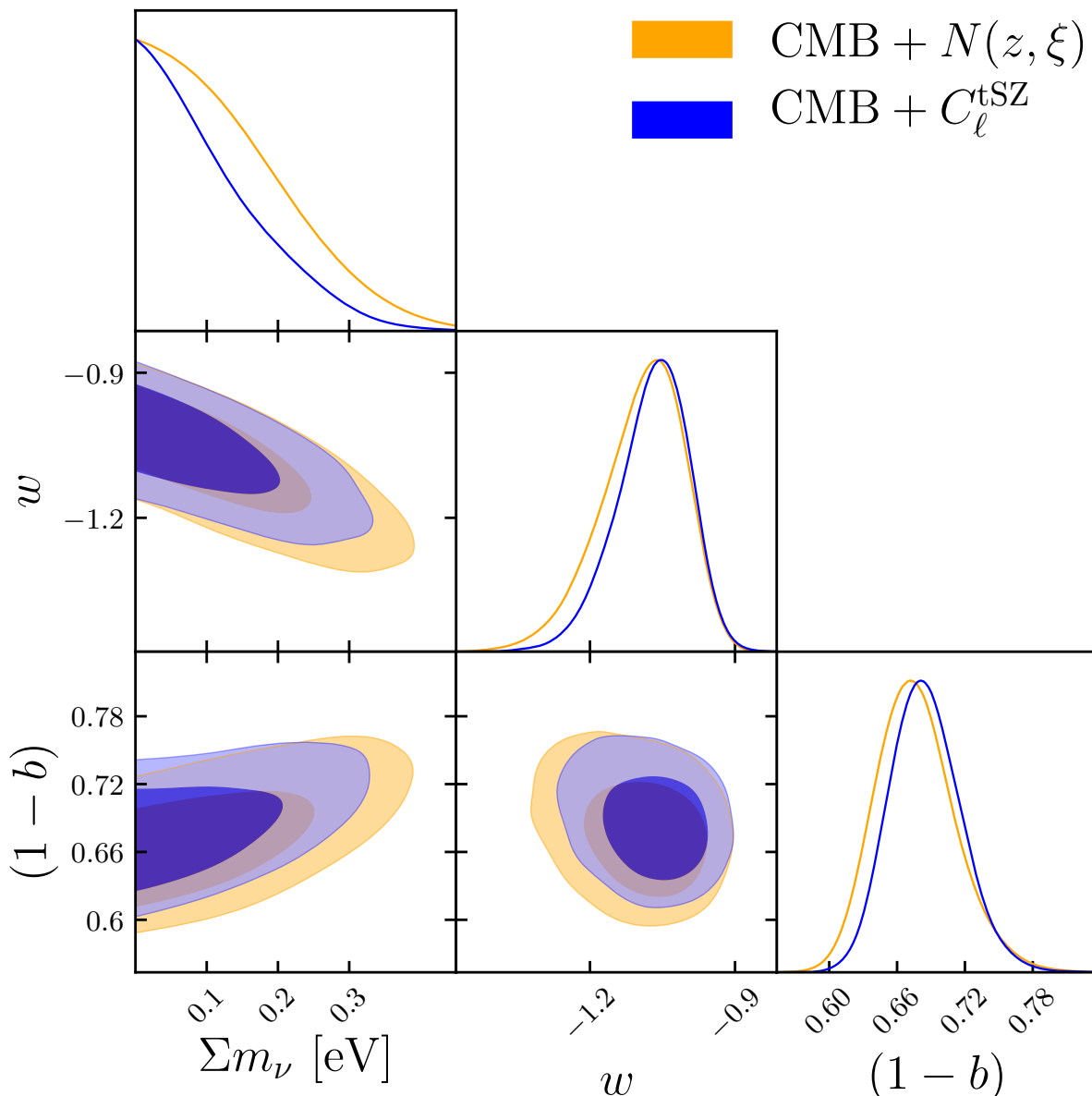
Remarkable consistency between power spectrum and cluster counts

Dark energy

Dark energy



Dark energy



CMB+SZ+BAO:
Data prefers to increase bias
(i.e., reduce $1-b$),
rather than changing w

Summary

$(1-b)=0.8$

- analytical work (Shi et al 2015)
- Hydro numerical simulation
- Weak lensing observation

with $(1-b)=0.8$

- Planck SZ agrees with SPT, DES, KIDS
- sigma8 from Planck SZ is 10% lower than from Planck Primary CMB

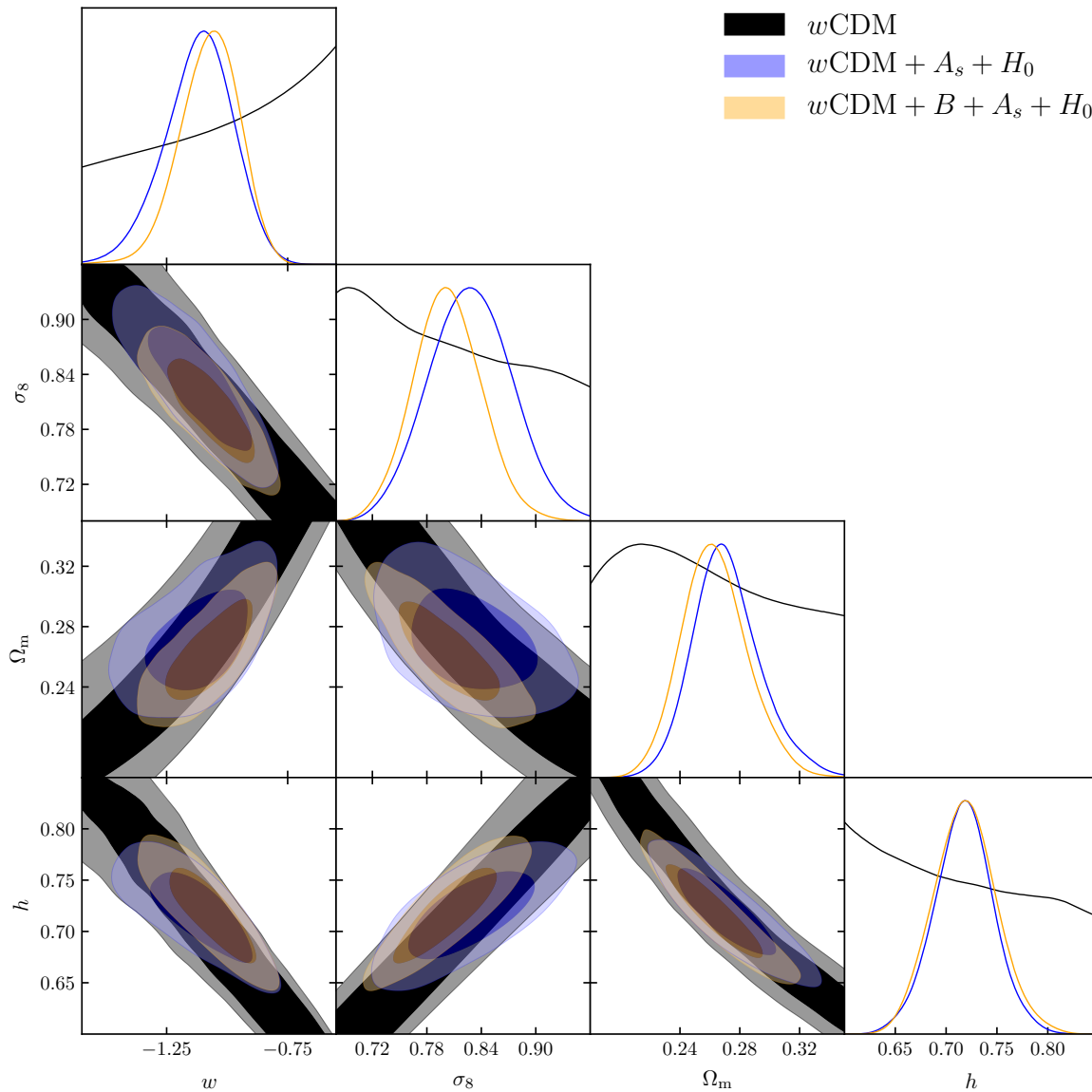
$(1-b)=0.6-0.7$

- preferred by CMB in LCDM, and extensions (neutrino, dark energy)

FUTURE OF SZ

Cosmological constraints?

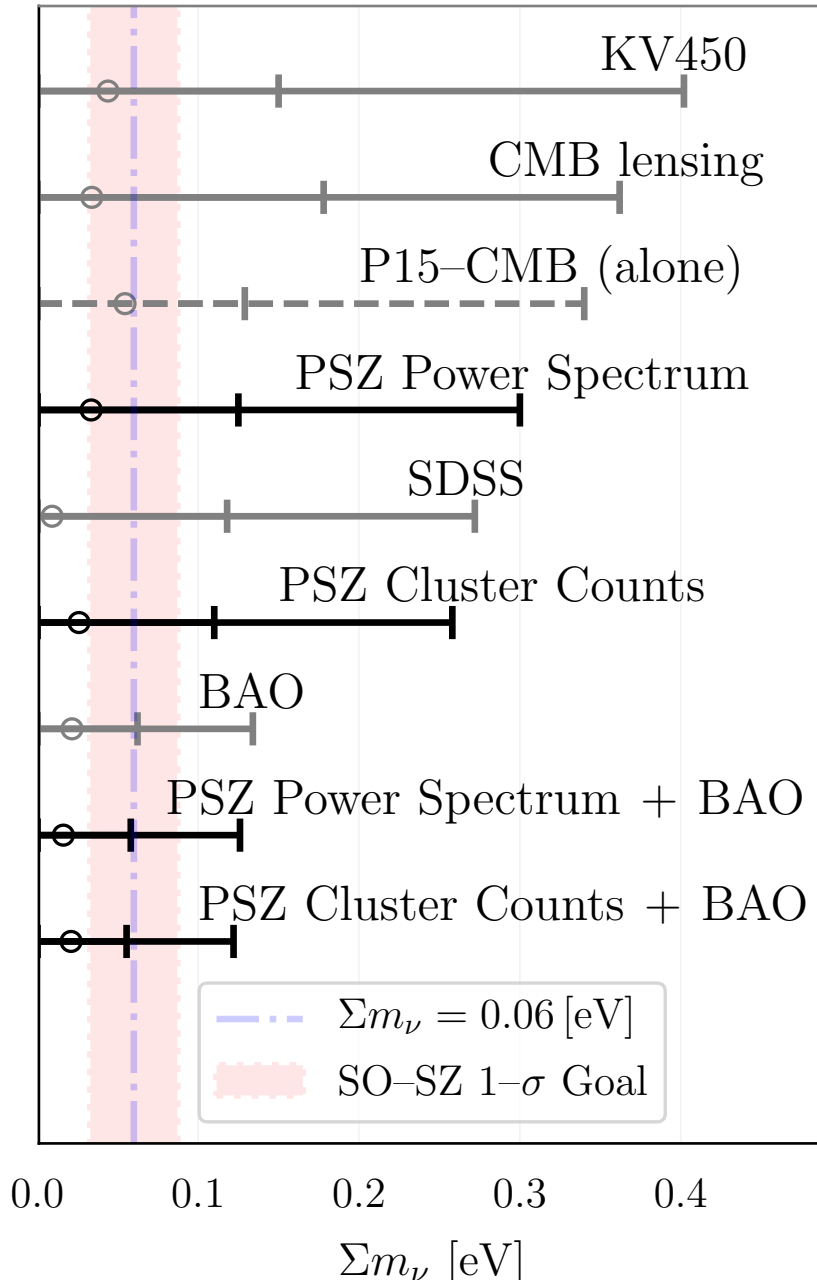
SZ as a cosmological probe



- only once issue of bias is solved
- measure dark energy
- measure neutrino masses

Current constraints with Planck SZ

P15–CMB combined with LSS probes



SZ competitive with
Galaxy surveys
and CMB lensing

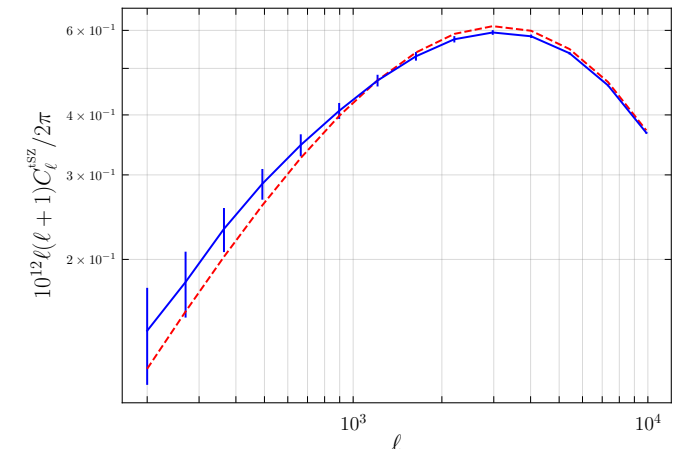
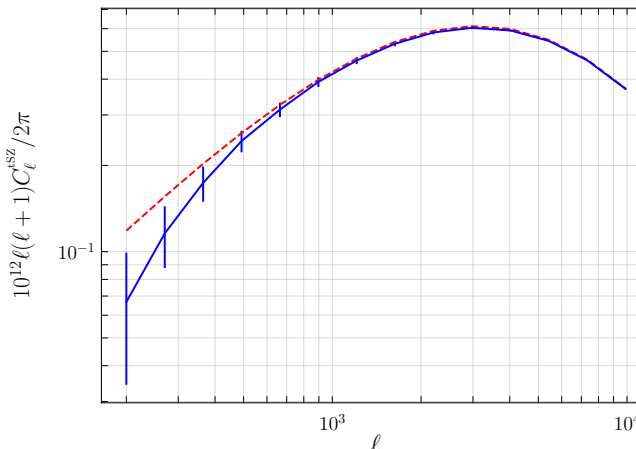
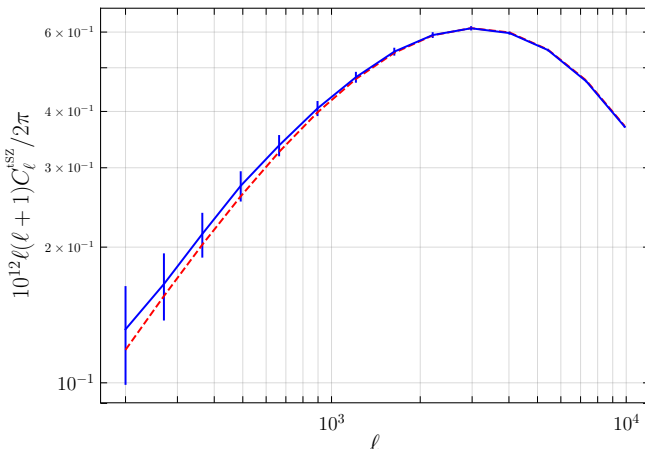
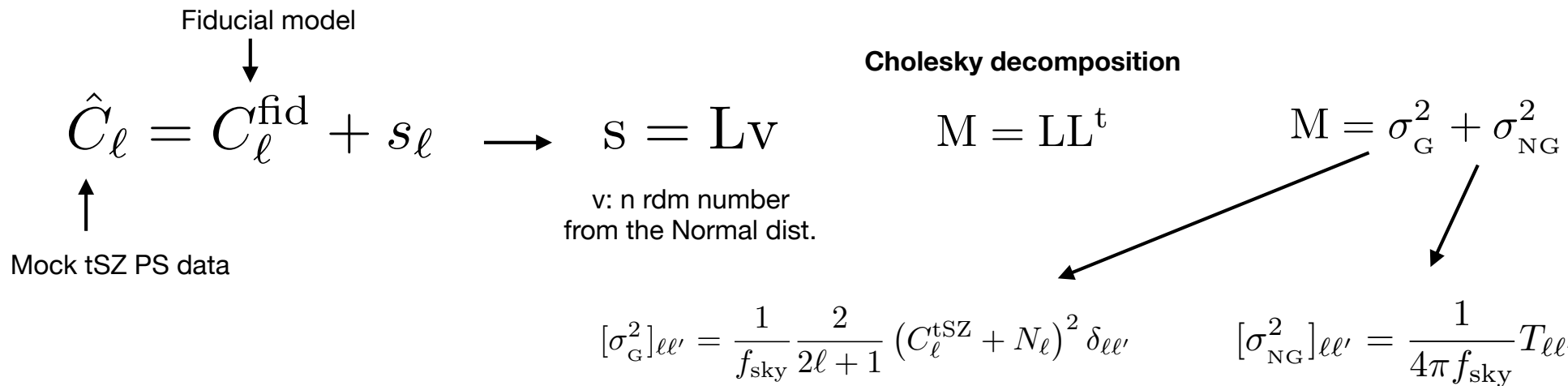
But the most powerful combination
remains CMB + BAO

addition of SZ to CMB+BAO:
very tiny improvement

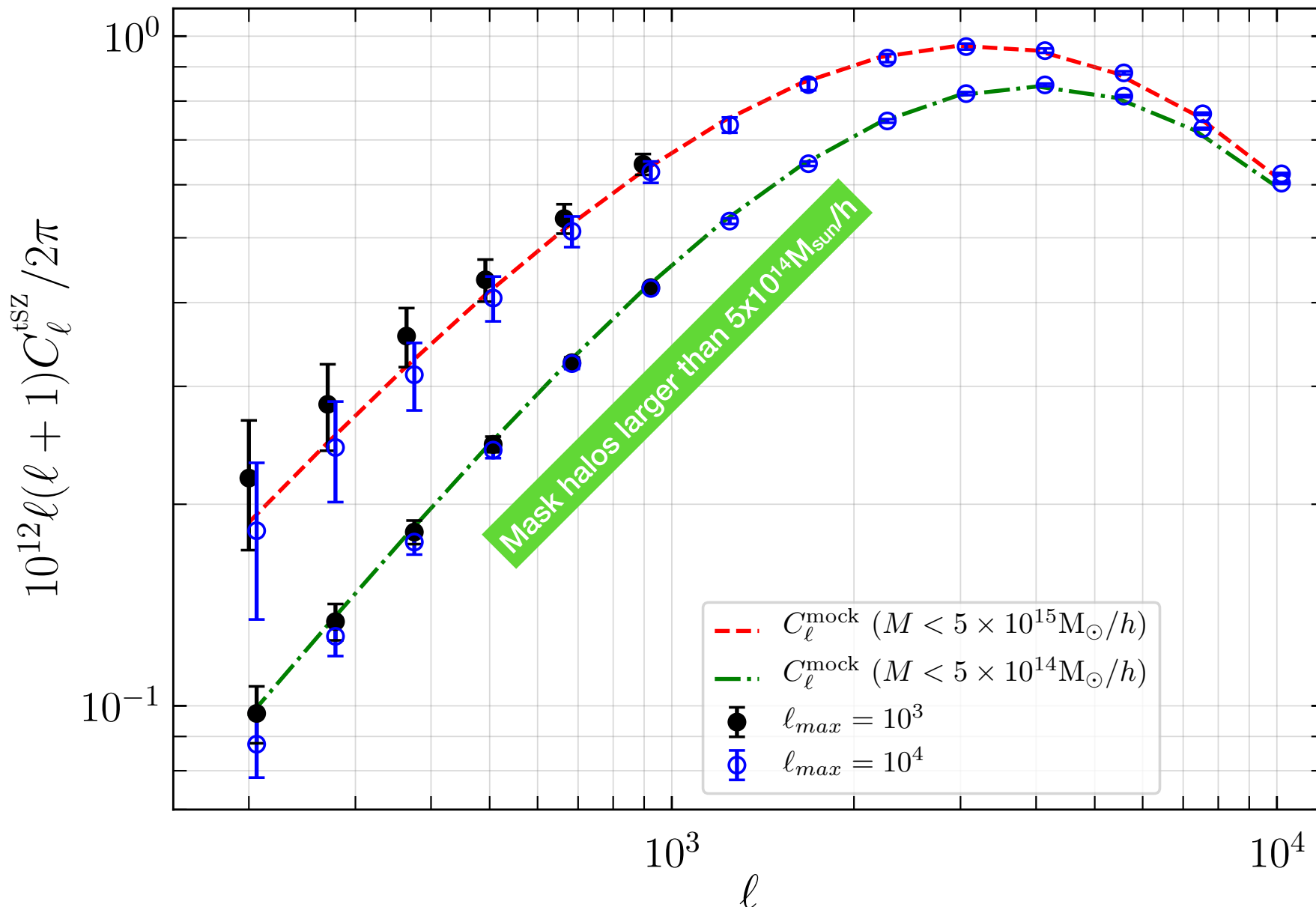
Forecasts for cosmic variance limited power spectrum

- Cosmic variance limited y -map power spectrum experiment

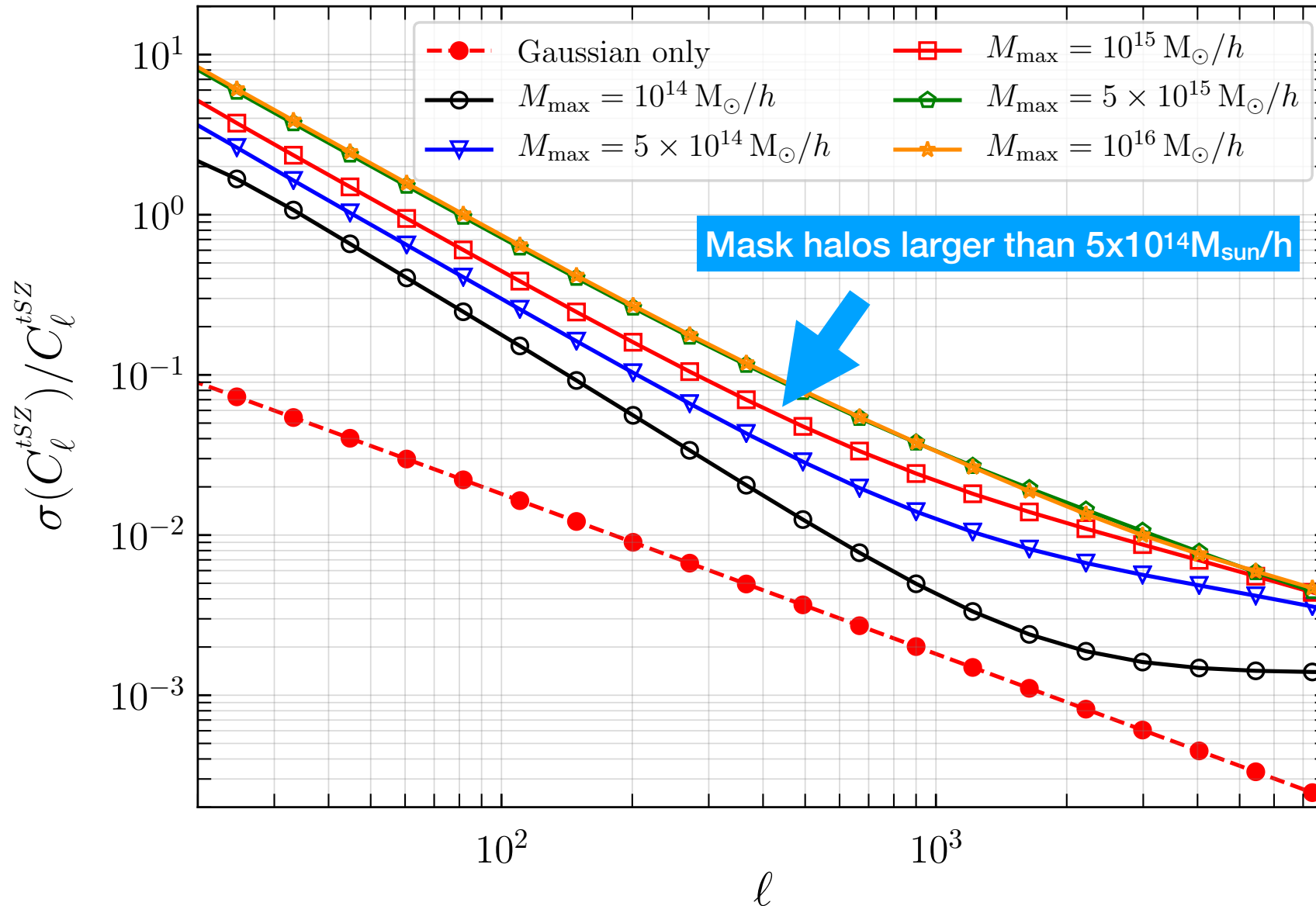
- ▶ Random draw the **Cl's from n-point PDF** of the tSZ PS (n =number of multipoles).
- ▶ **$n \gg 1$** : PDF **numerically hopeless** to evaluate.
- ▶ when **$\ell \gg 1$** : PDF \sim can use **multivariate Gaussian** (Zhang and Sheth 2007).

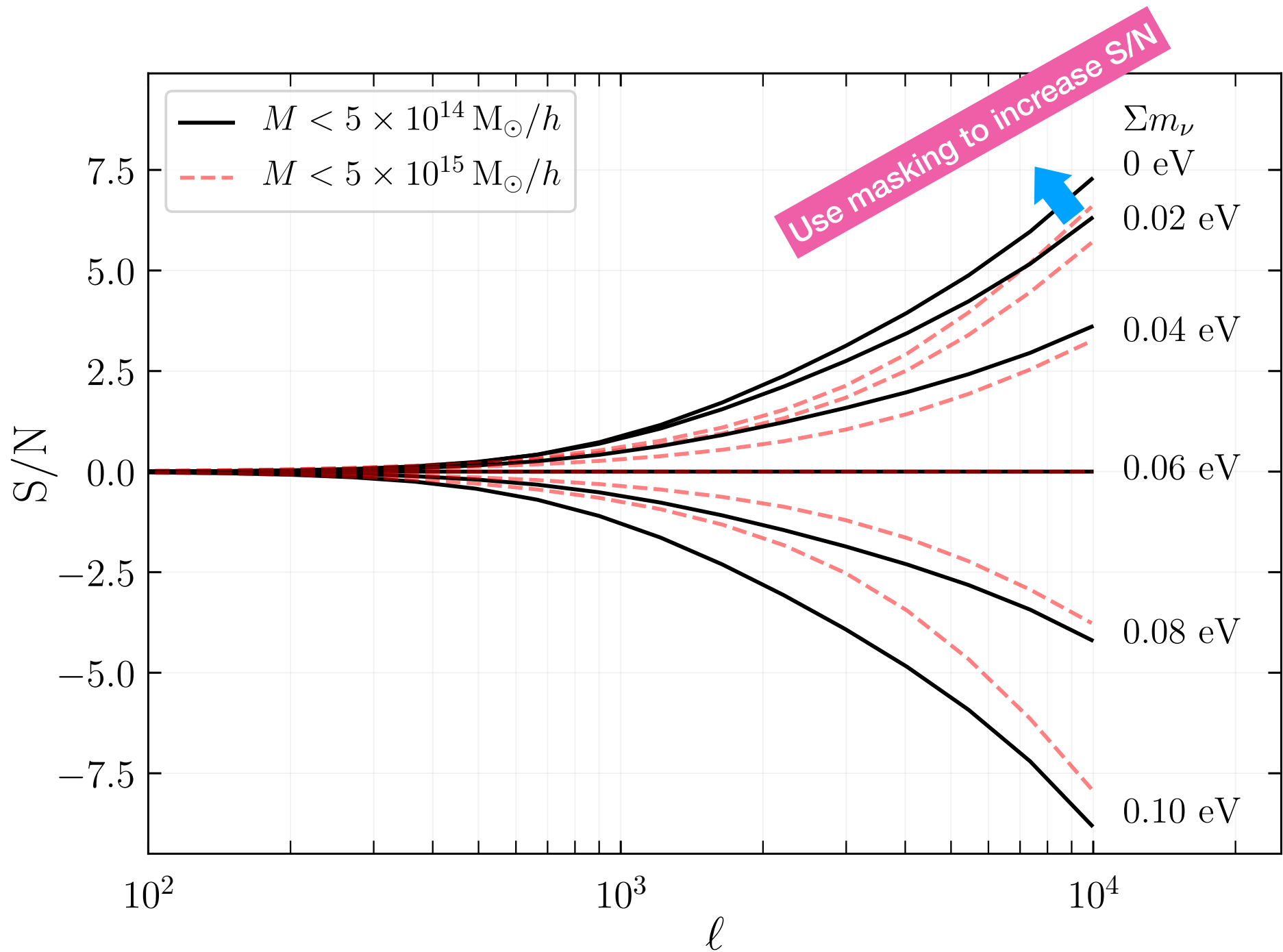


- Mock SZ power spectrum data

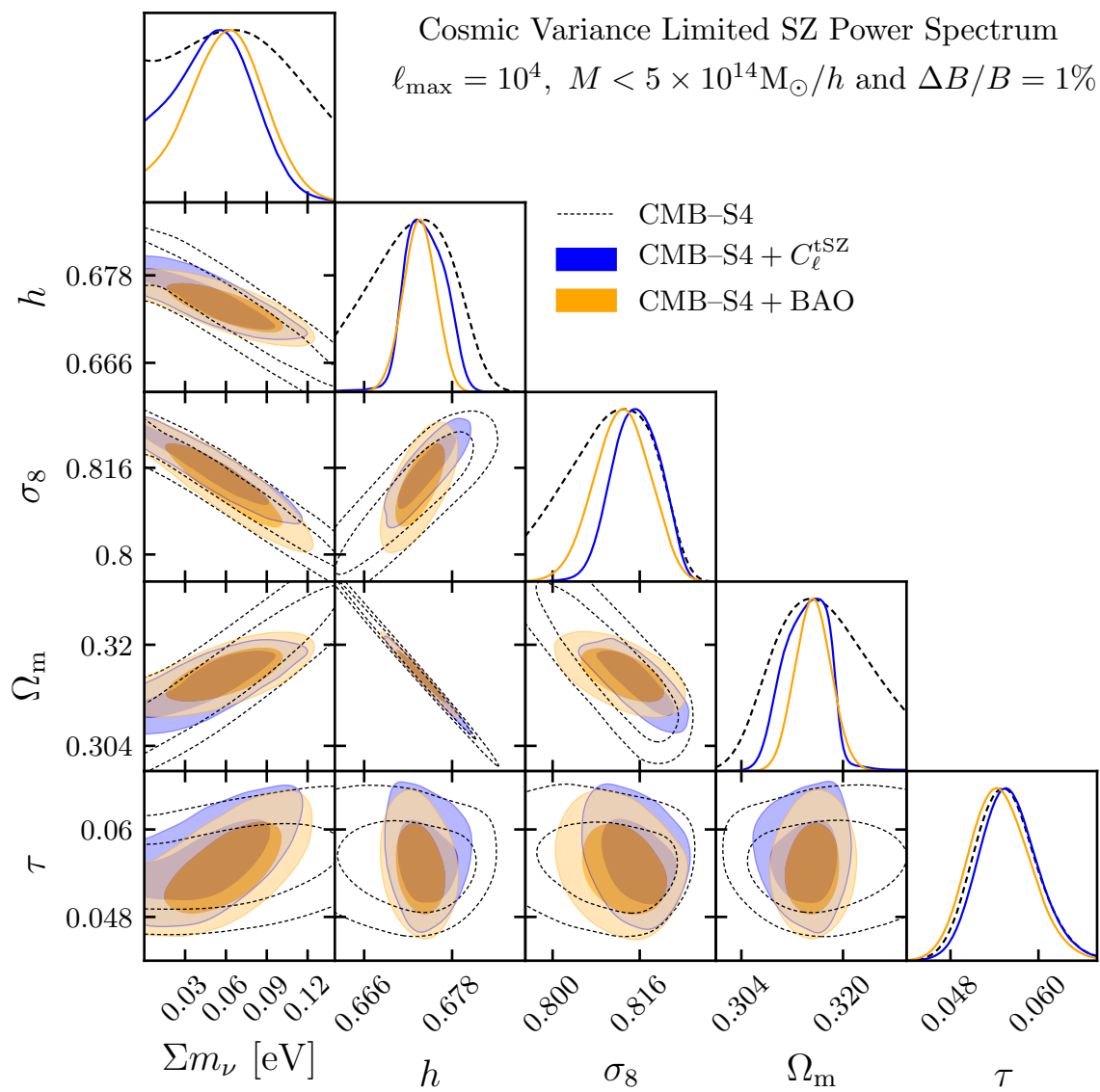


- Masking heavy clusters to reduce statistical errors

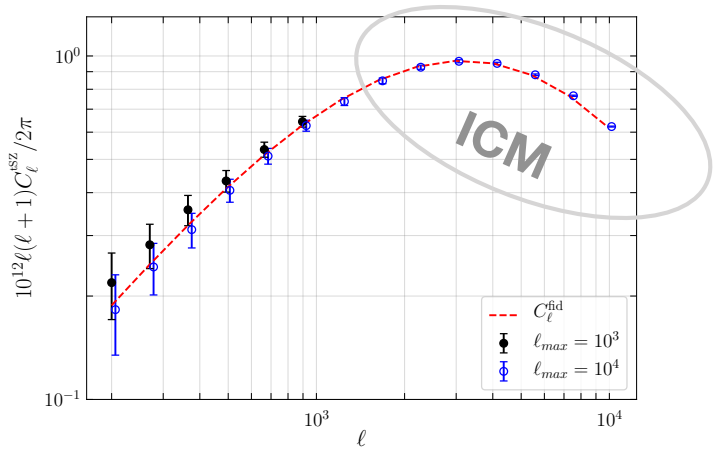




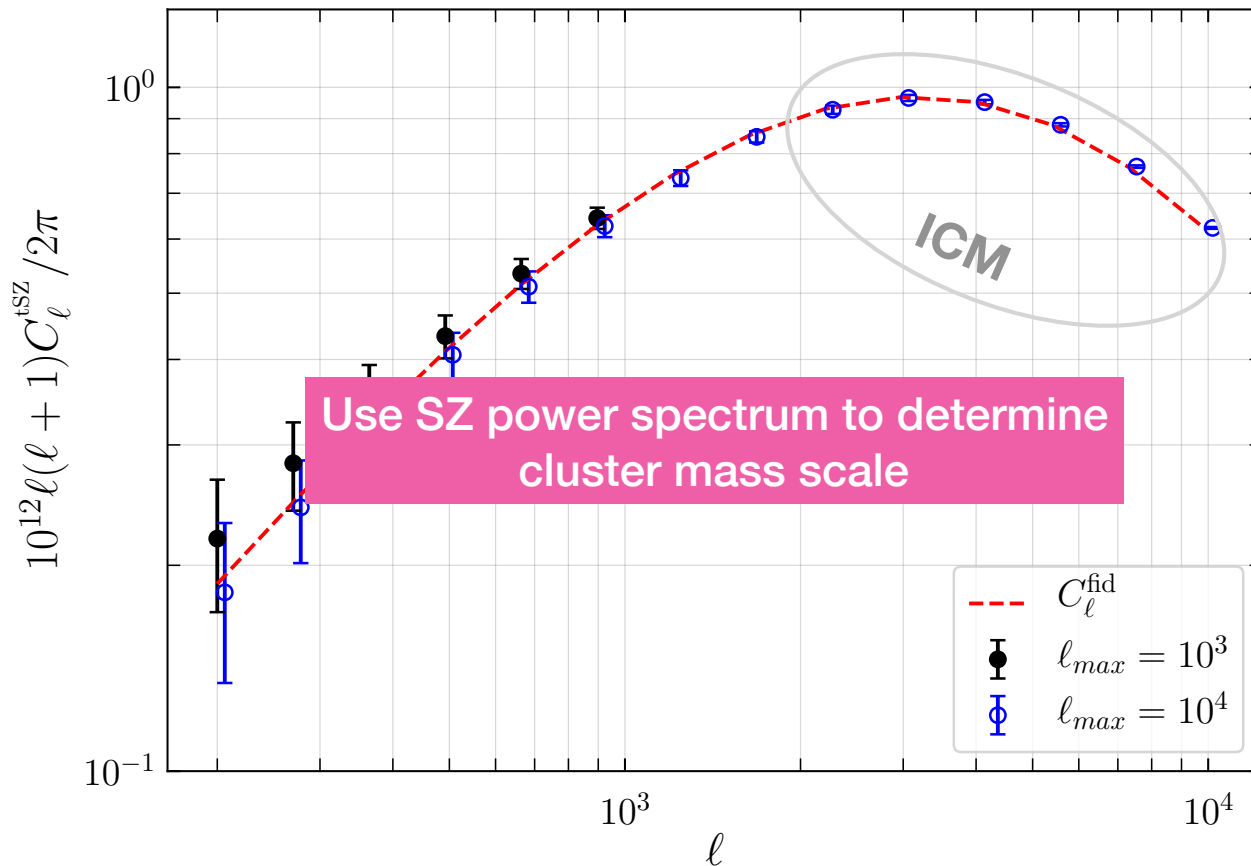
- To achieve 27meV goal:



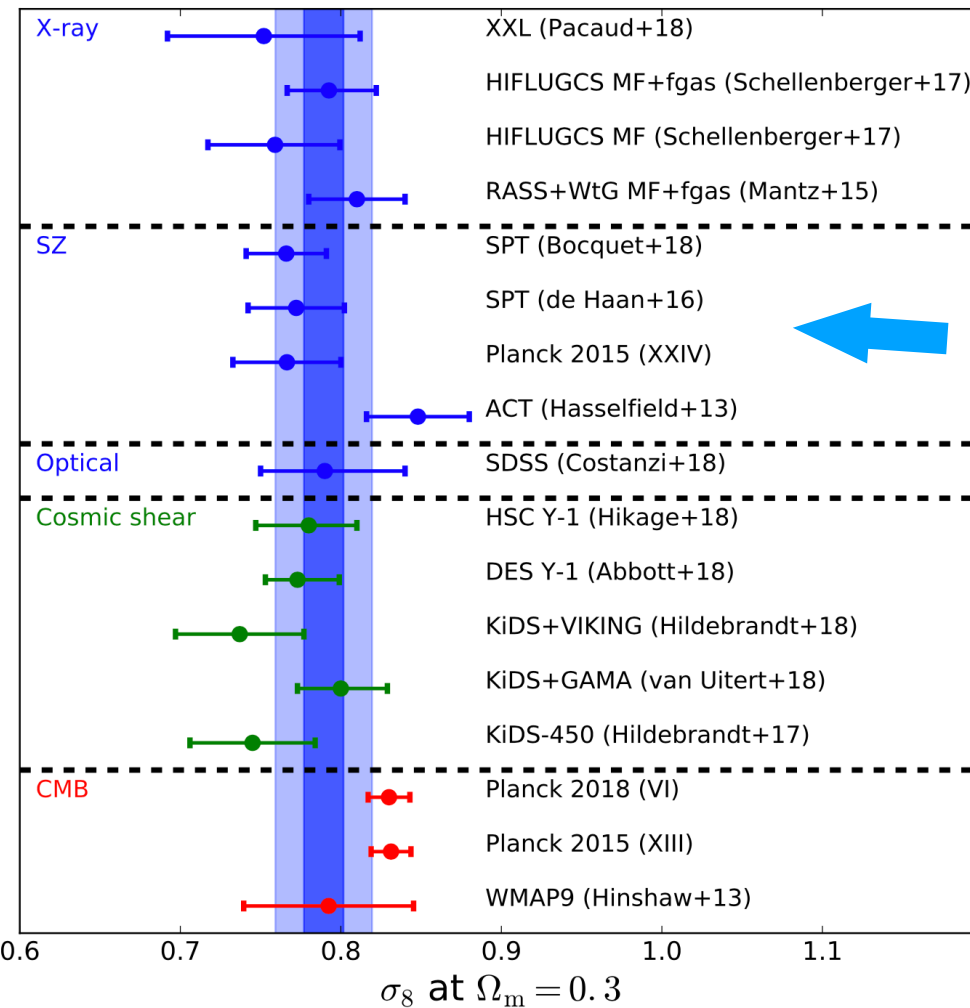
- But small scales: ICM



- Determine ICM properties from SZ power spectrum
- ➔ Easily get 2% precision on bias



FUTURE OF SZ



tSZ y-map power spectrum

Shed light on a tension:
 “CMB vs low-z probes”
 or
 “cluster mass scale”

Fig. 17 Constraints on σ_8 at $\Omega_m = 0.3$ from the cluster mass function (sometimes combined with f_{gas} constraints) are shown with blue symbols. Standard deviation ($= 0.033$) and error ($= 0.012$) around the unweighted mean ($= 0.789$) of all seven independent cluster analyses are shown as light and dark blue shaded bands, respectively. Also shown are constraints from WL/cosmic shear/galaxy clustering (green symbols) and from CMB (red symbols). Details on all the constraints are provided in Sections 5.2 and 5.3. Note that analysis details differ for the various works. Adapted from Schellenberger & Reiprich (2017b).

Figure from Pratt et al [1902.10837]

FUTURE OF SZ

- **ICM at large radii**

e.g., Ruppin et al [1712.09587]

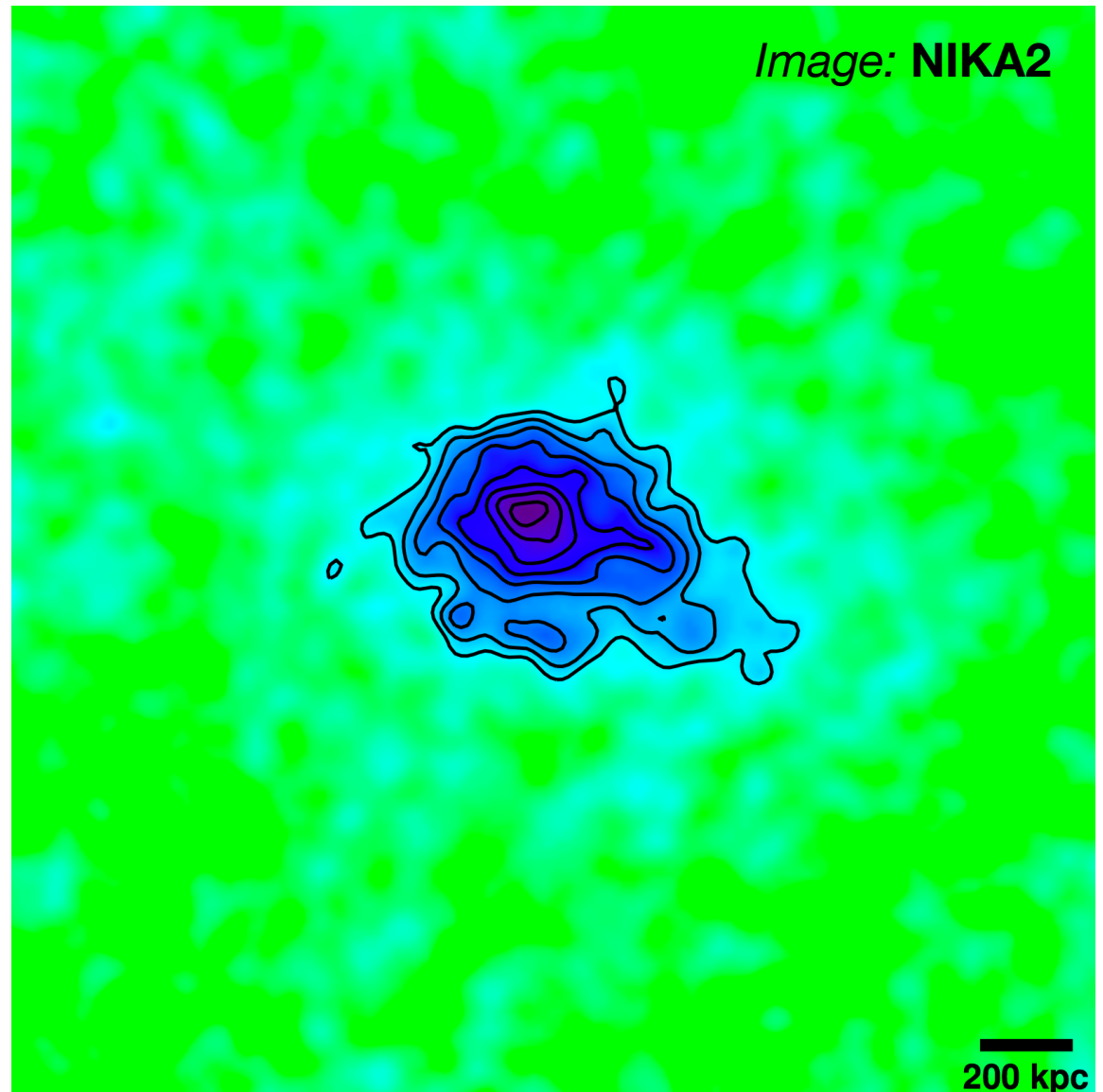
- **WHIM (e.g., missing baryons)**

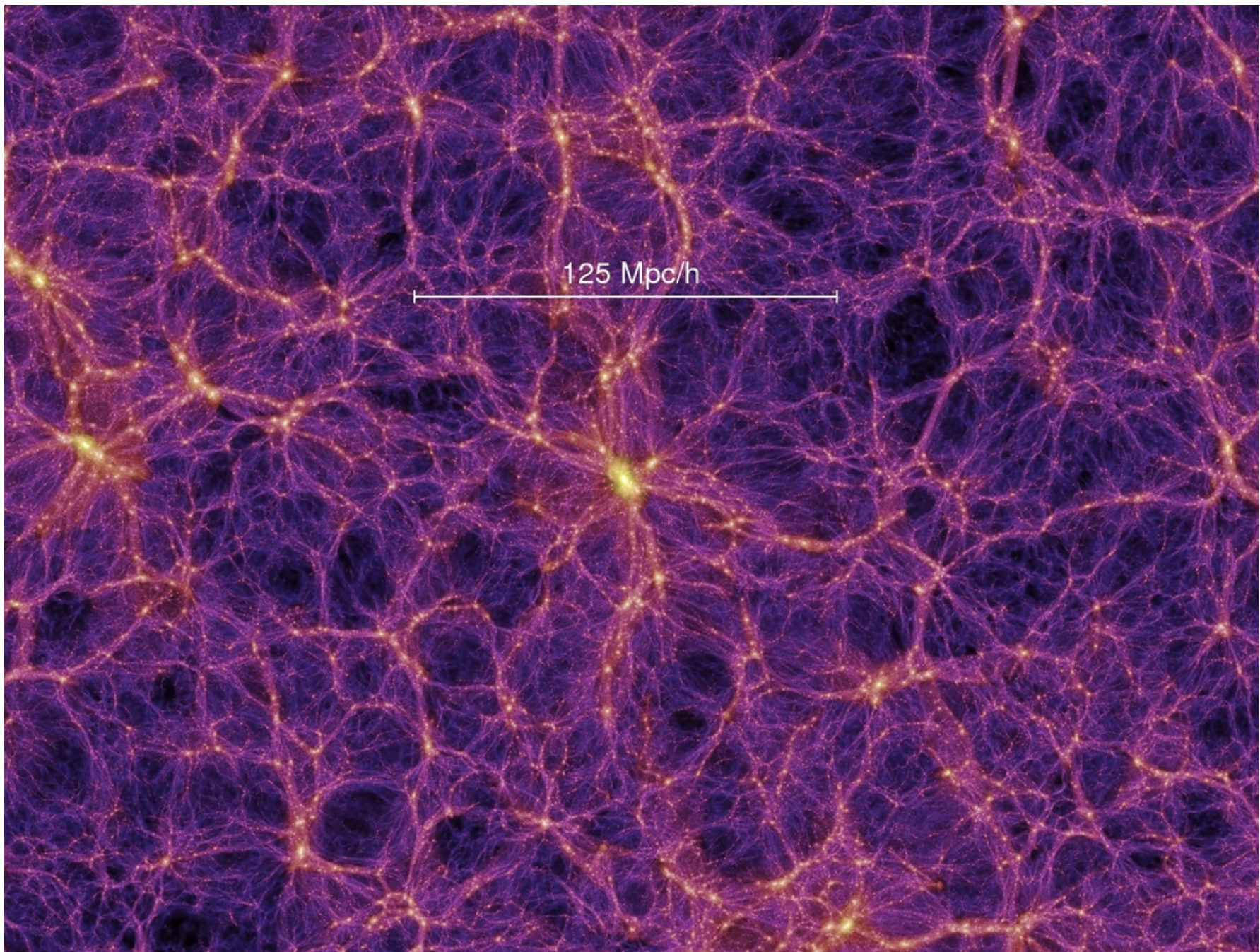
de Graaff et al [1709.10378]

Tanimura et al [1709.05024]

- **Cosmic voids**

Alonso et al [1709.01489]





Summary of the talk:

- Planck SZ cluster counts and power spectrum fully consistent with other SZ observation and galaxy surveys.
- Primary CMB predicts more clusters than we see:
 - ➔ larger bias or something exotic
- What will we learn from SZ in the next 15 years?
 - ➔ ICM properties and cosmic web

Cosmological constraints from tSZ power spectrum and cluster counts

Boris Bolliet

Jodrell Bank Centre for Astrophysics
The University of Manchester



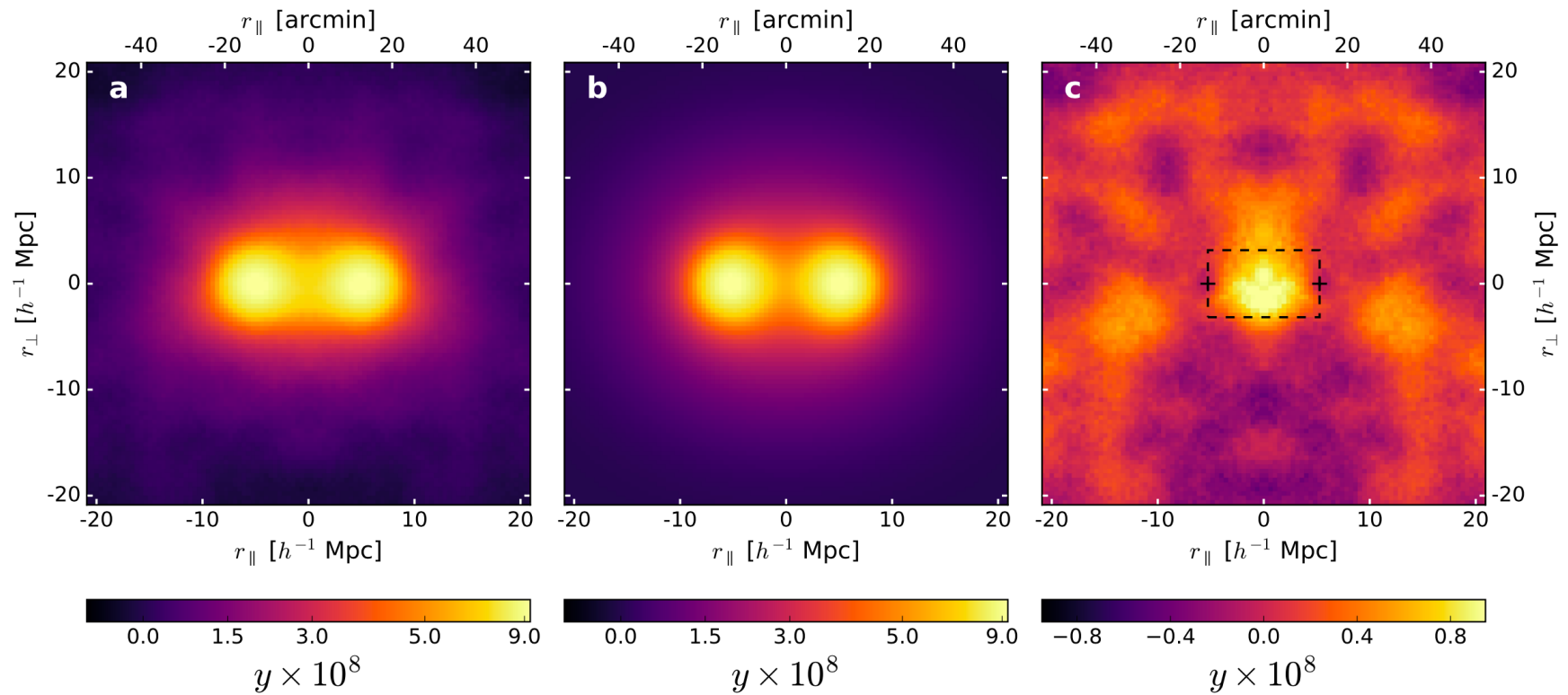


Fig. 1. (a) Symmetrically stacked Compton y -parameter maps for 1 million close pairs of CMASS galaxies; (b) the modelled signal from the galaxy host haloes only; and (c) the residual between the stacked data and model. The indicated horizontal and vertical distance scales (r_{\parallel} and r_{\perp} respectively) are calibrated using the mean galaxy pair separation of $10.5 h^{-1}$ Mpc. The mean projected angular separations are also shown for the horizontal axis. There is a bridge connecting the pairs of galaxies in the data (a) but not in the model (b), suggesting the presence of a filament in (a), which is highlighted in panel (c) by a dashed box with plus signs indicating the positions of the galaxy pairs.

de Graaff et al [1709.10378]

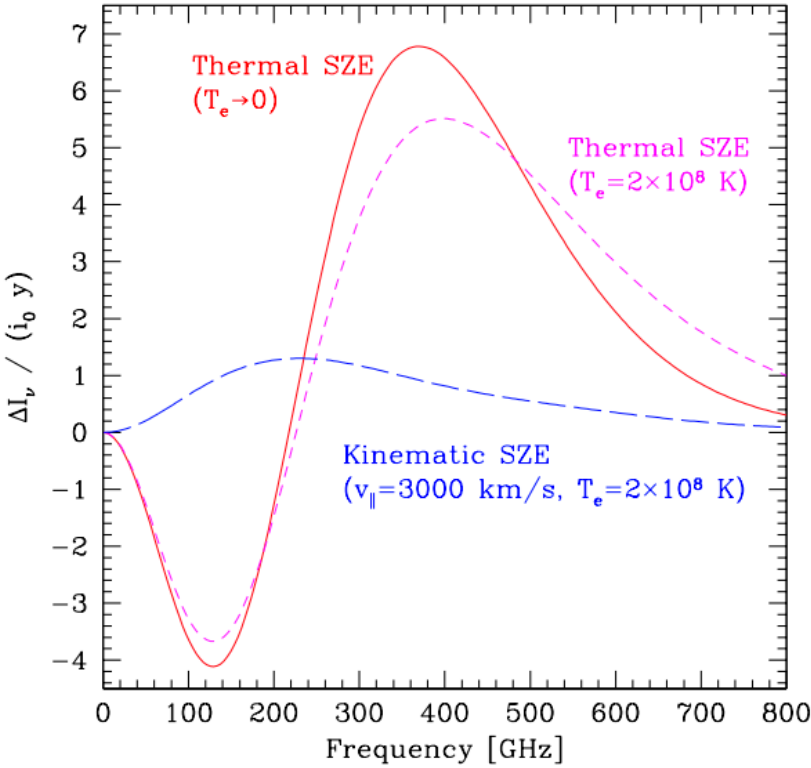


Fig. 2 Spectra of the Sunyaev-Zel'dovich effect (SZE). Intensity differences from the CMB normalized by i_0y are plotted for the non-relativistic thermal SZE (solid), the thermal SZE with the relativistic correction [39] for $T_e = 2 \times 10^8$ K (short dashed), and the kinematic SZE with the relativistic correction [40] for the bulk velocity 3000 km s^{-1} toward us and $T_e = 2 \times 10^8$ K (long dashed). The ratio between the kinematic SZE and the thermal SZE is proportional to v_{\parallel}/T_e in the non-relativistic limit.

Kitayama [1404.0870]

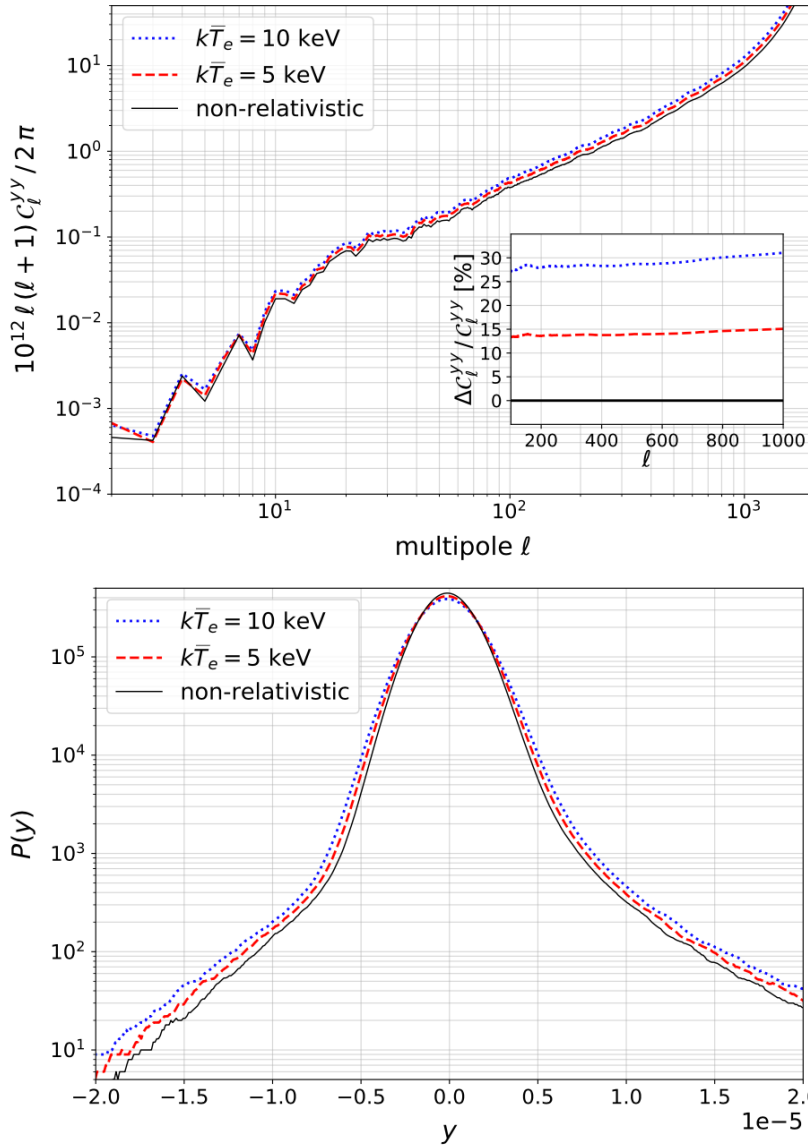


Figure 4. *Upper panel:* angular power spectrum of the NILC y-maps on 80% of the sky from *Planck* data obtained using different effective electron temperatures, $k\bar{T}_e$. The inlay highlights the relative difference in comparison with the non-relativistic case. *Lower panel:* corresponding one-point PDF of the y-maps on 40% of the sky.

Remazeilles et al (BB) [1809.09666]

Relativistic SZ Consequence for Planck y-map analysis

$$\frac{\Delta\sigma_8}{\sigma_8} \approx 0.02 \times \left[\frac{k_B \bar{T}_e}{5 \text{keV}} \right]$$

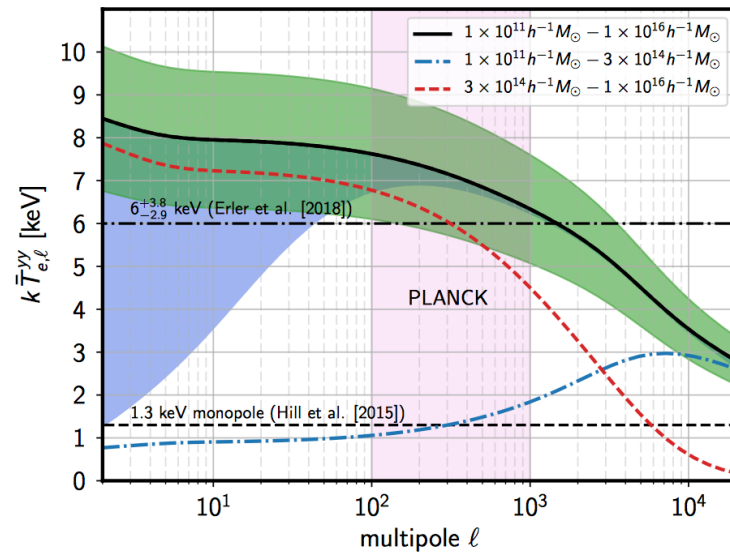


Figure 3. Effective C_ℓ^{yy} -weighted electron temperature for different multipoles computed using CLASS-SZ (Bolliet et al. 2018; Blas et al. 2011) with main settings like in Fig. 1. At high- ℓ , low-temperature systems dominate, giving effective temperature $k\bar{T}_{e,\ell}^{yy} \approx 2-3$ keV. Around $\ell \approx 10^2-10^3$, which is most relevant to the *Planck* tSZ analysis, we find $k\bar{T}_{e,\ell}^{yy} \approx 5-9$ keV. At $\ell \lesssim 10^2$, we obtain $k\bar{T}_{e,\ell}^{yy} \approx 6-10$ keV. However, uncertainties in the assumed mass-temperature relation and its redshift dependence and the total amount of diffuse gas lead to large ambiguities (green and blue bands) that will have to be quantified more carefully.

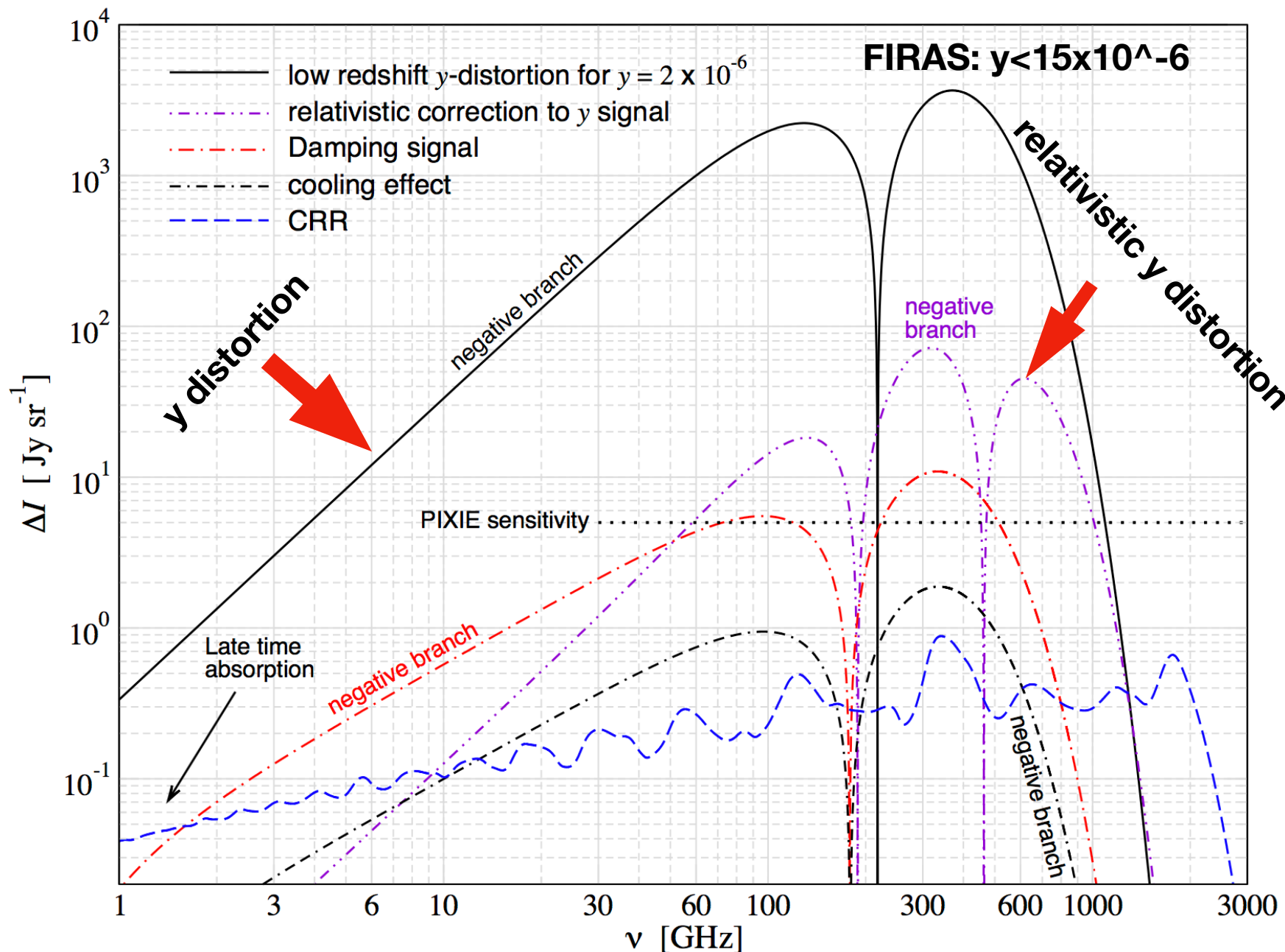
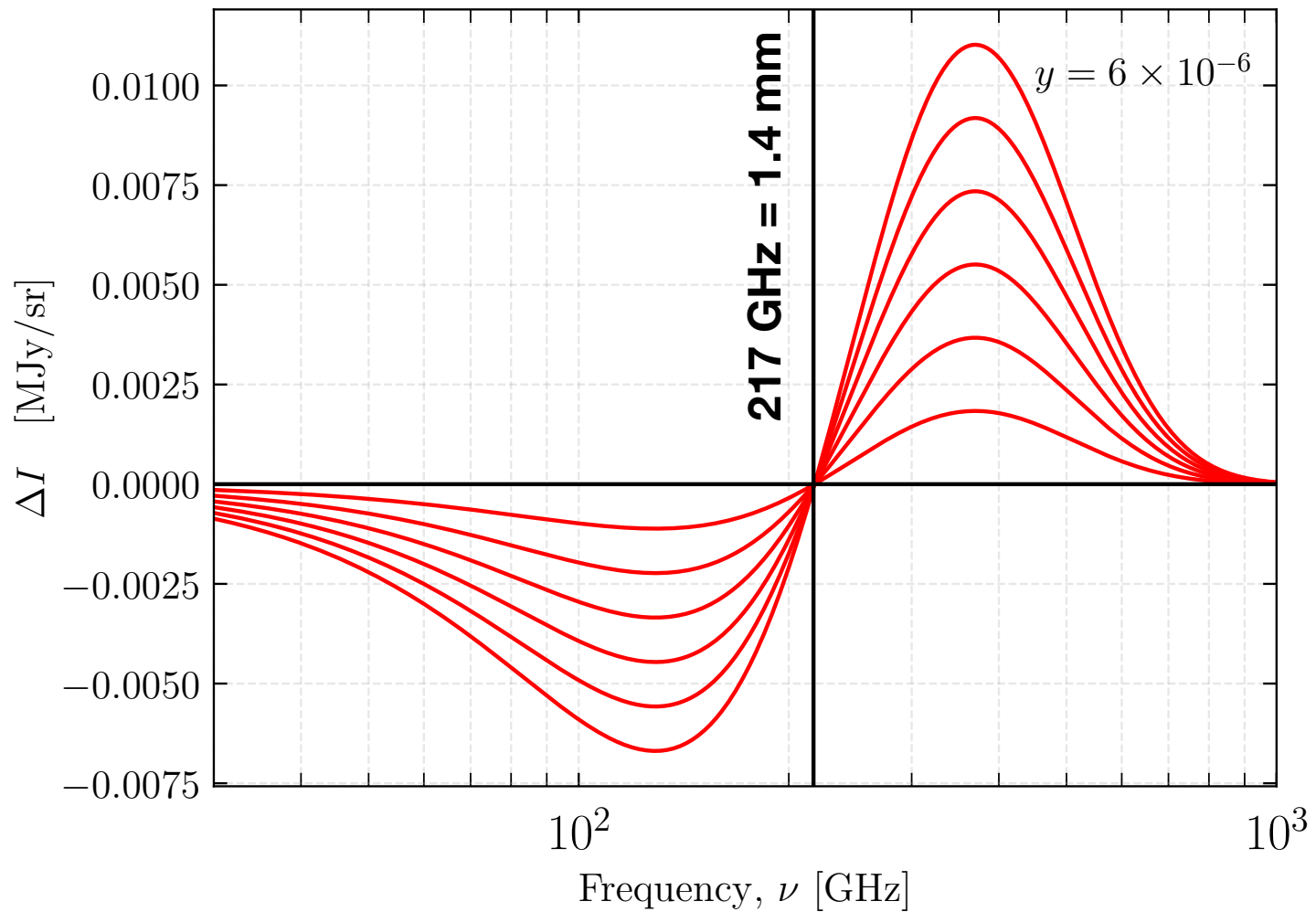


Figure from Chluba [1603.02496]



y distortion from cluster always positive
(energy goes to photons)

$$y = \frac{\sigma_T}{m_e c^2} \int P ds$$

Redshifts in PLC catalogues

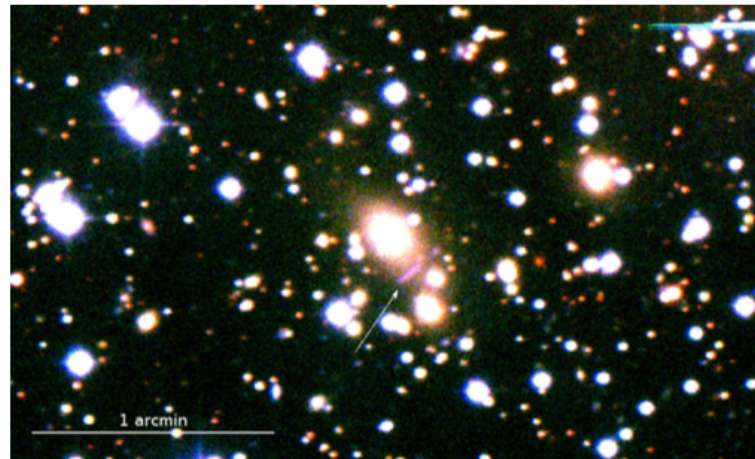


Fig. 6. RGB image of the cluster PSZ1 G060.12+11.42, obtained with the WFC/INT data. The white arrow shows the location of a gravitational arc.

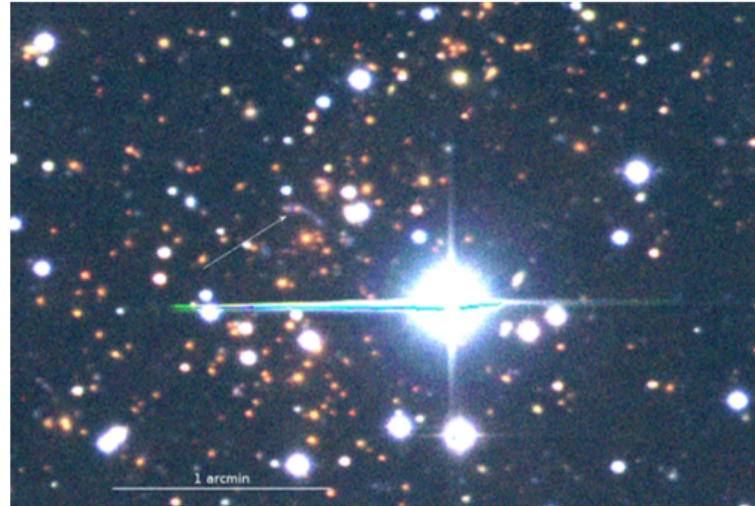


Fig. 7. RGB image of the cluster PSZ1 G078.67+20.06 obtained with our WFC/INT data. A gravitational arc (indicated by the arrow) is clearly visible around the cluster centre.

Fig from [Planck XXXVI [1504.04583]

Redshifts in PLC catalogues

Redshift->external surveys

*e.g. photometric redshift with telescopes at the Canary Island Observatory Planck XXXVI [1504.04583]

* CIO->72 sources

Based on g'r'i'-colour combinations, it is possible to identify the cluster candidates and to measure photometric redshifts (see e.g. Lopes 2007).

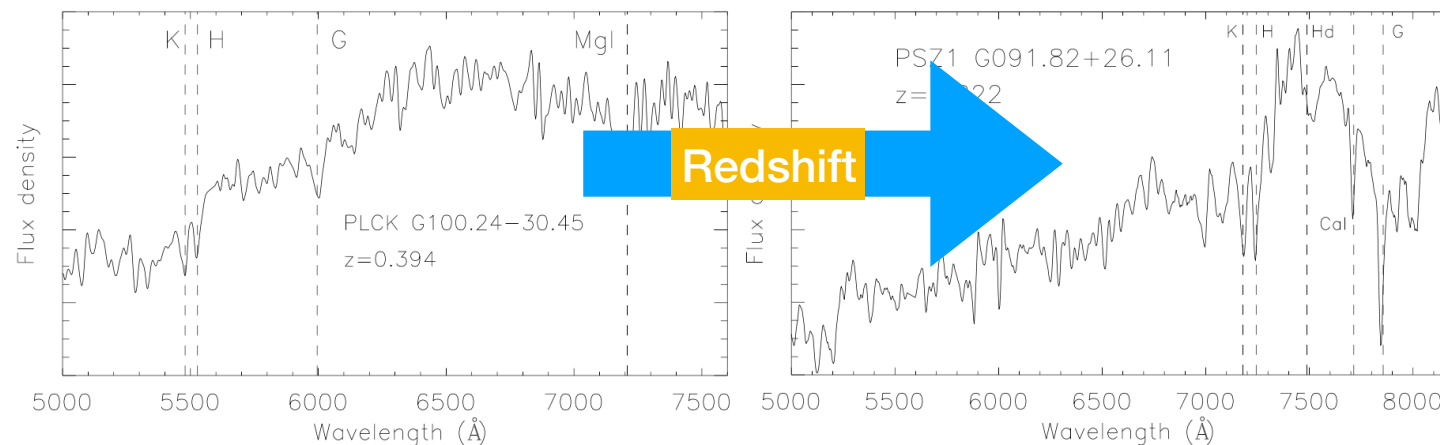


Fig. 1. Two examples of spectra of early-type cluster members (previously selected as candidates in the photometric sample) obtained with the TNG/DOLORES (left panel) and GTC/OSIRIS (right panel). Dashed lines show the location of the main absorption features identified in the spectra. The vertical axes are given in arbitrary units.

Angular diameter distance

What is the angle subtended by an object of size R at redshift z ?

$$\theta = \frac{R}{D_A(z)}$$

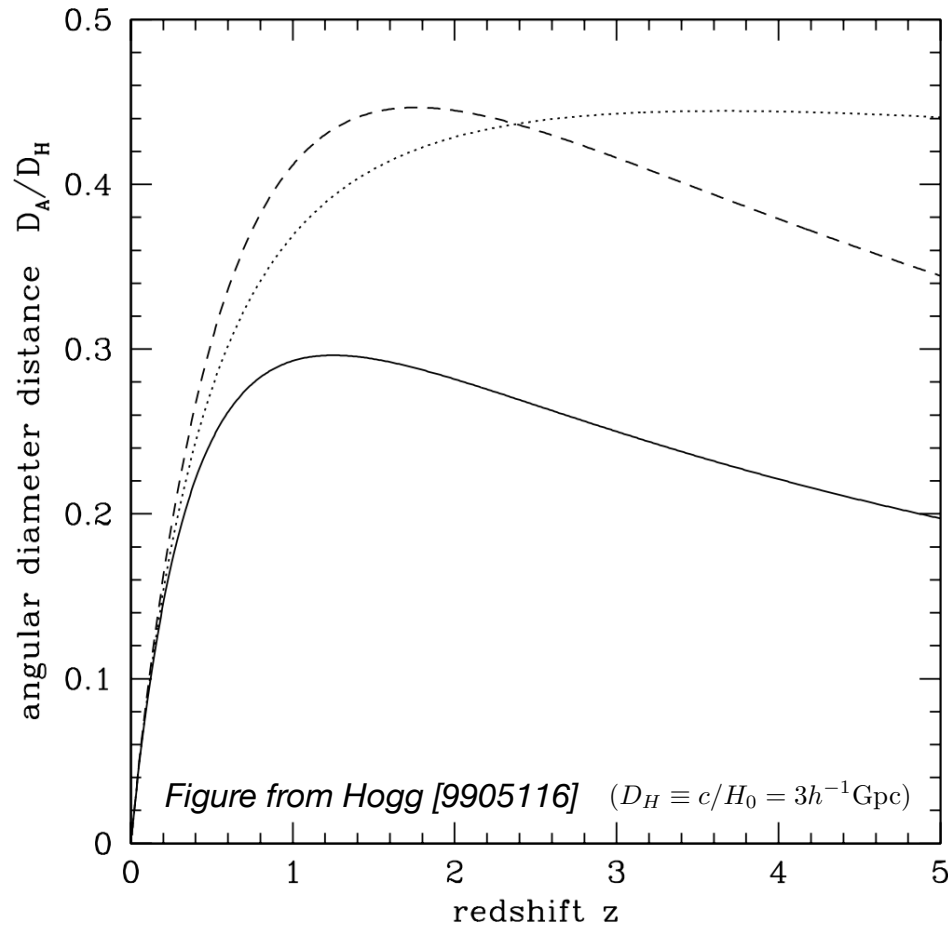
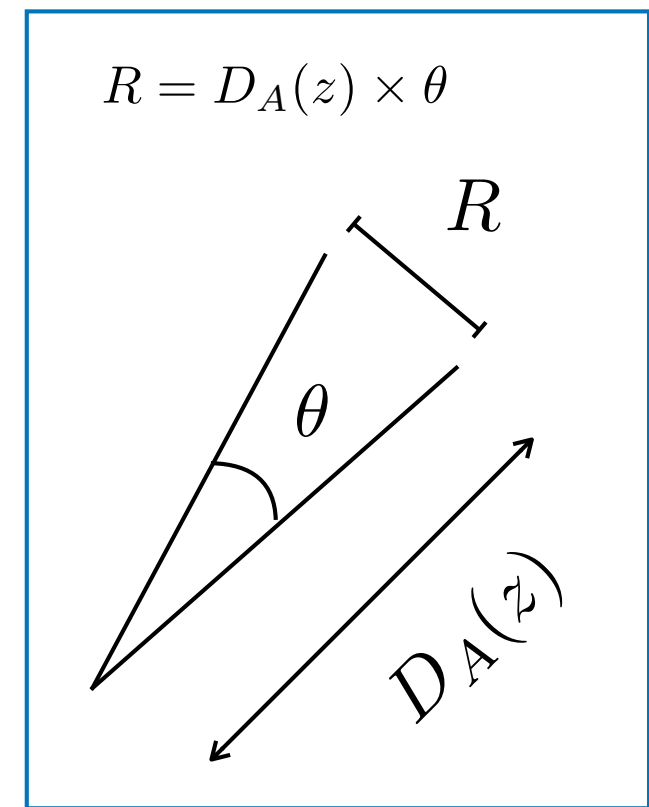


Figure 2: The dimensionless angular diameter distance D_A/D_H . The three curves are for the three world models, $(\Omega_M, \Omega_\Lambda) = (1, 0)$, solid; $(0.05, 0)$, dotted; and $(0.2, 0.8)$, dashed.



Planck SZ Cluster Catalogue

DETECTION (same method as ACT and SPT)

- Blind search (i.e., no prior info on location)
- Matched Multi-filters (Herranz et al 2002, Melin et al 2006)
 - Start with CMB temperature maps (6 HFI maps)
 - Divide the sky into ~500 patches (10x10 square degree)
 - Assume pressure profile (Arnaud et al 2010)
 - Use the SZ frequency spectrum
 - Use noise estimates (noise maps)
 - Combine the 6 CMB HFI maps
 - Find (cluster) angular size and flux that maximises S/N

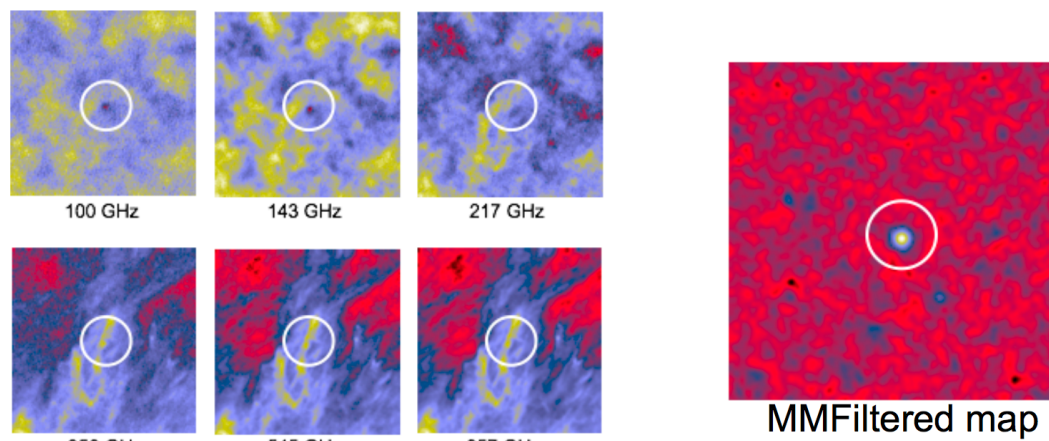


Image from Melin's talk

The Planck Y-M relation

Arnaud et al 2010: REXCESS (XMM-Newton) 20 relaxed clusters X-ray

$$E(z)^{-2/3} \left[\frac{Y_X}{2 \times 10^{14} M_\odot \text{ keV}} \right] = 10^{0.376 \pm 0.018} \left[\frac{(M_{500}/B)}{6 \times 10^{14} M_\odot} \right]^{1.78 \pm 0.06}$$
$$1.78 = \frac{5}{3} + 0.12$$

$Y_X \equiv M_{\text{gas}} \times T_X$ proportional to thermal energy
low-scatter mass proxy (Kravtsov, Vikhlinin, Nagai 2006)

Virial theorem (only gravity important, spherical symmetry)

$$-2 \text{ Kinetic energy} = \text{Gravitational potential energy} \quad T \propto M^{5/3}$$

$$\text{Hydrostatic Equilibrium (relaxed ICM)} \quad P \propto M^{2/3}$$

$$\text{Kinetic energy} = \text{Thermal energy}$$

(Kravtsov, Vikhlinin, Nagai 2006 [0603205] CHANDRA data plus Sims)

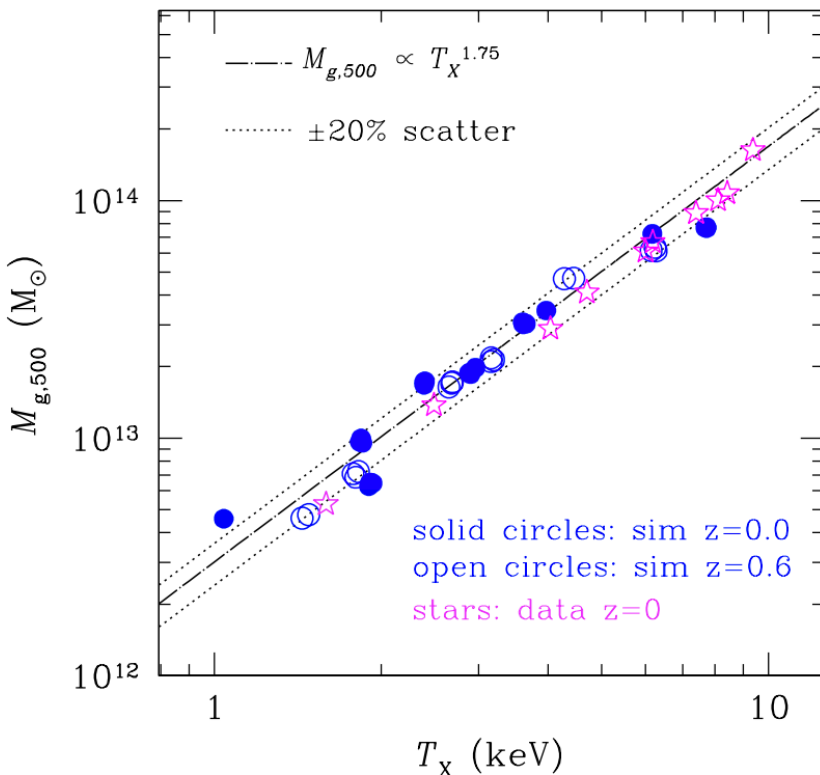


FIG. 5.— Relation between X-ray spectral temperature and gas mass for the relaxed subsample of simulated clusters (circles) and for a sample of relaxed *Chandra* clusters of Vikhlinin et al. (2006, stars). Both gas mass and temperature are the quantities derived from analysis of real and mock X-ray data. The error bars in the *Chandra* measurements are comparable to the symbol size and are not shown for clarity. The gas masses for the simulated clusters are rescaled by a factor of $0.17/0.143 = 1.19$ to reflect the difference between the universal baryon fractions adopted in the simulation and the value measured by the *WMAP*. The *dashed line* shows the best fit power law relation with the slope 1.75.

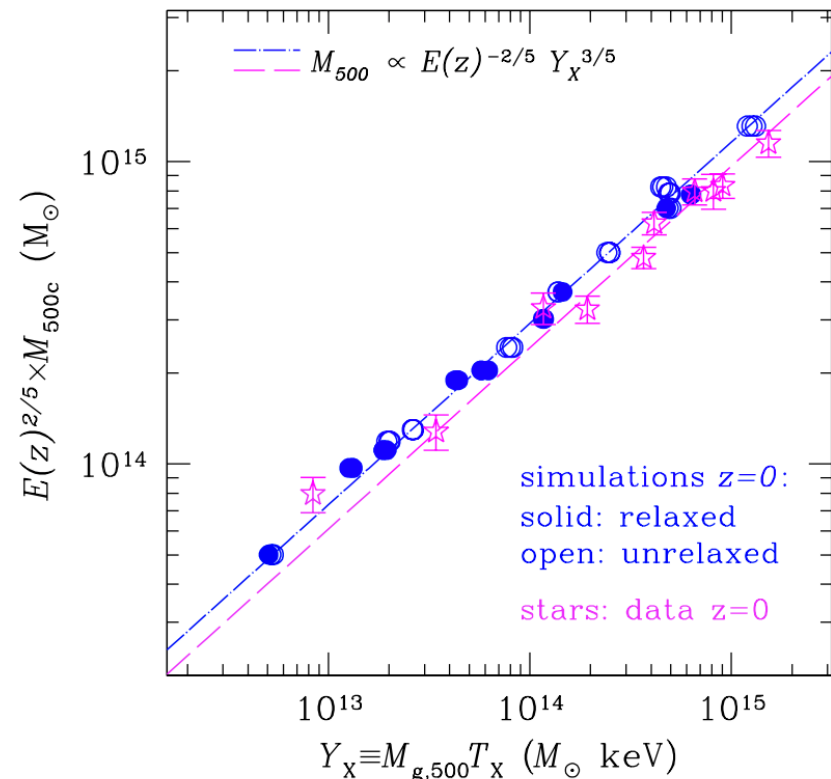


FIG. 6.— $Y_X - M_{500}$ relation for the $z = 0$ sample of the simulated clusters (circles) and for a sample of relaxed *Chandra* clusters of Vikhlinin et al. (2006, stars). The gas masses for the simulated clusters are appropriately rescaled (see caption to Fig.5). The *dot-dashed line* shows the best fit power law relation for the simulated clusters with the slope fixed to the self-similar value of $3/5$. The *dashed line* shows the same best fit power law, but with the normalization scaled down by 15% .

(*Also in [0603205] method to estimate Mass from Y_X)

Planck early SZ (Planck XI 2011)
 71 clusters with S/N>7 and XMM-Newton data

- Obtain M_{500} for each cluster from A10 Yx-M relations with method from V06

$$E(z)^{-2/3} \left[\frac{Y_X}{2 \times 10^{14} M_\odot \text{ keV}} \right] = 10^{0.376 \pm 0.018} \left[\frac{(M_{500}/B)}{6 \times 10^{14} M_\odot} \right]^{1.78 \pm 0.06}$$

- Estimate SZ signal Y_{500} within R_{500} (corresponding to M_{500} estimated above)
- Study Y_{500} against M_{500}
- Correct for Malmquist bias (Vikhlinin et al 2009, Pratt et al 2009)
- Obtain the Y-M relation

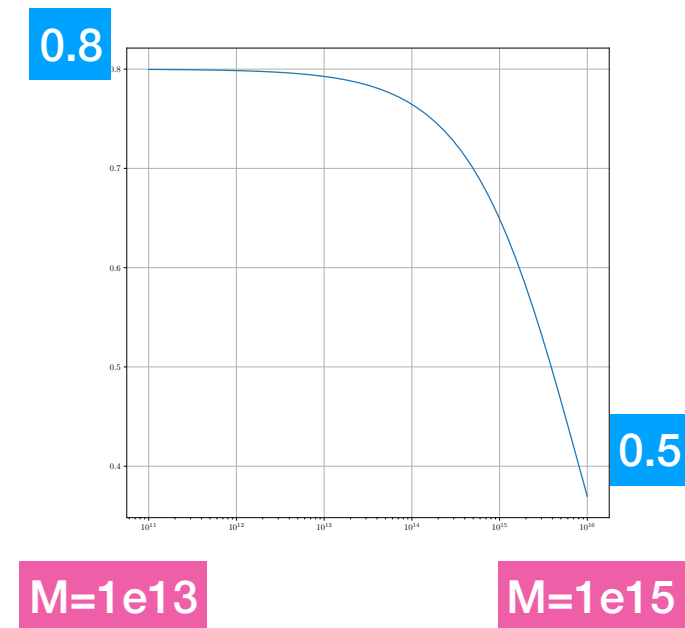
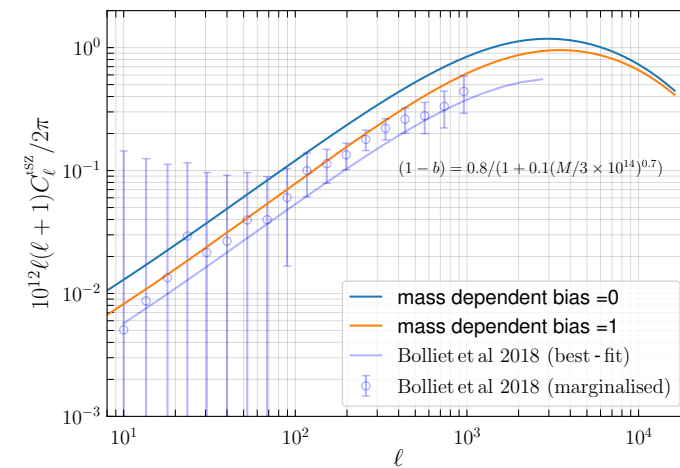
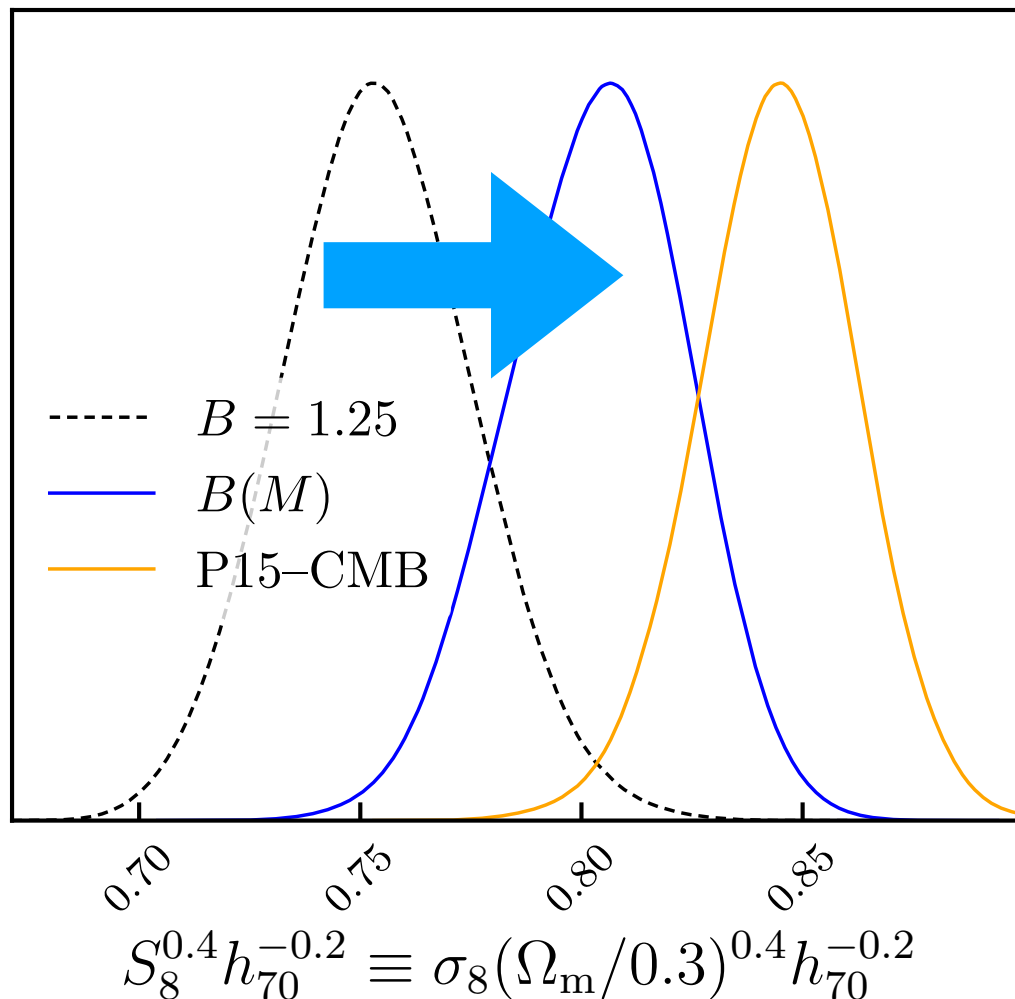
$$E(z)^{-2/3} \left[\frac{D_A(z)^2 Y_{500}}{10^{-4} \text{Mpc}^2} \right] = Y_\star h_{70}^{-2+\alpha} \left[\frac{(M_{500}/B)}{6 \times 10^{14} M_\odot} \right]^\alpha$$

$$\log_{10} Y_\star = -0.19 \pm 0.02 \quad \alpha = 1.79 \pm 0.08$$

$$\begin{aligned} \text{Bias} &= 20\% \text{ Hydrostatic} + 15\% \text{ Calibration (Mass dependent)} \\ &= 35\% \end{aligned}$$

See also Henson et al for sims.

Mass dependent bias



Mass function

The mass function, defined as the number of haloes of a given mass per unit volume, can be written as:

$$\frac{dN}{dM}(M, z) = f(\sigma_M) \frac{\rho_m(z=0)}{M} \frac{d \ln \sigma_M^{-1}}{dM}, \quad (42)$$

where $\rho_m(z=0)$ is the mean matter density at $z=0$, and σ_M is the power spectrum of density perturbations (Jenkins et al. 2001; Tinker et al. 2008). Its dependence on mass and redshift can be written as:

$$\sigma_M(M, z) = \sigma_M(M, z=0) D_{\text{grow}}(z)$$

with $\sigma_M(M, z=0) \sim \sigma_8 \left(\frac{M}{M_8}\right)^\alpha$ (43)

where $D_{\text{grow}}(z)$ is the growth factor, and considering that the present day power spectrum $\sigma_M(M, z=0)$ is close to a power law at cluster scales, with $\alpha \sim -1/3$. The logarithmic derivative term in Eqn. 42 is approximately constant, and the mass function depends on mass and σ_8 essentially as:

$$\frac{dN}{dM} \propto f(\sigma_8 M^\alpha)/M \quad (44)$$

The mass function is thus very sensitive to σ_8 , via the exponential behaviour of the function

$$f(\sigma) \propto [1 + (\sigma/b)^{-a}] \exp(-c/\sigma^2). \quad (45)$$

The determination of σ_8 will thus essentially be degenerate with any mass bias, expressed as $M_{\text{obs}} = (1-b) M_{\text{true}}$, along the degeneracy line $\sigma_8(1-b)^{-\alpha} = \text{cst}$, i.e. $\sigma_8 \propto (1-b)^{1/3}$ or $(1-b) \propto 1/\sigma_8^3$.

[Pratt et al [1902.10837]]

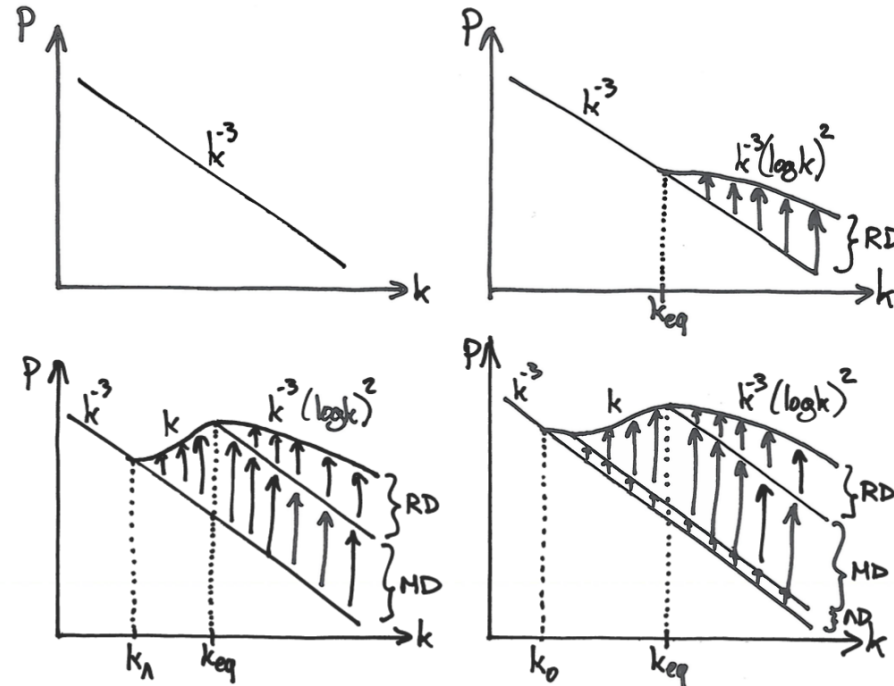


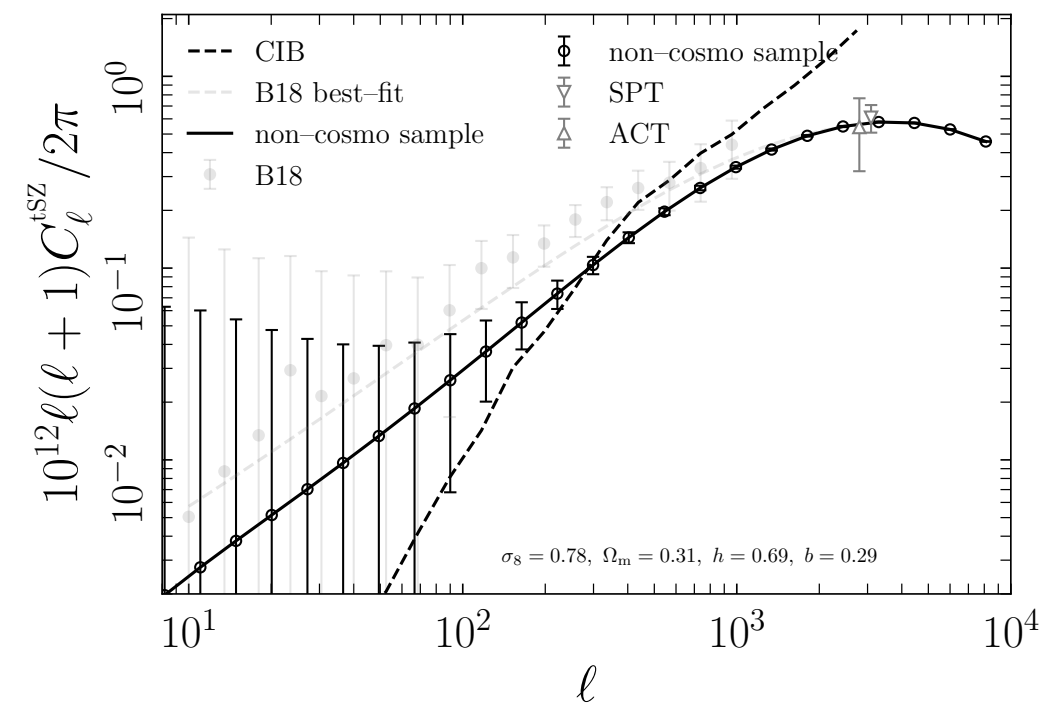
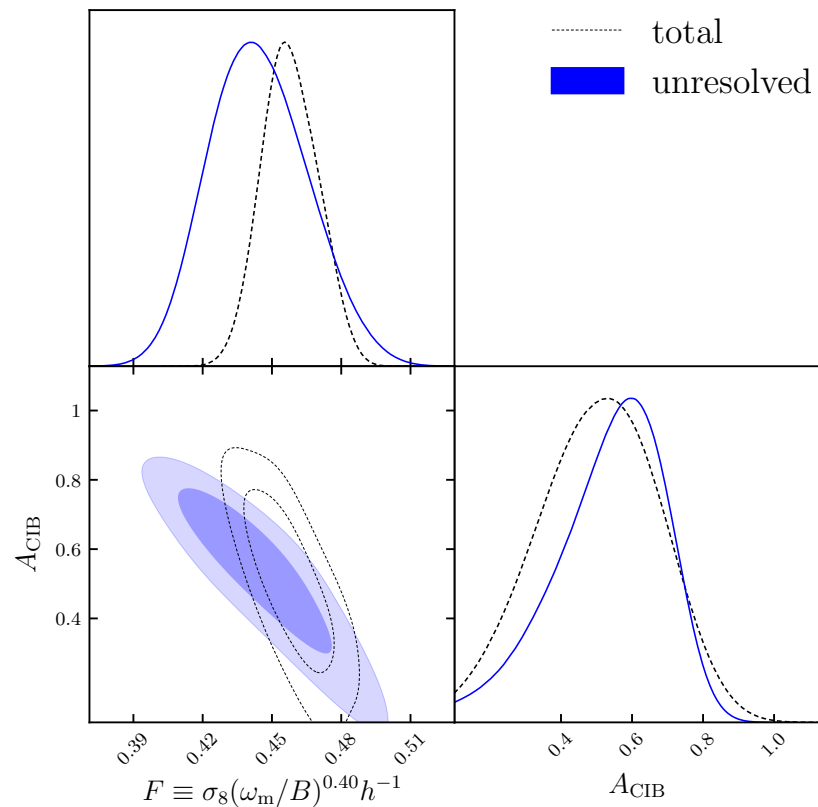
Fig. 14. Shape of the matter power spectrum $P(k)$ (log-log scale) at four different times: (upper left) when initial conditions are imposed (and all wavenumbers are super-Hubble); (upper right) at radiation/matter equality (arrows show the logarithmic growth during radiation domination); (lower left) at matter/ Λ equality (lower set of arrows show the growth during matter domination); (lower right) today (lower set of arrows show the growth during Λ domination).

[Lesgourges TASI lecture]

Idea of “anti-completeness” power spectrum

[Rotti, Battye, Bolliet, Chluba, Remazeilles - to appear]

compute power spectrum convolved with completeness of cluster count analysis

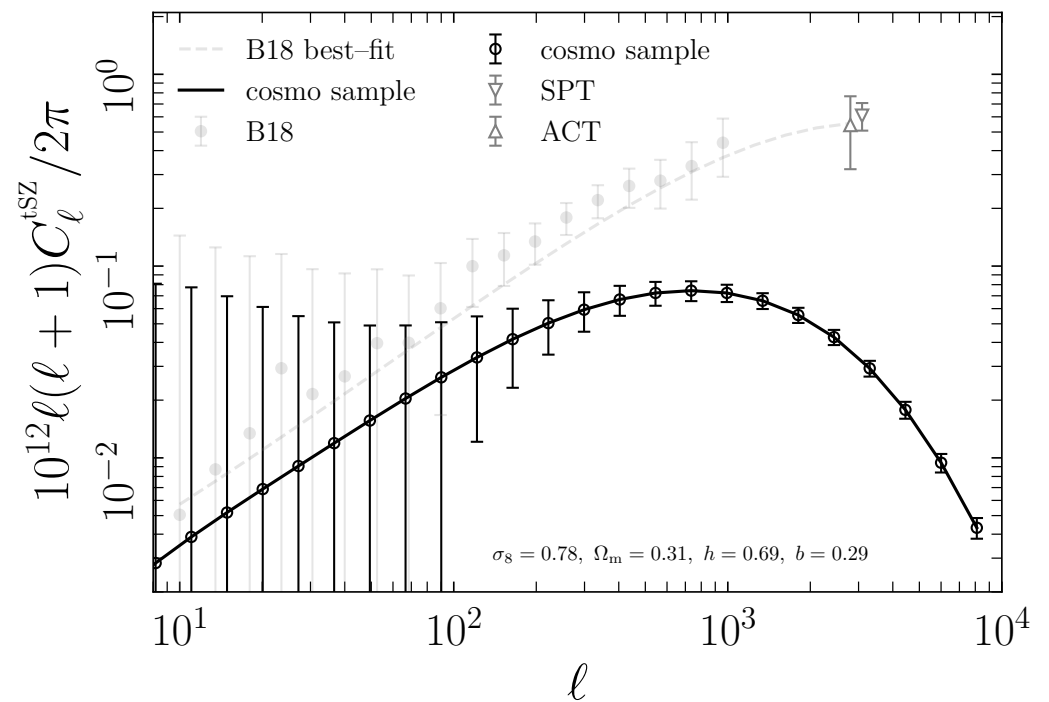
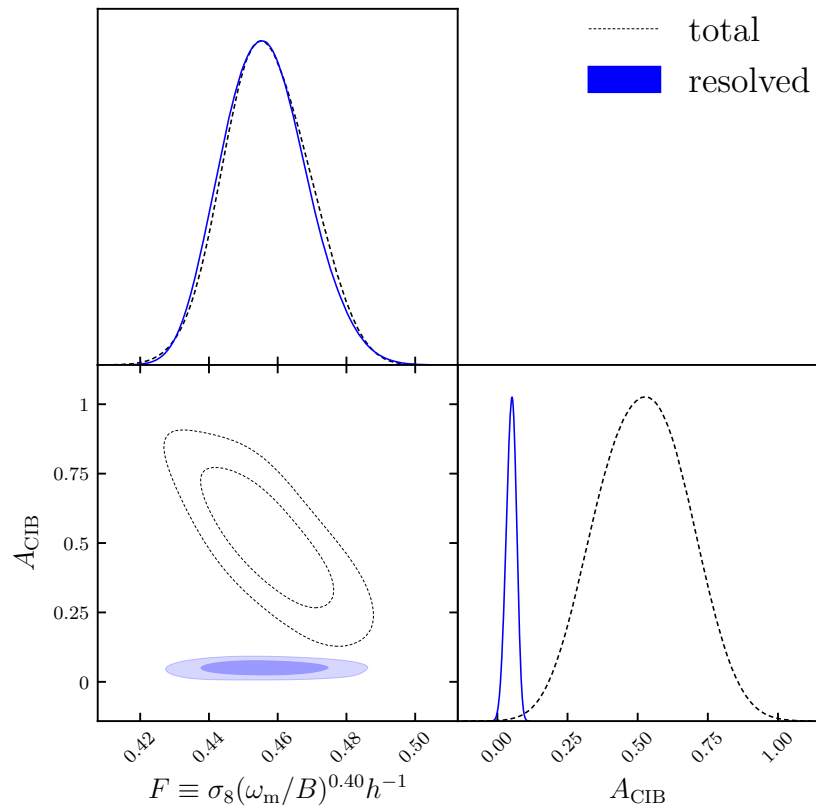


=> non-detected cluster info in y-map degenerate with CIB

Idea of “anti-completeness” power spectrum

[Rotti, Battye, Bolliet, Chluba, Remazeilles - to appear]

compute power spectrum convolved with completeness of cluster count analysis



Account for baryonic feedback in the halos:

.....

We model the effect of baryonic feedback within the halo by the relative gas fraction first introduced in (Mohammed et al. 2014), which appears as an overall normalization to the original gas pressure ρ_0 and therefore the Fourier transformed pressure profile \tilde{y}_l ,

$$f_{\text{gas}}(M_{\text{halo}}, M_{\text{crit}}) = \frac{1}{1 + \left(\frac{M_{\text{crit}}}{M_{\text{halo}}}\right)^2}. \quad (6)$$

In the limit that there is no feedback, $M_{\text{crit}} \rightarrow 0$, the gas fraction function goes to one. While feedback effects can expel the gas out to the virial radius and possibly beyond, the gas is not destroyed, and its thermal content is also unlikely to be changed, as also suggested by the weak lensing scaling relations of (Wang et al. 2016). We model this by enforcing integrated pressure conservation by exchanging the reduced pressure for a wide Gaussian profile,

$$y_l^{\text{new}}(x, r_{\text{vir}}) = f_{\text{gas}} y_l^0(x) + (1 - f_{\text{gas}}) y_l^{\text{feedback}}(x, r_{\text{vir}}), \quad (7)$$

with a Gaussian profile of the form

$$y_l^{\text{feedback}}(x, r_{\text{vir}}) = A(r_{\text{vir}}) e^{-x^2/2(4r_{\text{vir}})^2}. \quad (8)$$

Here $A(r_{\text{vir}})$ is a normalization coefficient calculated to preserve the overall integrated pressure. The spread of the Gaussian profile ($4r_{\text{vir}}$) will affect the power suppression of large scales versus small scales. While this is admittedly a rather simplified approach, we have chosen the parameter such that it roughly quantitatively agrees with the AGN feedback results of (McCarthy et al. 2014).

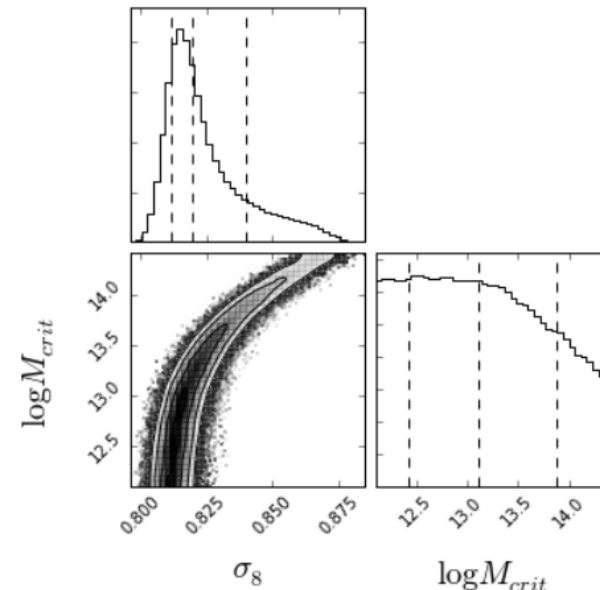
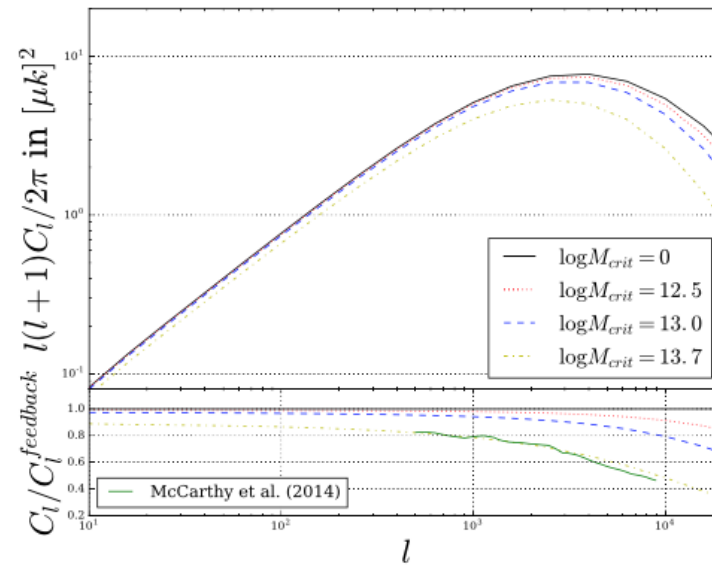
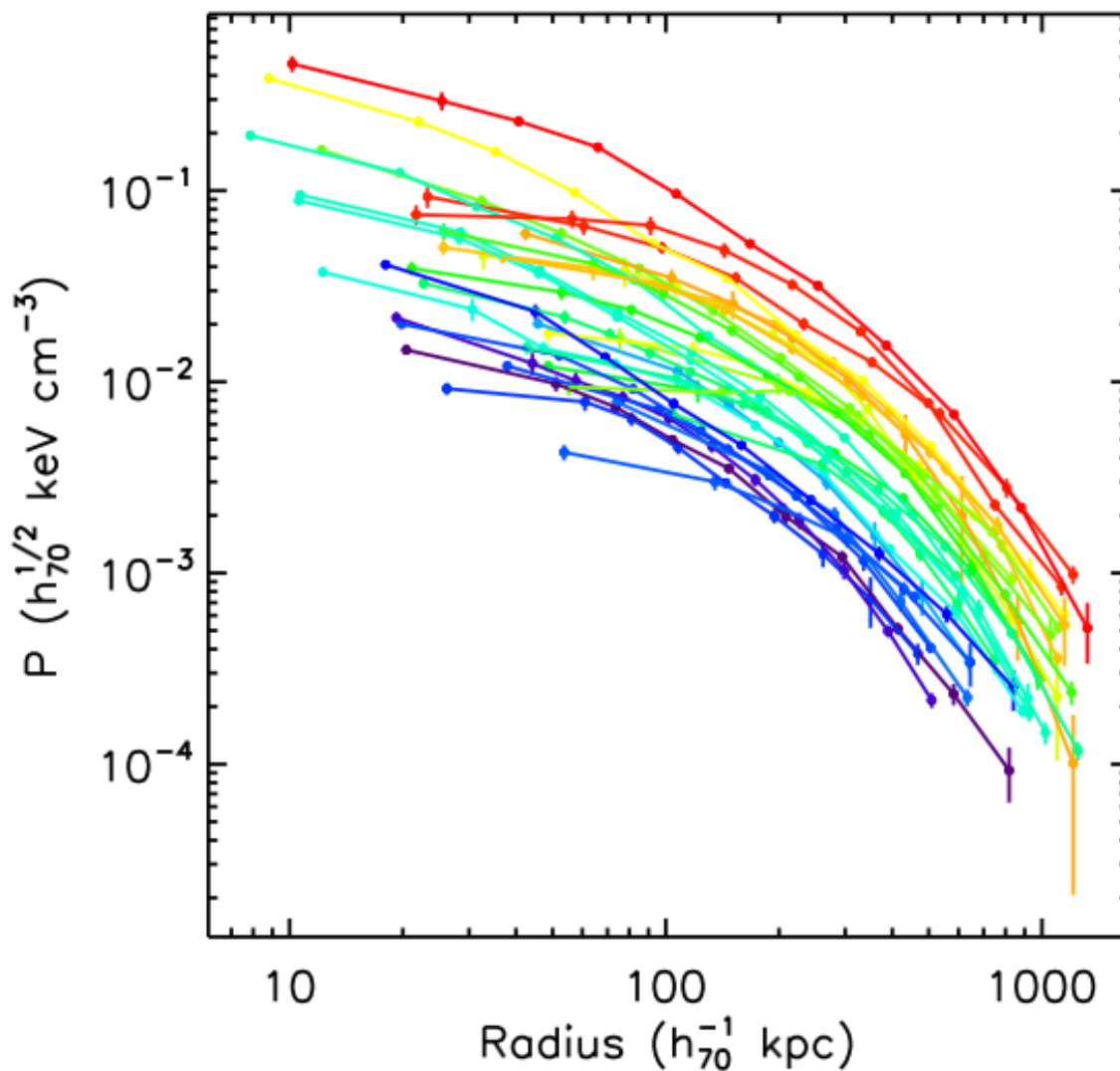


Figure 3. The result of our MCMC calculation with lines indicating the one standard deviation spread at the 16th, 50th, and 84th percentiles.

Horowitz and Seljak 2017



Universal pressure profile



*Fig from A10

Fig. 1. The pressure profiles of the REXCESS sample. Pressures are estimated at the effective radii of the temperature profile (points with errors bars). A line connects the data points for each cluster to guide the eye. The data are colour coded (from cold–blue to hot–red) according to the spectroscopic temperature, T_X .

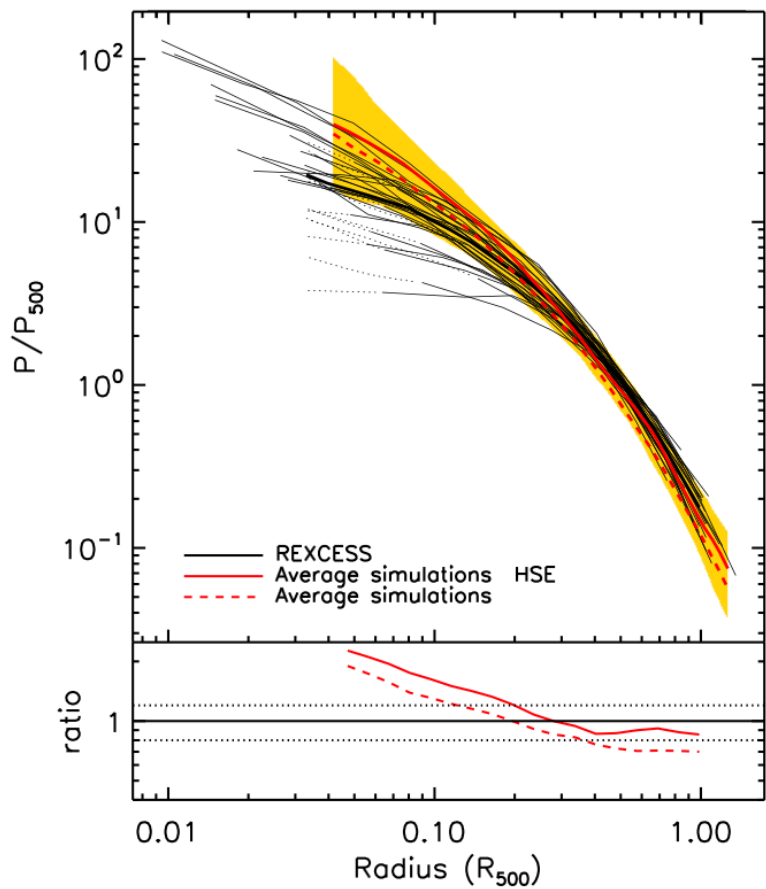
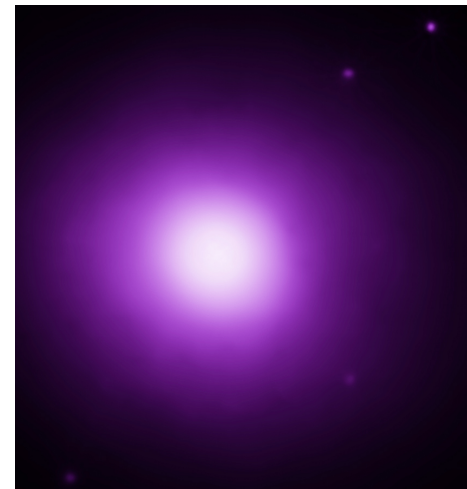


Fig. 7. Comparison of the REXCESS scaled profiles with the prediction of numerical simulations. Black lines: REXCESS data (as in Fig. 2). Thick black line: average REXCESS scaled profile. Red line: average simulation profile and dispersion around it (orange area) using the hydrostatic mass. Dotted red line: same using the true mass. Bottom panel: ratio of these average simulation profiles to the REXCESS average profile.



Universal pressure profile

Figure from P13 V

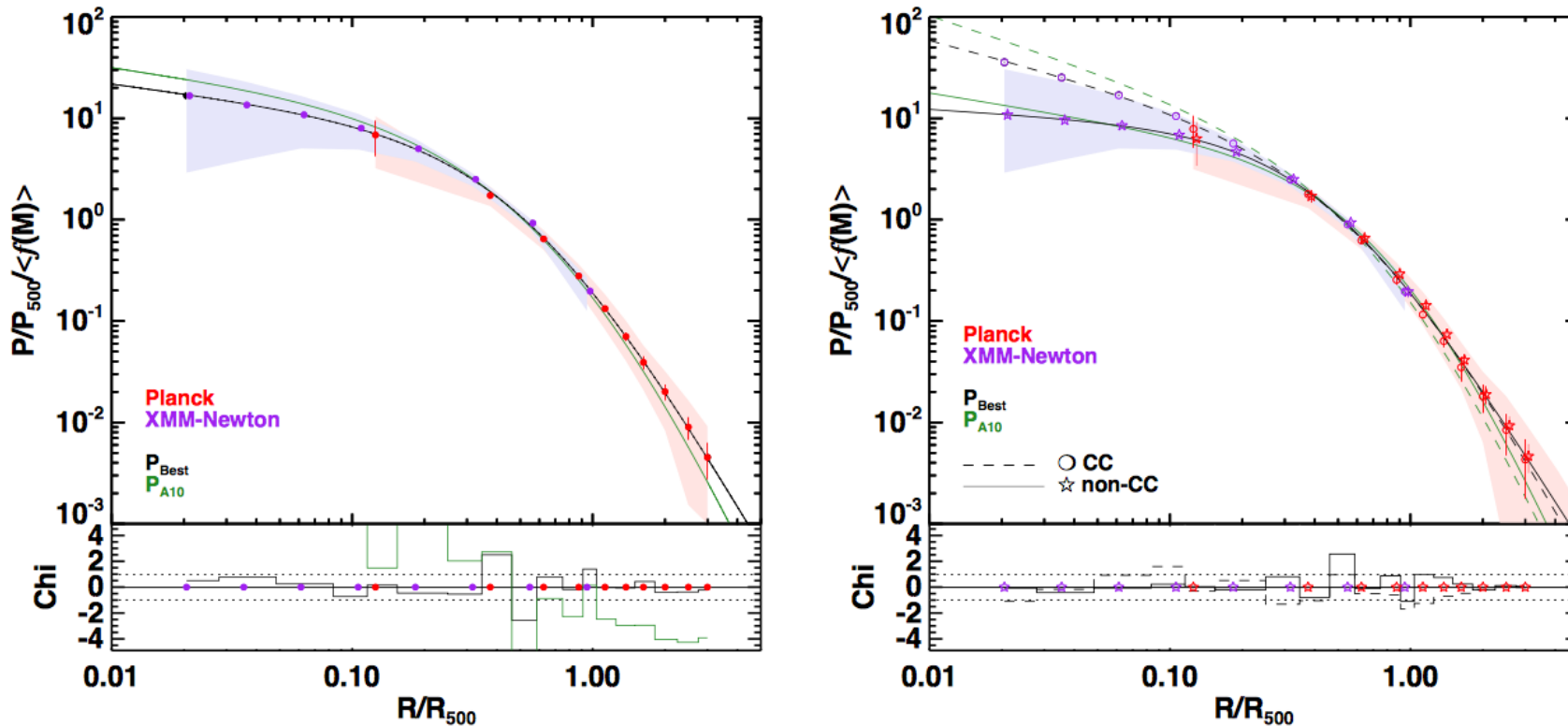


Fig. 4: Left: *Planck* pressure profile obtained from the average of the individual pressure profiles across our sample (red points) shown together with the stacked pressure profile derived from the *XMM-Newton* data for the same sample (purple points). The dispersions about the SZ and X-ray profiles are depicted, respectively, by the red and purple shaded areas. Our best fit GNFW profile is shown as a solid black line and that of A10 as a solid green line. The lower panel shows the χ profile of these two best models taking into account the statistical errors and dispersion about the observed profile. Right: stacked profile from *Planck* and *XMM-Newton* for the sub-samples of cool-core (open circles) and non cool-core (open stars) clusters within the ESZ-*XMM* sample. The shaded areas are identical to the one shown in the left panel. Our best fit models for each sub-sample are shown as black solid and dashed lines for the cool-core and non cool-core clusters, respectively (see Table 1). The best A10 fit for cool-core and non cool-core clusters are shown as green solid and dashed lines, respectively. The lower panel gives the χ profiles of our best fit models with respect to the measured profiles and associated errors (including dispersion). On both panels the *Planck* data points are correlated at about the 20% level (see Sect. 4.3.1). As for the stacked SZ profile, the error bars on the *Planck* points are purely statistical and correspond to the square root of the diagonal elements of the covariance matrix. For the *XMM-Newton* points they correspond to the statistical error on mean.

Universal pressure profile

Figure from Ruppin et al 2019

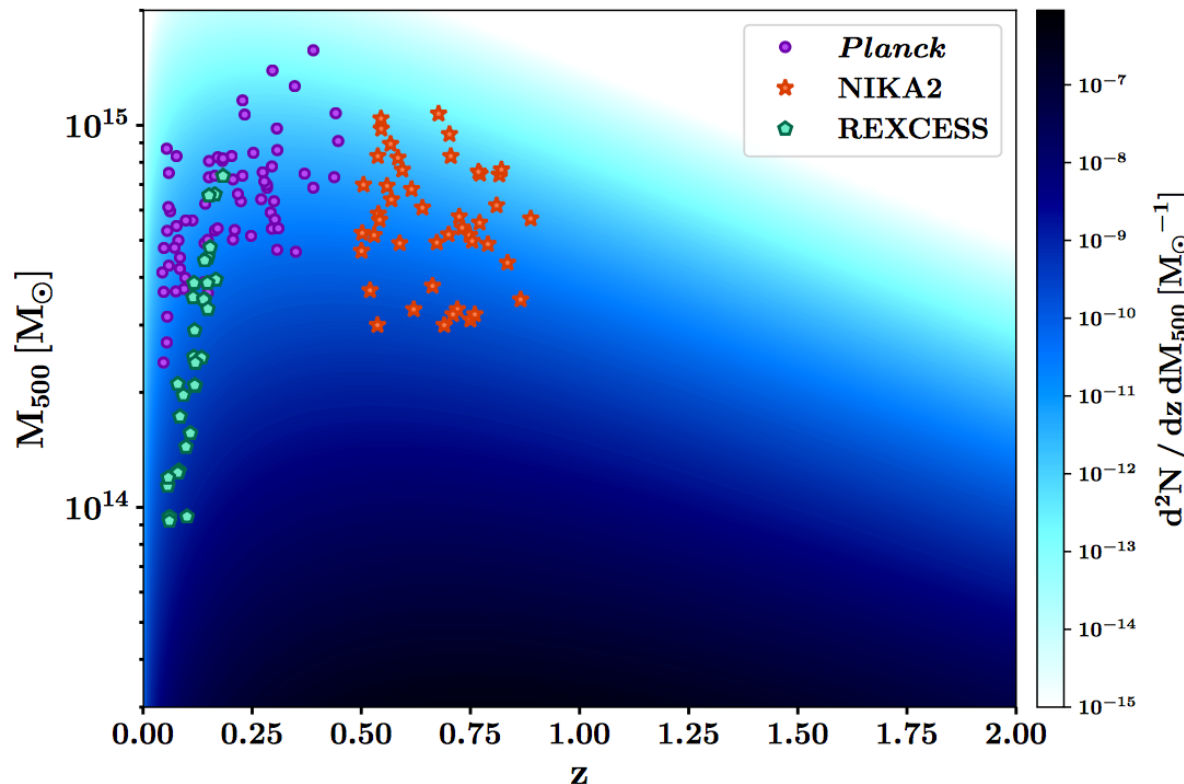


Figure 3. Distribution of the 62 *Planck* clusters used in order to estimate the mean normalized pressure profile at low redshift (purple) in the mass-redshift plane. The NIKA2 and REXCESS samples are also shown in orange and green respectively. The different shades of blue give the expected cluster abundance, *i.e.* the cluster number per unit of mass and redshift computed from Eq. (10).

REXCESS = 33

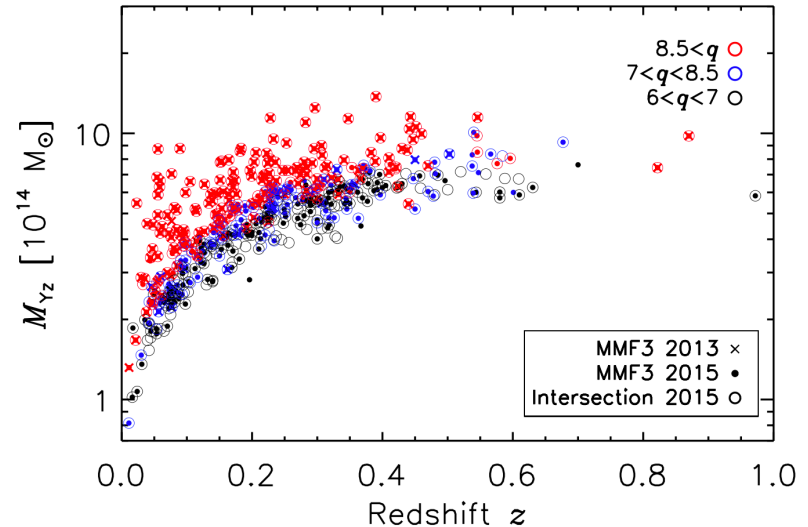
Planck = 62 (fitting the stacked XMM and SZ profile)

Total number of cluster:

$$N_{\text{tot}} \propto \sigma_8^{4.3} \Omega_m^{1.5} h^{0.5}$$

With Planck completeness:

$$N_{\text{tot}} \propto \sigma_8^{9.8} \Omega_m^{2.9} B^{-3.2} h^{-0.5}$$



depends on bias because completeness ~ see clusters above certain mass

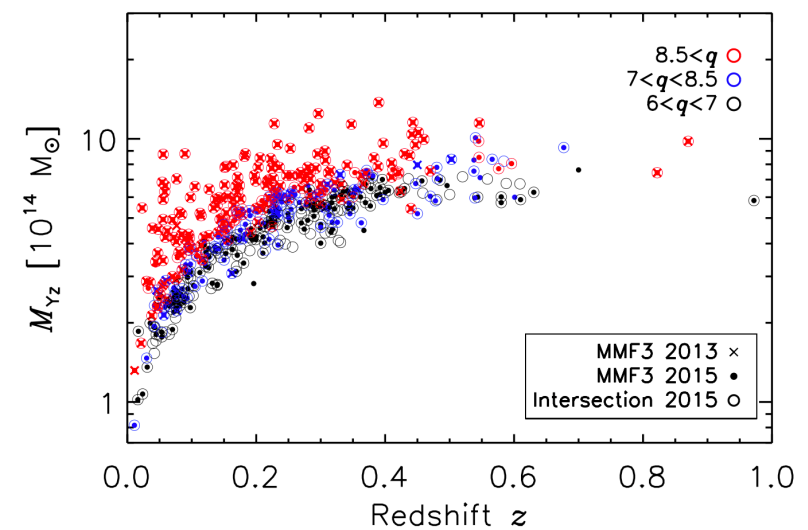
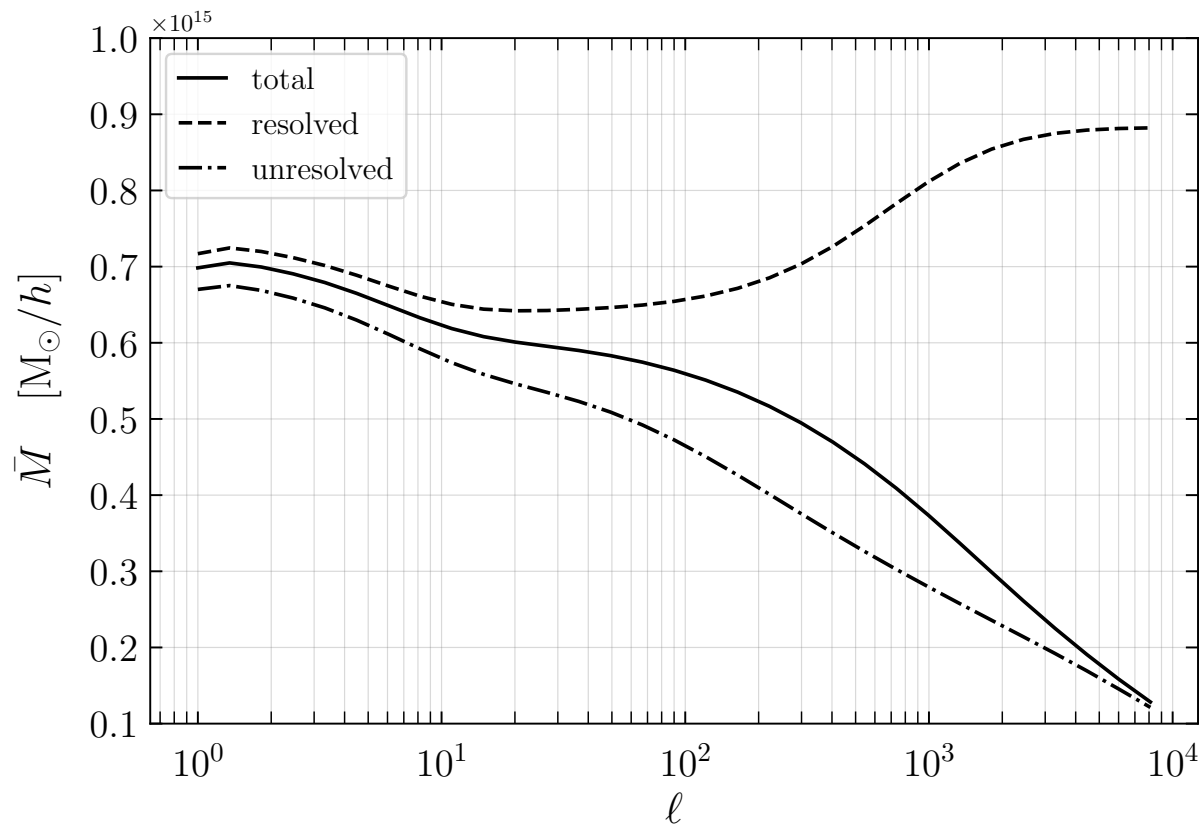
sensitive to mass definition and therefore bias

If bias is left undetermined:

$$\frac{dN}{dM} \propto f(\sigma_8 M^\alpha) / M \quad \alpha \approx -1/3$$

Expect degeneracy: $\sigma_8 B^\alpha \approx \text{constant}$

- Which masses contribute more to tSZ power spectrum?



Which redshift contribute more to tSZ power spectrum?

Figure from Kitayama [1404.0870]

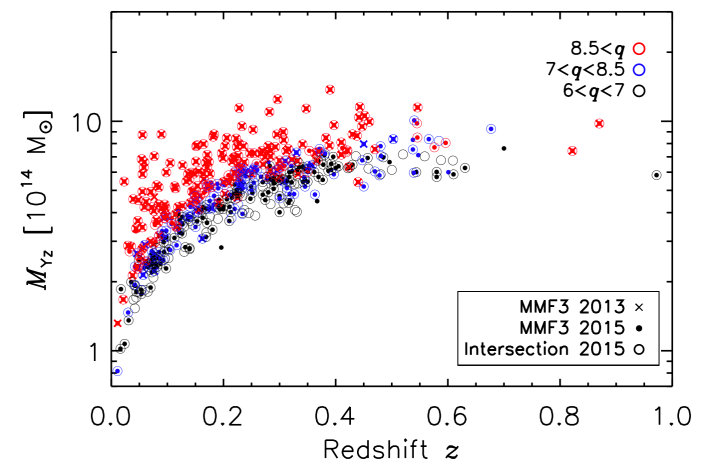
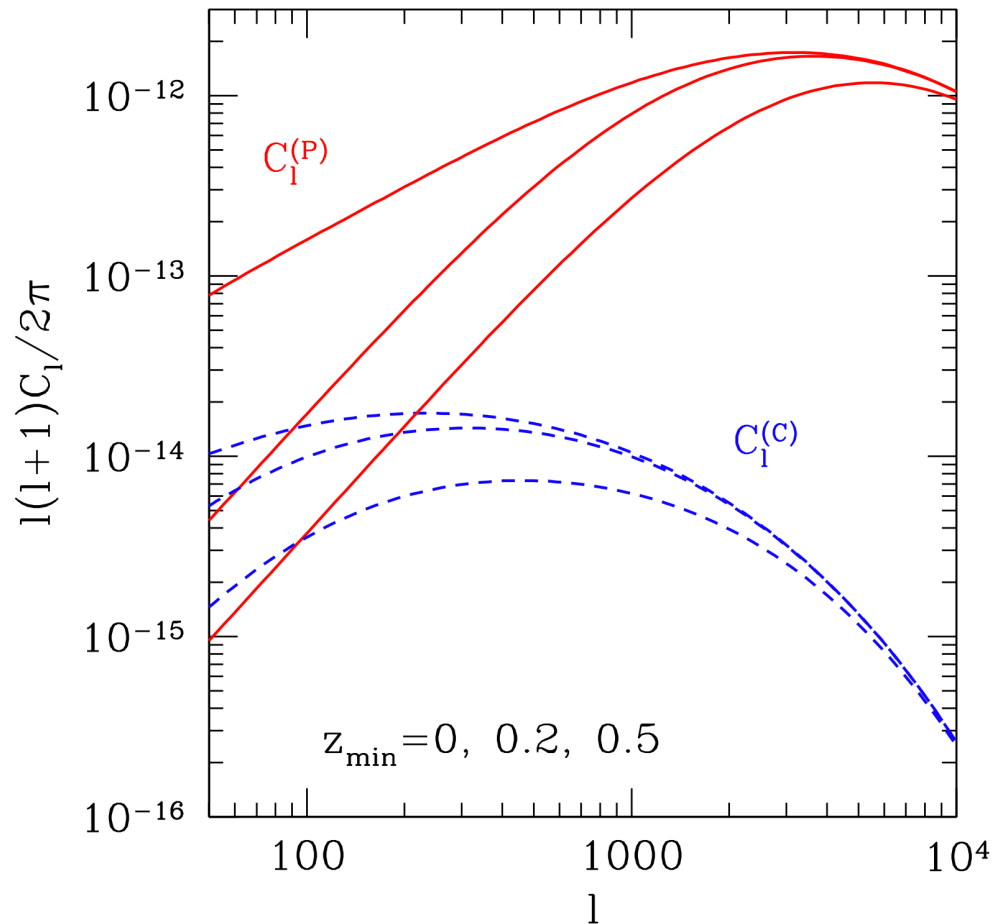


Figure from Planck 2015 cluster paper

- large scales: low redshift contribute more ($z < 0.2$)
- small scales power: determined by high z halos